



Investigation of the influence of asymmetric long chain ceramides [NP] and [AP] on *stratum corneum* lipid matrix architecture with neutron diffraction

DISSERTATION

Zur Erlangung des akademischen Grades:

Doktor rerum naturalium (Dr. rer. nat.)

Vorgelegt der

Naturwissenschaftlichen Fakultät I Biowissenschaften

der

Martin-Luther-Universität Halle-Wittenberg

am

14.06.2018

von

Herrn M. Sc. Thomas Schmitt

geboren am 16.06.1991

Gutachter/in

1. Prof. Dr. Dr. R. H. H. Neubert
2. Prof. Dr. Gerald Brezesinski
3. Prof. Dr. Bodo Dobner

Tag der Verteidigung:

18.10.2018

Rechtserklärung

Hiermit erkläre Ich laut § 5 Absatz 2b der Promotionsordnung der Naturwissenschaftliche Fakultät I (Biowissenschaften) der Martin-Luther-Universität Halle-Wittenberg, dass ich die vorliegende Arbeit selbständig verfasst und keine anderen als die angegebenen Quellen und Hilfsmittel verwendet habe. Alle Textstellen, die wörtlich oder sinngemäß aus veröffentlichten oder noch nicht veröffentlichten Quellen entnommen sind, sind als solche kenntlich gemacht.

Die Grafiken oder Abbildungen in dieser Arbeit wurden vom Autor selbst erstellt oder sind mit einem entsprechenden Quellennachweis versehen. Diese Arbeit ist in gleicher oder ähnlicher Form noch bei keiner anderen Prüfungsbehörde eingereicht worden.

Declaration of regulations

According to §5 Absatz 2b of the PhD regulations of the Naturwissenschaftliche Fakultät I (Biowissenschaften) of the Martin-Luther-University Halle-Wittenberg, I ensure that have written the presented thesis myself and used no other sources or materials other than the indicated ones. All passages taken literally or textural from published as well as unpublished work are indicated as such.

All graphics and pictures shown in this thesis are created by the author himself or labelled with an indication of the corresponding source. The same or a modified version of it has so far not been submitted to another academic examination office.

Halle (Saale), den

Thomas Schmitt

14.06.2018

Danksagungen und Anmerkungen (Acknowledgements)

Hiermit möchte ich mich ganz herzlich bei allen Kollegen, Freunden und sonstigen Involvierten bedanken, die mir auf die eine oder andere Art und Weise die Anfertigung dieser Dissertationsarbeit ermöglicht haben.

Als aller erstes herzlichen Dank an meinen Doktorvater **Herrn Prof. Dr. Dr. h.c. Reinhard H. H. Neubert**, der ungeachtet seiner wohlverdienten Emeritierung das entsprechende Forschungsthema bereitstellte, mir die Möglichkeit gab, dieses zu bearbeiten und mir als Betreuer immer wieder mit Rat und Tat zur Seite stand.

Mein besonderer Dank gilt ebenfalls **Herrn Dr. Peter Lersch** und **Frau Dr. van Logchem** stellvertretend für die **Firma Evonik Industries AG** für die Gewährung meines Stipendiums und damit der Grundlage nicht nur zur Erstellung dieser Arbeit sondern auch für eine äußerst interessante, lehrreiche und vor allem wissenschaftlich konstruktive Reise zur Gordon Research Conference „Barrier Function of Mammalian Skin“ in den USA im August 2017.

Einen Dank an dieser Stelle auch an **Frau Dr. Adina Eichner** für die Einführung in den praktischen Teil der Arbeit und einige weitere anfängliche Hilfestellungen.

Ebenso vielen Dank an **Herrn Dr. Thomas Hauß** für die Einführung in die Neutronendiffraktionsexperimente, deren Auswertung und Interpretation, sowie für diverse weitere Hilfestellungen während meiner Arbeit, ebenso wie die ausgezeichnete Betreuung am **V1 am HZB** Berlin. Auch einen Dank an **Herrn Dr. Bruno Demé** für die gleichfalls ausgezeichnete Betreuung am **D16 am ILL** in Grenoble. Und natürlich auch allen anderen die an der Entstehung und am Erhalt des HZB und ILL sowie der Zuteilung von Beamtime beteiligt waren.

Ebenfalls besonderer Dank gebührt **Herrn Prof. Dr. Bodo Dobner** und seinen beiden Doktoranden **Herrn Stefan Sonnenberger** und **Herrn Stefan Lange** für die Synthese, Reinigung, Analyse und Zurverfügungstellung der meisten verwendeten Lipide. Der Rest des Dankes speziell hierfür gebührt der **Firma Evonik Industries AG**, die ebenfalls einen großen Teil an Substanzen für die getätigten Experimente zur Verfügung stellte.

Ein großes Dankeschön weiterhin an **Herrn Rakesh Gupta**, **Frau Prof. Dr. Beena Rai** sowie **TATA Research incorporated**, die die gezeigten MDS Resultate ermöglichten. Ebenfalls gilt mein Dank **Herrn Dr. Gert Gooris** und **Frau Prof. Dr. Joke Bouwstra**, die die gezeigten SAXD Ergebnisse ermöglichten.

Auch ein extra Dankeschön an **Herrn Prof. Dr. Johannes Wohlrab** für die Unterstützung an diverser Stelle, sowie **Herrn Prof. Dr. Stefan Ebbinghaus** und **Herrn Dr. Christoph Wagner** für die Zurverfügungstellung der Pulverdiffraktometer für diverse Voruntersuchungen.

Weiterhin natürlich herzlichen Dank an **Herrn Prof. Dr. Gerald Brezesinski** und **Herrn Prof. Dr. Bodo Dobner** für die fachliche Beurteilung der Arbeit. Ebenso an all die **Reviewer** und **Editoren** meiner Publikationen, sowie **sonstige Mitarbeiter der entsprechend Journale** die das Erscheinen dieser ermöglichten. Gleichfalls einen Dank an alle interessierten **Leser** der Entsprechenden Zeitschriften die wiederum deren Erscheinen ermöglichen und hoffentlich zumindest teilweise mit Interesse meine Arbeit verfolgten.

Danke ebenfalls an **Herrn Dr. Tobias Schrader**, **Herrn Dr. Andreas Ostermann** und **Herrn Dr. Robert Georgii** für Gerätebetreuung am MLZ in Garching.




Ein herzliches Dankeschön auch an alle netten Kolleginnen und Kollegen der Einfachheit halber in alphabetischer Reihenfolge: **Dr. Alexander Vogel, Angelica Avila, Andrea Stennett, Anika Kaiser, Anke Nies, Carmen Ballstaedt, Christian Sporn, Claudia Bruhne, Prof. Dr. Daniel Huster, Dr. Efreem Tessema, Dr. Elfie Sommer, Felix Otto, Hina Hussain, Dr. Julia Michael, Kathrin Fleischhauer, Khaled Alkassam, Dr. Konstanze Bosse, Nick Härtling, Moritz Niemöller, Selina Watzlaw, Dr. Sören Stahlberg, Stefanie Münch, Sylke Faßhauer, Dr. Yahya Mrestani** und der **Firma Skinomics**, der **Hautklinik der UK-Halle** und dem **IADP e.V.** jeweils als Ganzes, für das angenehme Arbeitsklima, spannende Seminare, interessante Konversationen, gelegentliche Unterstützung und mehr.




Danke auch an den **Promotionsausschuss**, das **Dekanat** der **Naturwissenschaftlichen Fakultät I** und dessen direkte und indirekte Vertreter **der Martin-Luther-Universität Halle-Wittenberg** die meine Promotionsarbeit ermöglicht haben.

Zu guter Letzt geht mein Dank an meine **Freunde**, meine **Eltern Reiner und Silke Schmitt** meine **Tante Ortrud Götz** mich auch in schwierigen Zeiten weithin unterstützten, so gut sie konnten. Ebenfalls in **Gedenken an** meinen **Onkel Winfried Hennig**, der bedauerlicherweise nicht mehr erleben wird, wie ich diese Arbeit zu einem Abschluss bringe.

Die notwendige Finanzierung dieser Arbeit wurde ermöglicht durch die **Deutsche Forschungsgemeinschaft** (DFG NE427/30 1 und DO463/6-1) sowie die **Firma Evonik Industries AG (Essen, DE)**.

Für alle Studenten denen diese Arbeit möglicherweise als Vorbild oder auch nur Copy & Paste Vorlage dient Arbeitet hart, haltet durch und versucht immer Euch in jeder möglichen Hinsicht zu verbessern, denn nur so werdet Ihr eure Ziele Erreichen!

Anmerkung: Sofern Sie die **interaktive PDF-Version** dieses Dokuments in einem geeigneten Leseprogramm (z.B. Adobe® Reader®) verwenden, besteht die Möglichkeit zur Navigation durch das Dokument über vorhandene interaktive Felder. Diese Felder sind unter anderem Index of contents (Inhaltsverzeichnis), of tables (Tabellenverzeichnis) of figures (Grafikverzeichnis), Grafik und Tabellenverweise, Querverweise, Quellen und Abkürzungen im Text sowie einige Grafiken. Wird der Mauszeiger zu , drücken Sie Maustaste 1 (für gewöhnlich linke Maustaste) um zum entsprechenden Element zu springen. Um zum ursprünglichen Bereich/Textabschnitt zurückzukehren kann unter Windows die Tastenkombination **Alt** und  „links“ und unter MacOS **Cmd** und  „links“ verwendet werden.

Note: If you are using the **interactive PDF-version** of this document together with a suitable reading program (e.g. Adobe® Reader®) please note, that there are some interactive fields, which can be used to navigate the document. These include the index of contents, index of tables, index of figures, table, figure and other cross references, sources and abbreviations in the text as well as some Figures. If your mouse cursor turns into , press mouse button 1 (usually left mouse trigger), to jump to the corresponding element. To return to the original spot/paragraph on windows the key combination **Alt** and  „left“ and on MacOS **Cmd** and  „left“ can be used.

Index of contents

Abbreviations.....	8
Index of Figures.....	9
Index of Tables.....	11
Kurzzusammenfassung.....	12
Abstract.....	13
1. Introduction.....	14
2. General Background.....	15
2.1 The Epidermis.....	15
2.1.1 Layer by Layer.....	17
2.1.2 The Barrier Layer.....	18
2.1.3 The Matrix Lipids.....	20
2.1.4 Asymmetric Long-Chain Ceramide [NP] and [AP].....	24
2.1.4.1 CER[NP].....	24
2.1.4.2 CER[AP].....	26
2.1.5 The Very Long ω -hydroxy-Ceramides.....	26
2.1.6 The Molecular Nanostructure of the Lipid Matrix.....	27
2.1.6.1 The Lamellar Structure.....	27
2.1.6.2 The Short Periodicity Phase.....	28
2.1.6.3 The Long Periodicity Phase.....	28
3. Materials and Methods.....	30
3.1 Materials.....	30
3.2 Sample Preparation.....	32
3.3 Neutron Diffraction Experiments.....	33
3.3.1 General Principles of Neutron Diffraction.....	33
3.3.2 Diffraction in Ordered Multilamellar Systems.....	34
3.3.3 Membrane Diffraktometer V1.....	35
3.3.4 Small Momentum Transfer Diffractometer D16.....	36
3.3.5 Evaluation and Implications of Diffraction Data.....	38
3.4 X-ray Diffraction.....	42
4. Results and Discussion.....	44
4.1 Investigation of a CER[NP] and [AP]-Based <i>Stratum Corneum</i> Modelling Membrane System: Using Specifically Deuterated CER Together with a Neutron Diffraction Approach.....	45
4.1.1 Materials and Methods.....	45
4.1.1.1 Ceramide Mixtures.....	45
4.1.1.2 Sample preparation.....	46
4.1.1.3 Neutron diffraction experiments.....	46
4.1.2 Results.....	47
4.1.3 Discussion.....	51
Dissertation Thomas Schmitt.....	5

4.1.4	Conclusion	53
4.2	Determination of the influence of C24 D/(2R)- and L/(2S)-isomers of the CER[AP] on the lamellar structure of <i>stratum corneum</i> model systems using neutron diffraction.....	54
4.2.1	Materials and Methods	54
4.2.1.1	Preparation and Separation of the CER[AP] Diastereomers	54
4.2.1.2	Sample PreparationBN	55
4.2.1.3	Neutron Diffraction Experiments.....	55
4.2.1.4	Small angle X-Ray diffraction	56
4.2.2	Results	56
4.2.3	Discussion	60
4.2.4	Conclusion	62
4.3	The structure organisation of CER[NS] and CER[AP] in SC modelling membrane systems is surprisingly similar yet noticeably different: A Neutron diffraction study	63
4.3.1	Abstract.....	63
4.3.2	Introduction.....	63
4.3.3	Materials and Methods.....	64
4.3.3.1	Ceramide Mixtures.....	64
4.3.3.2	Sample Preparation.....	65
4.3.3.3	Neutron Diffraction Experiments.....	65
4.3.3.4	Molecular Dynamics Simulations.....	66
4.3.4	Results	67
4.3.4.1	Phase behaviour	67
4.3.4.2	Lamellar repeat distance.....	68
4.3.4.3	Head group region	69
4.3.4.4	Water distribution	70
4.3.4.5	CHOL distribution	70
4.3.4.6	Molecular nanostructure: Overlapping long chains.....	71
4.3.4.7	Molecular nanostructure: Chain tilt and chain opening angles:	73
4.3.5	Discussion	73
4.3.5.1	Repeat distance	74
4.3.5.2	Phase behaviour of lipids	74
4.3.5.3	Water distribution	75
4.3.5.4	CHOL distribution and its influence	75
4.3.5.5	Nanostructure overlapping in middle-layer	75
4.3.5.6	Nanostructure conformation	76
4.3.6	Conclusion	77
4.4	The long periodicity phase (LPP) controversy Part I: The influence of a natural-like ratio of the CER[EOS] analogue [EOS]-br in a CER[NP]/[AP] based stratum corneum modelling system: A Neutron diffraction study	78
4.4.1	Abstract.....	78
4.4.2	Introduction.....	78

4.4.3	Materials and Methods.....	80
4.4.3.1	Ceramide Mixtures.....	80
4.4.3.2	Sample preparation.....	80
4.4.3.3	Neutron Diffraction Experiments.....	80
4.4.4	Results.....	81
4.4.5	Discussion.....	85
4.4.6	Conclusion.....	90
4.5	Co-authored publications.....	91
4.5.1	Synthesis of specific deuterated derivatives of the long chained stratum corneum lipids [EOS] and [EOP] and characterization using neutron scattering.....	91
4.5.1.1	Materials and Methods.....	92
4.5.1.2	Neutron Diffraction Experiments.....	92
4.5.1.3	Results and discussion.....	93
4.5.1.4	Conclusion.....	94
4.5.2	The Influence of a Novel Dimeric Ceramide Molecule on the Nanostructure and the Thermotropic Phase Behavior of a Stratum Corneum Model Mixture.....	95
4.5.2.1	Introduction.....	96
4.5.2.2	Materials and Methods.....	96
4.5.2.2.1	Sample Preparation for Neutron Diffraction Measurements.....	96
4.5.2.2.2	Neutron Diffraction Experiments.....	97
4.5.2.3	Results and Discussion.....	98
4.5.2.3.1	Lipid Organization in the SC Lipid Model System in the Presence of the Dimeric Ceramide.....	98
4.5.2.3.2	Localization of the Central Segments of the Dimeric Ceramide in the SC Lipid Model System.....	99
4.5.2.4	Conclusions.....	100
5.	Final Conclusions.....	101
6.	References.....	102
7.	Appendix.....	109

Abbreviations

BA	Behenic acid	SA	Stearic acid
br	Branched	SAXD	Small angle X-ray diffraction
CA	Cerotic acid	SC	<i>Stratum corneum</i>
CER	Ceramide	SPP	Short periodicity phase
ChE	Cholesterol esters	SPR	Small proline rich proteins
CHOL	Cholesterol	UV	Ultraviolet
ChS	Cholesterol sulfate	WAXD	Wide angle X-ray diffraction
dim	Dimeric		
DSC	Differential scanning calorimetry		
eM	Electron microscopy		
<u>FFA</u>	<u>Free</u> fatty acids		
FTIR	Fourier transformed infrared spectroscopy		
FTRa	Fourier transformed Raman spectroscopy		
HbN	Hydrogen-bonding network	CER[___]	
HG	Head group	[EO___]	Esterified at ω -hydroxy group
HOPG	Highly oriented pyrolytic graphite		
HPLC	High performance liquid chromatography	[OE___]	Esterified at C1-hydroxy group
HRMS	High resolution mass spectrometry	[__N__]	Non-hydroxy (fatty acid)
ILL	Institut Laue Langevin	[__A__]	Alpha-hydroxy (fatty acid)
IR	Infrared	[__O__]	Omega-hydroxy (fatty acid)
LA	Lignoceric acid		
LM	Multilamellar lipid matrix		
LPP	Long periodicity phase	[___S]	Sphingosine (sphingoid base)
MDS	Molecular dynamics simulations	[___P]	Phytosphingosine (sphingoid base)
NMR	Nuclear magnetic resonance	[___H]	6-Hydroxysphingosine (sphingoid base)
NSLD	Neutron scattering length density profile	[___DS]	Dihydroxysphingosine (sphingoid base)
PA	Palmitic acid		
PU	Poly-unsaturated	[___T]	Dihydro-dihydroxy-shpingosine (sphingoid base)
PyBOP®	Benzotriazol-1-yl-oxytripyrrolidinophosphonium-hexafluorophosphat		
R.H.	Relative humidity		
Rac	Racemic mixture (D/R and L/S)		
RT	Room temperature		

Index of Figures

Figure 1: Overview of the skin layers and important structures located within them	Seite 17
Figure 2: Schematic representation of the epidermis with its multiple layers	Seite 18
Figure 3: Schematic representation of the corneocyte envelope	Seite 19
Figure 4: Penetration pathways through the SC	Seite 20
Figure 5: Chemical structure of the 5 known sphingoid bases.....	Seite 21
Figure 6: Chemical structure of the 18 confirmed ceramides from human	Seite 22
Figure 7: Three basic CER chain conformations depending on the chain tilt angle α	Seite 23
Figure 8: Lateral chain packing of CER in the SC lipid matrix	Seite 24
Figure 9: Different cases of interference of two waves	Seite 33
Figure 10: Diffraction in different complex systems.....	Seite 34
Figure 11: The V1 and the beam path at this Instrument.....	Seite 36
Figure 12: Representative diffraction pattern for a sample measured at the V1	Seite 36
Figure 13: Specifications of the D16	Seite 37
Figure 14: Representative diffraction pattern for a sample measured at the D16	Seite 38
Figure 15: Example for the determination of the F_n using a three point measurement	Seite 40
Figure 16: NSLD-profiles for multilamellar lipid model systems.....	Seite 41
Figure 17: Comparison of the NSLD-profiles for multilamellar lipid model systems	Seite 41
Figure 18: Comparison of the NSLD-profiles at 8 % D2O and 100 % D2O	Seite 42
Figure 19: Example for a typical diffractogram as observed using X-ray	Seite 42
Figure 20: Relevant interactions of X-rays with matter.....	Seite 44
Figure 21: Structures of the lipids used for these experiments.....	Seite 46
Figure 22: Representative physical data for the CER[NP]-D3/[AP]/CHOL/LA system	Seite 48
Figure 23: NSLD for the three different H2O/D2O contrasts.....	Seite 49
Figure 24: NSLD for the two investigated model systems	Seite 50
Figure 25: Proposed arrangement for the CER[NP]/[AP] 2:1 and 1:2 ratio model system	Seite 52
Figure 26: Structures of the deuterated lipids used for these experiments.....	Seite 55
Figure 27: Resulting neutron scattering length density profiles for the investigated samples ..	Seite 58
Figure 28: Resulting SAXD profiles for the investigated base mixtures.....	Seite 59
Figure 29: Resulting neutron scattering length density profiles for the investigated samples ..	Seite 59

Figure 30: Structures of the deuterated lipids used for these experiments	Seite 65
Figure 31: Representative diffraction data for the investigated systems.....	Seite 67
Figure 32: Comparison of the 4th order peak of the two different molecular ratios	Seite 68
Figure 33: The structure of each triple layer structure in the end of 300 ns simulation.....	Seite 68
Figure 34: Calculated (non-normalized) neutron scattering length density profiles	Seite 69
Figure 35: Overall system density along the bilayer normal z	Seite 70
Figure 36: Comparison of the CHOL peaks	Seite 71
Figure 37: Calculated normalized neutron scattering length density profiles.....	Seite 71
Figure 38: The schematic of the triple layer	Seite 72
Figure 39: Structures of the deuterated lipids used for these experiments.....	Seite 80
Figure 40: NSLD for the three H ₂ O/D ₂ O contrasts.....	Seite 82
Figure 41: NSLD for the investigated CER[NP]/[AP]/[EOS]-br based model system	Seite 83
Figure 42: Relative neutron diffraction profiles	Seite 83
Figure 43: Comparison of the corrected and uncorrected NSLD and deuteration profiles	Seite 85
Figure 44: Neutron scattering length density profiles	Seite 94
Figure 45: Structures of the dimeric ceramide (dim-Cer) and the deuterated variant dim-Cer-d ₁₂	Seite 96
Figure 46: NSLD profiles $\rho_s(x)$	Seite 99
Figure 47: Structural model of the lipid mixture based on Cer[AP18], Chol, SA, Chol-S, and dim-Cer..	Seite 100

Index of Tables

Table 1: Fatty acid composition within the LM	Seite 20
Table 2: Overview of the ratios with which, CER are found in the LM.....	Seite 23
Table 3: Used Chemicals	Seite 30
Table 4: Used Instruments and Utensils	Seite 31
Table 5: Used software	Seite 32
Table 6: Overview of the scattering length of elements found in biological molecules.....	Seite 38
Table 7: Used mixtures of CER[NP]/CER[AP]/CHOL/	Seite 46
Table 8: Different conditions, applied for all mixtures	Seite 47
Table 9: Structure factors F_n for diffraction orders 1-5 at 100 % D2O and 98 %	Seite 48
Table 10: Used mixtures of CER[NP]/CER[AP]/CHOL/	Seite 55
Table 11: Structure factors F_n for diffraction orders 1-5 at 100 % D2O and 98 % R.H.....	Seite 57
Table 12: Structure factors F_n for diffraction orders 1-5 at 100 % D2O and 98 % R.H.....	Seite 69
Table 13: Structure factors F_n for diffraction orders 1-5 at 100 % D2O and 98 % R.H.....	Seite 81
Table 14: Observed and estimated peak positions for the second phase	Seite 84
Table 15: Measurement conditions for the neutron scattering measurements.....	Seite 92
Table 16: Overview of the composition of the SC lipid model systems studied in neutron diffraction experiment	Seite 97

Kurzzusammenfassung

Die oberste Hautschicht, *Stratum corneum*, ist eine der wichtigsten Barrieren gegen exogene Noxen wie Pathogene oder Chemikalien. Sie besteht aus stark keratinisierten toten Korneozyten mit mehrschichtiger Hülle. Der Interzellularraum ist gefüllt mit einer Lipidmatrix aus Cholesterin, freien Fettsäuren und Ceramiden in äquimolarem Verhältnis, welche die Hauptbarriere bilden. Die Ceramide bestehen aus einer Sphingoidbase und einer Amid-gebundenen Fettsäure mit variabler Länge und Kopfgruppe. Sie sind der Haupteinflussfaktor für die Barrierefunktion. Da die natürliche Lipidmatrix zu komplex ist um diese direkt zu untersuchen werden vereinfachte Modellsysteme mit wenigen synthetischen Lipiden, mit definierten Kettenlängen und Kopfgruppen, eingesetzt. Diese werden in definiertem Verhältnis, Ceramide/Cholesterin/freie Fettsäuren (1/ 0,7/1), gemischt und auf ein Träger aufgesprüht. Durch wiederholte Heiz-/Kühlzyklen wurde eine Selbstorganisation zu einer der naturnahen multilamellaren Struktur induziert. Die Proben wurden mittels Neutronendiffraktion analysiert. Verursacht durch die geordnete multilamellare Struktur ergibt sich aus der Überlagerung der kugelförmig gestreuten Neutronenwellen ein spezifisches Diffraktionsmuster. Aus diesem Muster kann das Neutronenstreuulängendichteprofil errechnet werden. Dieses Profil zeigt die Streueigenschaften entlang der Einheitszelle, einer virtuellen Repräsentation einer einzelnen Lamelle. Dies liefert Informationen über die Verteilung der Kopfgruppen, Lipidketten und des Wassers, was die Analyse der detaillierten lamellaren Mikrostruktur ermöglicht. Neutronen können weiterhin Isotope unterscheiden, was die Verwendung von Deuterium als Markierung, ohne starke Veränderung der molekularen Eigenschaften, ermöglicht. Auf diese Weise kann auch die molekulare Nanostruktur erfasst werden. Zwei der häufigsten Ceramide sind [NP] und [AP]. Die Ketten der Ceramide sind meist gesättigte C22 - 32 Fettsäuren und C18 Sphingoidbasen. Asymmetrische C24/18 Varianten wurden daher als natürlichste verfügbare Ceramide ausgewählt. Diese beiden wurden mit Cholesterin und Lignocerinsäure gemischt. Für beide Ceramide im Verhältnis 1:2 und 2:1 wurde trotz der Einfachheit der Mischungen die Bildung einer naturnahen Struktur beobachtet. Der höhere Ceramid-[NP]-Anteil führte zu einer lineareren Kettenausrichtung mit überlappenden C24 Ketten, der höhere [AP] Anteil zu einer lateral geneigten Anordnung mit weniger Überlappung. Die gebildete 5.45 nm Phase war, abgesehen von einer stärkeren Kettenneigung, nahezu unbeeinflusst vom Zusatz eines langen Ceramid-[EOS]-Analog in einem naturähnlichen Verhältnis von 10 %. Es führte nicht zur Bildung zusätzlicher Phasen sondern wurde lediglich integriert und durchspannte mehrere Schichten. Der Austausch des natürlichen D-Isomers des Ceramids [AP] durch das synthetische L-Isomer störte die lamellare Struktur und führte zu kristallinem Verhalten. Grundsätzlich zeigte das L-Isomer ein fundamental unterschiedliches Verhalten und formte trotz Zusatz des Ceramids [NP] keine lamellare Phase. Der Austausch von [NP] durch [NS] führte zu einer kürzeren Phase und besserer Mischbarkeit mit Cholesterin. Insgesamt konnte die Bedeutung beider Ceramide gut herausgestellt werden. Eine lediglich minimale funktionale Redundanz zwischen den unterschiedlichen Ceramiden konnte gezeigt werden.

Abstract

The uppermost skin layer, the *stratum corneum*, is one of the main barriers against exogenous noxae like pathogens, or chemicals. It is constructed of heavily keratinized dead corneocytes with a complex multi-layered shell surrounding them. Located in between the cells is the lipid matrix, consisting of cholesterol, free fatty acids and ceramides in an equimolar ratio, providing the main barrier. The ceramides consist of a sphingoid base and an amide bound fatty acid with varying chain and head group structure. They are the main influencing factor for the structure and function of the lipid matrix. Because the natural lipid matrix is much too complex to study, simplified model mixtures with only a very limited number of synthetic lipids, with predefined head groups and chains are used. They are mixed in defined ratios ceramides/cholesterol/free fatty acids (1/0.7/1) and are applied to a substrate by spraying. Repeated heating/cooling cycles, induce a self-assembly to a native-like multilamellar structure. The samples are analysed using neutron diffraction. As a result of the ordered multilamellar structure, the spherically scattered neutron waves interfere at defined points generating a specific diffraction pattern. From this pattern, a neutron scattering length density profile can be calculated. This profile shows the scattering properties, along the unit cell, a virtual representation of a single lamellae. This holds information on the head group, tail and water localisation, allowing a detailed assessment of the lamellar microstructure. Neutrons can also distinguish between different isotopes, making deuterium usable as a label, without largely changing the molecules properties. This way, also the molecular nanostructure can be determined. Two of the most common ceramides are [NP] and [AP]. The ceramide chains are mostly saturated C22 - 32 fatty acids and C18 sphingoid bases. Asymmetric C24/18 variants were thus chosen as most natural available ceramides. These two were combined with cholesterol, and lignoceric acid. The two ceramides in 1:2 and 2:1 ratios were shown to form a very native-like structure, despite the simplicity of the mixtures. The higher ceramide [NP] content yielded a straight chain arrangement with overlapping C24 chains, the higher [AP] content a tilted chain arrangement with less overlapping. The formed 5.45 nm phase was almost resistant to the addition of a long ceramide [EOS] analogue in an about native ratio of 10 %, except for the induction of a small lateral chain tilt. It did not led to the formation of additional phases but was simply integrated, spanning multiple layers. The exchange of the natural D-isomer of ceramide [AP] for the synthetic L-isomer disturbed the lamellar structure and led to a crystalline-like behaviour. In general the L-isomer could be shown, to behave fundamentally different and did not form a lamellar phase without the addition of ceramide [NP]. The exchange of ceramide [NP] for [NS] led to a shorter phase and better miscibility with cholesterol. Overall this study could demonstrate the importance of the two ceramides very well. A low functional redundancy between the different ceramides, despite their small chemical differences could also be shown.

1. Introduction

The skin is a very important organ for higher differentiated organisms. This is especially true for terrestrial mammals, including humans. With 1.2 - 2.3 m² for the average adult^[1], it is the largest area sensory organ. It houses multiple different receptor types, sensitive for different types of touch as well as temperature^[1,2]. It however not only receives but also sends an assortment of signals. The skin can partially show our health status and even give an emotional response by wrinkling, blushing or turning pale. By the secretion of substances from specialized glands, it can also transfer olfactory signals^[2]. The skin furthermore holds several important physiological regulatory functions. The secretion of sweat for example also has a thermoregulatory role, as have skin hair, which uphold a buffering air cushion around the body^[1,2]. The skin also regulates the body's retention of a constant moisture content, by inhibiting the loss of water through the skin or by secreting solutes and/or water through sweating^[3]. It also fulfils a metabolic role, by synthesizing vitamin D^[1]. Since this vitamin has hormone-like functions this gives the skin even an endocrine-like function^[4].

The skin furthermore represents the bodies main barrier against most exogenous noxae no matter, if they are physical like UV-radiation, biological like pathogens or chemical like penetrating substances. Especially the uppermost skin layer, the *stratum corneum* (SC), is of utmost importance for a functional skin barrier^[5]. It contains a complex multilamellar organized lipid matrix (LM) mainly consisting of ceramides (CER), cholesterol (CHOL) and free fatty acids (FFA)^[6], which upholds this barrier function^[7,8]. The skin has thus a very interesting duality. On the one hand it represents the main interface for the interaction between the organism and its environment. On the other hand it also is the main barrier, separating and protecting the organism from its surroundings. The skin is thus basically the outer border, which defines a single living being as a multicellular biological individual. Despite its important function, the barrier layer of the skin, the SC is still only poorly understood. Due to its efficient barrier function, the SC also still represents an almost impenetrable barrier for most pharmaceuticals. This massively limits the applicability of a number of possible pharmaceutical treatments. Thus far most medications have to be either ingested or injected to reach their designated target region or organ or to be spread systemically. Application through the skin in the form of creams, lotions or plasters only works in certain cases and always brings huge limitations with it, especially concerning the effective absorption through the skin without strongly disturbing the barrier^[9].

Beyond the hindrance for medical applications, there is a lack of applicable model systems. Right now there is no way to bypass animal testing for pharmaceuticals intended for dermal application, without having to deal with mayor drawbacks^[10]. Simple synthetic skin substitutes could be an effective replacement for many basic assays. Such skin substitutes, if they emulate the native skin well enough, might even be applicable as a grafts for damaged skin after injurie or surgery^[11]. Unfortunately, up to date too little is known about the detailed structure and function of the skin barrier, to reconstruct it well

enough. There are for example many skin conditions like psoriasis^[12-14] atopic dermatitis^[15-17] or lamellar ichthyosis^[18,19], which disturb the skin barrier function and are known to be a result of an altered skin structure and composition. Unfortunately, still very little is known about their exact pathophysiology. This is also halting possible treatments, since too little is known about the induced structural changes. A substantiated knowledge of the skin and especially the SC structure and function, as well as its biophysical properties would thus be most desirable, not only out of pure scientific curiosity but especially for all the above mentioned practical reasons.

Several former studies already used basic mixtures of CER together with FFAs, CHOL and sometimes small amounts of other components to generate simple model membranes, simulating the SC structure and function. These simplified model systems combined with a variety of measurement methods could be shown to be a valuable tool for understanding the lipid matrix architecture as well as its properties. With these model systems in most cases only consisting of a minimal amount of components, it is possible, to study the influence of individual constituents, conditions like temperature and hydration or ratio between different components. Especially neutron diffraction was identified to be a very powerful tool for the assessment of the influence of single components on the lamellar structure^[20-24].

This thesis mainly focused on the dependence of the multilamellar arrangement of the SC LM on the asymmetric long chain CER[NP] C24 and [AP] C24. These CERs are among the most common single species within the SC^[25,26]. They should thus have a mayor contribution to the overall structure of the LM. Neutron diffraction was utilized as a tool, to get an insight into structures induced by these CER, in simplified CER/CHOL/FFA model membranes.

A special property of neutrons is their interaction with the atomic nuclei rather than the electron shell^[27]. Because of this they can distinguish not only different elements but even different isotopes^[28]. Due to this effect it is possible, to use deuterations as a detectable tag without fundamentally changing the chemical and physical properties^[27]. By using CERs deuterated at a specific position, in this thesis mostly the terminal carbon of the long acyl chain, the molecules can be precicely located within the lamellar system. This allowed for a special focus not only on the lamellar but on the inner nanostructure of the different model systems. This can reveal a much greater amount of detail on the individual influence of each CER.

2. General Background

2.1 The Epidermis

The skin or cutis covers most of the body of any vertebrate, with for example about 1.2 to 2.3 m² for adult humans^[1]. It is comprised of two mayor layers. Below the cutis is the subcutis or hypodermis which is important for its maintenance. This layer serves mainly as an energy storage and supply route. It is housing fat cells, embedded in connective tissue

which supply dividing cells with energy rich molecules for their metabolism. The soft consistency of this cell layer also serves as a pressure cushion and helps with thermoregulation, due to its insulating effect. This layer furthermore contains larger blood vessels, which transport oxygen and other important nutrients, growth factors and immune cells to the smaller capillaries. The thick connecting neurons which collect and transfer signals from sensory neurons are also located in this layer. It furthermore contains a few sensory neurons, specialized on sensing strong pressure signals^[1,2].

The majority of sensory neurons are however located within the dermis, the lower layer of the cutis. These neurons have a variety of functions from sensing temperature over slight touch up to strong pressure. This layer can be defined as the vital and regenerative part of the cutis. It harbours the vital and dividing cells, which constantly replenish the dead cells in the epidermis (the upper layer of the cutis). It is traversed by small blood vessels and even smaller capillaries which transport and release nutrients and other important chemicals, to sustain the metabolism of these cells. These blood vessels furthermore also influence the skin's thermoregulation through either widening or contracting and thus regulating the blood flow. This layer also houses the hair follicles. From these grow the body hair, which help to maintain a protective air cushion around the body, helping to keep the body temperature constant. The hair can also serve as an additional protection against mechanical stress. The dermis also fulfils a secretory role, containing sweat and sebaceous glands. The sweat glands also support the thermoregulative role of the skin since evaporation of the sweat offers a cooling effect. The liquid however also contains a variety of volatile chemicals or their precursors which get degraded by the skin bacteria and become volatile in the process. These chemical signals can transfer a variety of information like health status, gender or receptiveness^[1,2].

The sebaceous glands secrete a film of small lipids, mainly short and intermediate fatty acids. The resulting lipid film on the skin surface has a couple of different functions. The smaller fatty acids are proposed to have a certain amount of antimicrobial function^[29]. They also are responsible for the so called acid mantle which keeps a low pH at the surface of the skin of about 4.7^[30]. By maintaining these constant conditions and feeding our natural skin flora, the sebum lipids help, to repel or kill pathogens and keep the organism healthy. The sebum also keeps the uppermost skin layer smooth and helps to retain both the water repelling and water retaining properties of the skin^[2].

The uppermost or outer skin layer is the epidermis, in contrast to the dermis it is a stiff and rigid tissue and mostly consists of highly or terminally differentiated non-dividing cells. Even though the cells are mostly inactive, the epidermis exhibits a very important function as well. It represents the organism's main barrier against most harmful environmental factors^[31]. It protects against biological hazards like pathogens, physical hazards like UV-radiation and also prevents penetration of harmful chemicals^[1]. Since it is also mostly impermeable for water, it furthermore minimizes the trans-epidermal water loss, keeping the underlying viable cells moisturized^[3]. Pigment cells or melanocytes produce melanin, which is transferred to the surrounding epidermal cells to induce protection against the

harmful influence of UV-radiation. This layer also contains some sensory cells, the Merkel cells, which play some part in fine spatial resolution of touch^[32] and special immune cells, the Langerhans cells which take up process and present antigens^[1]. Together these cells can detect skin injuries or invading pathogens and initiate an immune response to defend and repair the tissue^[1]. Figure 1 gives an overview over the skin layers and important structures located within them.

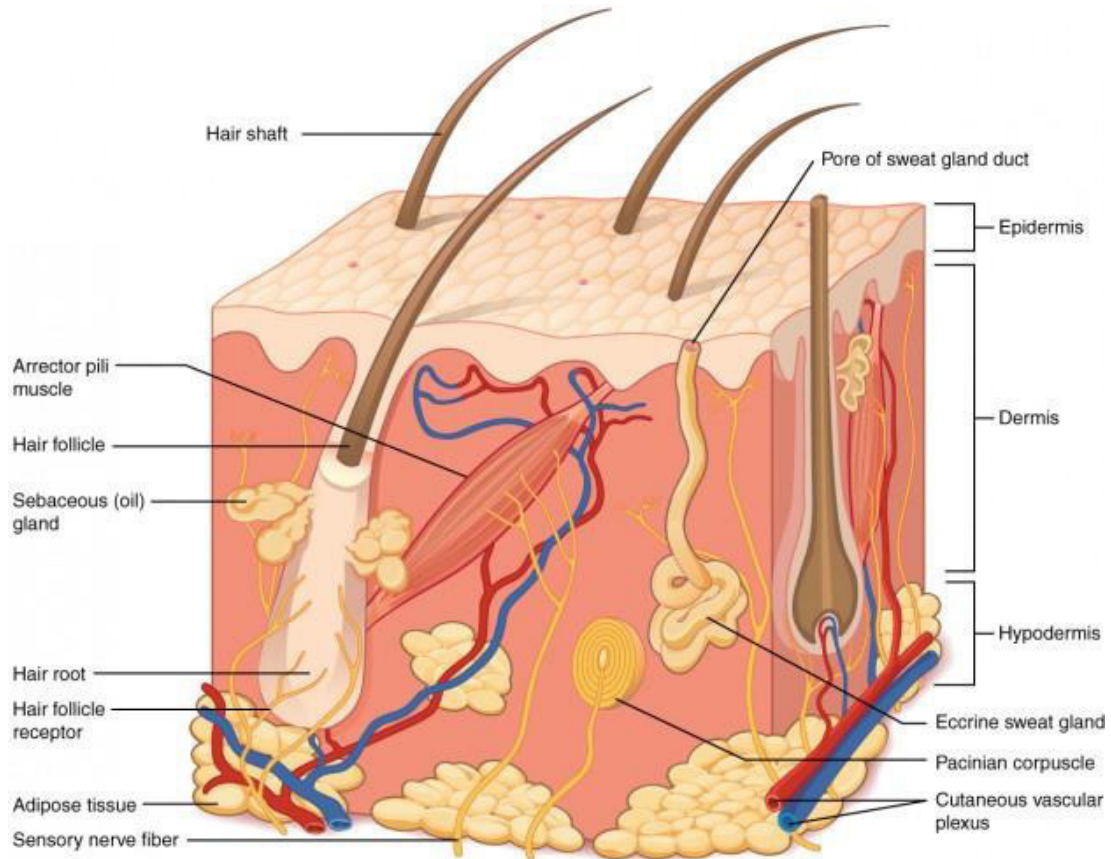


Figure 1: Overview of the skin layers and important structures located within them^[33].

For complex multicellular vertebrates the skin thus shows a variety of very important functions. Overall this organ shows an intriguing dualism, with all its sensory and expressing functions, it represents the main interface for communication between the organism and its environment on the one hand. On the other hand it represents the main barrier, separating and protecting the organism from the outside world.

2.1.1 Layer by Layer

The epidermis itself can be further subdivided into multiple layers with each of them exhibiting specific structural properties. Between the dermis and the epidermis, the basal lamina is located. This is a layer of extracellular matrix, excreted by the epithelial cells it serves as a basis for the attachment of the cells which excrete it. These cells form the *stratum basale*, a single basal layer of viable keratinocytes, which constantly divide. The cells differentiate while migrating upwards through the other layers, replenishing the non-dividing and dead cells in the upper layers. The next layer is the *stratum spinosum*. In this layer, the cells are tightly connected via desmosomes and start to differentiate. Within the

cells large amounts of keratin precursors are formed^[1]. The cells also contain membrane enclosed granules, the so called Odland bodies^[34]. These contain hydrolytic enzymes special lipids and other proteins, important for the formation of the typical structure of the uppermost layer later on^[35]. In the *stratum granulosum*, the cells differentiate into granular cells. They are more flattened and additionally to the lamellar granules, (Odland bodies) they contain keratohyalin granules. Within the *stratum lucidum*, the keratohyalin granules start to interconnect to large keratin networks, initiating the process of cornification. The lamellar bodies are excreted and release the multilamellar organized lipids into the extracellular space. After about 20 days, the originally keratinocytes reach their final stage of differentiation in the uppermost layer of the epidermis, the SC^[36]. The cells, which are transformed into corneocytes at this point are now fully cornified. Inside they have a heavily crosslinked network of keratin filaments and other proteins. At the outside, they are surrounded by the multilamellar lipids excreted from the lamellar bodies^[1]. Atop the SC only a thin undistinguished layer of dysfunctional cells and cell fragments, referred to as the *stratum disjunctum* follows. In this region, the cells have lost their integrity and function, the cell-cell connections dwindle and the damaged cells are finally desquamated on their own or due to outer physical forces^[37] (Figure 2).

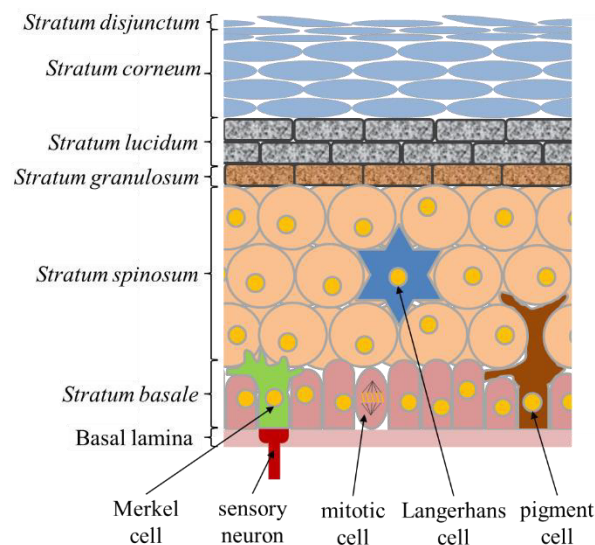


Figure 2: Schematic representation of the epidermis with its multiple layers.

The constant cycle of desquamation at the outside and division and migration from the inside leads to a complete renewal of the SC every few days. The epidermis can furthermore adapt to various environmental conditions. With increased mechanical stress for example at the palms of the hands or feet, the *stratum lucidum* as well as the SC can thicken, forming the more flexible and stable thick skin^[1].

2.1.2 The Barrier Layer

The SC, even though its cells are dead and metabolically inactive, is everything but functionless. It is a very rigid strongly interconnected tissue, with a total thickness of about 9 - 13 μm . It has a very low water content which is typically between 18 and 58 %^[38]. The SC is constructed of about 15 - 30 layers of heavily keratinised, flattened, hexagonal

corneocytes^[31,39-41]. These terminally differentiated dead cells without a nucleus are connected to each other via corneodesmosomes, a special modification of normal cell-cell connecting desmosomes. These desmosomes are mainly made up of the protein desmoplakine and are connected to the keratin network^[42]. The corneocytes do not have a regular cell membrane, instead they are enclosed by the corneocyte envelope. This mantle is constructed of three very different layers. The basal layer is the cornified envelope, which consists of a complex array of various cross-linked proteins, forming a dense continuous layer. It is connected to the keratin and gives the cells their outer shape and mechanical stability^[43]. It also serves as a basis for the next layer, the lipid envelope. This layer is formed by a special class of lipids, the very-long-chain ω -hydroxy-ceramides. These are covalently bound to the cornified-envelope-proteins. This layer is often proposed, to serve as an anchor^[44] or template for lamellar organization of the intercellular lipids^[45,46]. This third layer, the LM is occupying the space in between the cells (Figure 3).

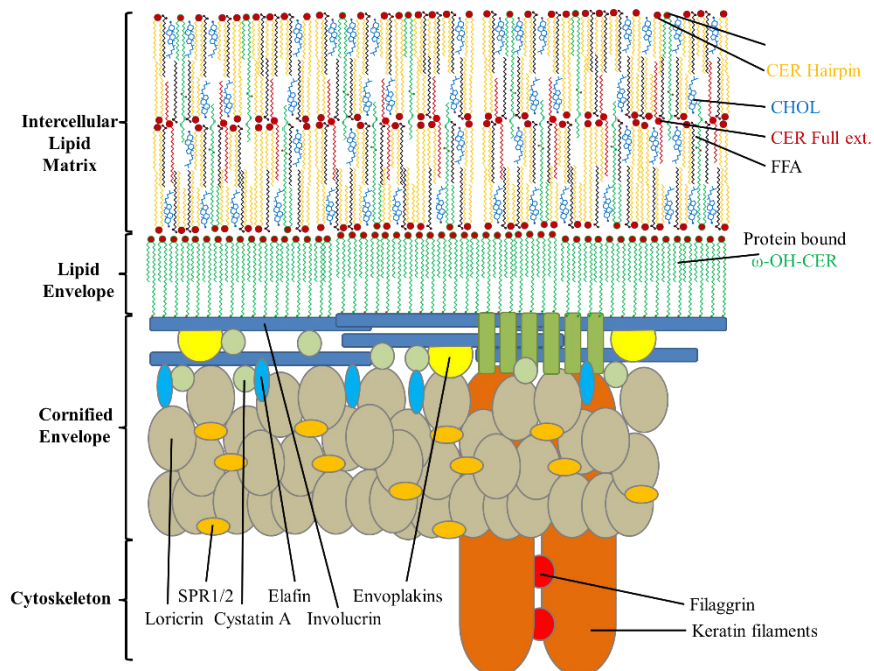


Figure 3: Schematic representation of the corneocyte envelope.

The LM is recognised as the most important structure for a proper barrier function of the skin^[41]. The cell bodies with the structures bound to it on the one hand and the LM on the other hand are generally described as a two compartment system. This general architecture is depicted by the brick and mortar model^[47]. This model pictures the corneocytes as bricks and the lipid matrix as mortar in between them. For chemicals penetrating through the SC, this architecture leaves two possibilities, not considering the trans-follicular pathway. For such, the substance moves along the hair shaft into the follicle and is thus actually penetrating in the dermal layer, not involving the SC or through the folded in SC there. The other two possible pathways however solely involve penetration through the SC. The first of these is the transcellular pathway, with the substance penetrating through the cell bodies. The second is the intercellular pathway, where the substance migrates along the cells, only through the LM surrounding them^[48]. However, independent of which of

these two pathways shows the main contribution for which substance, any substance has to pass through notable proportion of LM (Figure 4). The LM is thus the most important functional element for the SC's barrier^[49].

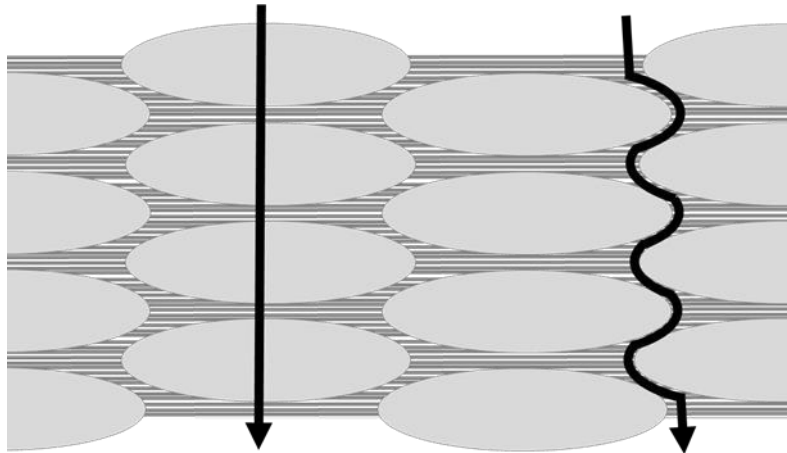


Figure 4: Penetration pathways through the SC. Intracellular (L) and intercellular (R).

2.1.3 The Matrix Lipids

Compared to other lipid systems like the cellular or nuclear membrane, the LM has a very unique composition. It mainly consists of about 46 wt% CER, 27 wt% CHOL and 27 wt% mostly long chain $\geq C_{20}$ FFA^[6,25,50,51] (see Table 1).

Table 1: Fatty acid composition within the LM^[50].

	Carbons	M [g•mol ⁻¹]	Saturated		Mono-Unsaturated	
			[wt%]	[mol%]	[wt%]	[mol%]
Pamitic acid (PA)	16	256.43	4.0	2.8	0.2	0.1
	17	270.46	0.1	0.1	0.1	0.1
Stearic acid (SA)	18	284.48	5.6	4.3	2.3	1.8
	19	298.51	0.1	0.1	<0.1	<0.1
	20	312.54	0.7	0.6	0.1	0.1
	21	326.56	0.1	0.1	<0.1	<0.1
Behenic acid (BA)	22	340.59	3.8	3.5	<0.1	<0.1
	23	354.62	2.8	2.7	<0.1	<0.1
Lignoceric acid (LA)	24	368.64	33.7	33.6	0.1	0.1
	25	382.67	8.0	8.3	0.1	0.1
Cerotic acid (CA)	26	396.70	25.2	27.1	0.1	0.1
	27	410.72	2.3	2.6	<0.1	<0.1
	28	424.75	7.1	8.2	0.1	0.1
	29	438.78	0.7	0.8	<0.1	<0.1
	30	452.81	1.0	1.2	0.2	0.2
	>30	501.89 ^{*1}	0.1	0.1	0.2	0.3
Summe			95.3	96.0	3.5	3.0
					Poly-unsaturated	
$\bar{M}_{PU}(C16 - 30)^{*2}$			~315.69*		[wt%]	[mol%]
					~1.2	~1.0

*1 Estimated assuming an equal distribution of C31 - 34

*2 Estimated assuming about the same chain length distribution as for monounsaturated FFA and two double bonds.

The molar ratio between these three major components is almost 1:1:1 with about 31 mol% CER, 33 mol% CHOL and 36 mol% FFA^[6,25,50,51]. A small amount of cholesterol sulfate (ChS) and cholesterol esters (ChE) is also present^[52]. Other lipids, including the

phospholipids, which are typically the main constituents of other biological membranes, are only found in traces^[53]. The most complex component within the LM are the CERs. This is already apparent by the fact that they are the main component mass wise, with almost double the mass of the fatty acids, even though they have a slightly lower molar ratio than the other components. This difference is a result of their architecture, basically consisting of two building blocks. One is a sphingoid base, covalently bound to this base via an amide-bond, is a fatty acid. Currently, there are 5 different known sphingoid bases with slight variations within their head groups (HGs) at positions C4 - 6. These bases according to the current CER nomenclature, are each assigned a letter identifier. The sphingosine with a C4,5 double bond (S), the phytosphingosine with a C4 hydroxy-group (P), the 6-hydroxy-sphingosine with a C6 hydroxy group and C4,5 double bond (H), the dihydrosphingosine without any C4 - 6 modifications (DS). Most recently a study claimed to have discovered yet another sphingoid base, the dihydro-dihydroxy-sphingosine abbreviated (T). This is proposed to have a C4 hydroxy group, as well as an additional one. The position of this additional group would most likely be the C6 position, since in skin CER, hydroxyl groups were not observed at any other positions so far. This could however not be verified in the original work^[51]. The bases show almost no variation in aliphatic carbon chain lengths. Most feature a length of C18 a smaller portion C20, other lengths are rare. Odd carbon numbers are almost not present for the sphingoid bases^[54-57] (Figure 5).

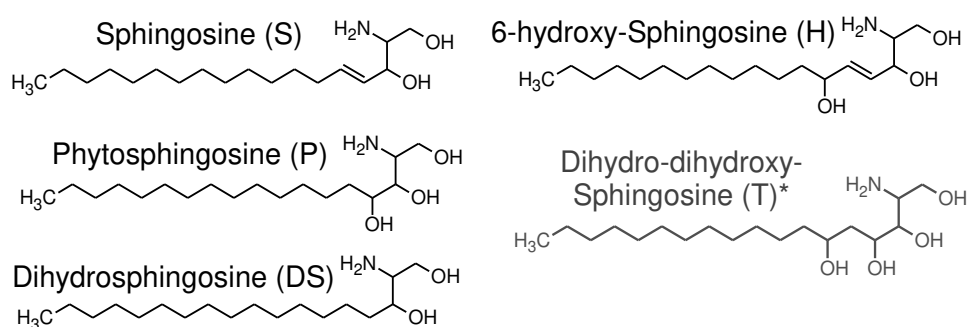


Figure 5: Chemical structure of the 5 known sphingoid bases. * For the structure of (T) an estimated structure is displayed, since in the original publication no definitive structure could be determined^[51]

The second building block, the amide-linked FAs, are quite a bit more variable, concerning their chain length and unsaturation. The majority of the bound FAs, just like the FFAs have a chain length of >20 carbon atoms with C24 being the most common^[25,51]. This makes the CER asymmetric with a longer FA than base chain. This relation also explains the content values, since they are slightly less than double the size of the fatty acids. There is also a small amount of 3.42 % mono-unsaturated and 1.63 % di-unsaturated bound FAs^[51]. Like the base-chains, the FAs can also be chemically modified. Each modification is also assigned a letter code, which for CER nomenclature is added in front of the letter code for the base. About 41.30 % of them have an additional hydroxyl group in the α -/C2 position (A), about 9.00 % of them have an additional hydroxyl group at the ω -position (terminal carbon atom) (O). This terminal OH-group is mostly esterified (EO)^[51]. In 2013 another species of CER, the 1-O-acyl-CER (OE or 1-OE) was described. This species is

esterified with another fatty acid at the hydroxyl-group at the C1 of the sphingoid base, it has thus three acyl chains, much like a triglyceride^[58,59]. These variations allow for a wide variety of combinations between different building blocks. So far the 18 different CER species depicted in Figure 6 could be isolated from human skin with a notable ratio.



Figure 6: Chemical structure of the 18 confirmed ceramides from human SC. * For the structure of the CER[NT], an estimated structure is displayed, since in the original publication no definitive structure could be determined^[51].

It could be shown, that the CER are a major contributing factor for the proper function of the penetration barrier of the skin^[5]. A small amount of age or season related as well as inter-day variation in CER composition is possible^[25,60,61]. In some cases however even slight changes in CER ratios can have enormous effects. Changed CER ratios are associated with an impaired LM structure and skin barrier function. This is the case for example in pathological skin conditions like psoriasis^[12–14], atopic dermatitis^[15–18,62,63] or different forms of ichthyosis^[18,19]. A representation of the typical CER composition of the native LM is given in Table 2.

Table 2: Overview of the ratios with which, CER are found in the LM.

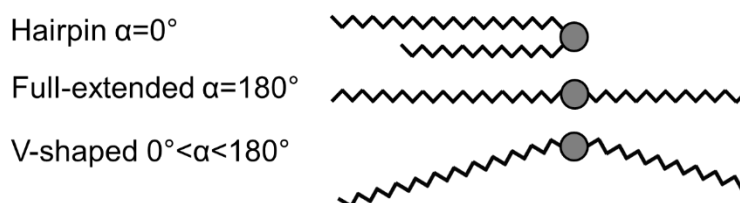
CER	$\bar{M} \left[\frac{g}{mol} \right]^{*1}$	Masukawa 2009 ^{[25]*2}		Kindt 2012 ^[51]		Smeden 2014 ^[50]		Overall ratio [mol%]
		ratio [wt%]	ratio [mol%]	ratio [wt%]	ratio [mol%]	ratio [wt%]	ratio [wt%]	
NS	677.69	6.35	5.95	7.44	7.96	6.8	6.35	5.95
NP	695.70	21.31	20.48	22.10	23.04	26.19	21.31	20.48
NH	693.69	22.58	21.64	14.51	15.17	12.59	22.58	21.64
NDS	679.70	5.95	5.59	9.83	10.49	8.73	5.95	5.59
AS	693.69	3.56	3.41	9.58	10.02	3.86	3.56	3.41
AP	711.70	16.11	15.84	8.78	8.95	13.6	16.11	15.84
AH	709.69	15.73	15.42	10.77	11.01	12.59	15.73	15.42
ADS	677.69	0.82	0.76	1.63	1.74	1.93	0.82	0.76
EOS	1025.98	4.28	6.07	6.48	4.58	5.48	4.28	6.07
EOP	1043.99	0.86	1.23	1.14	0.79	2.74	0.86	1.23
EOH	1041.98	2.5	3.60	4.26	2.97	5.48	2.5	3.60
EODS ^{*3}	1027.99	---	---	0.40	0.28	---	---	---
OS ^{*3}	775.56	---	---	0.73	0.68	---	---	---
OP ^{*3}	793.57	---	---	0.17	0.16	---	---	---
OH ^{*3}	791.55	---	---	0.43	0.39	---	---	---
NT ^{*3}	711.70	---	---	1.73	1.76	---	---	---

*1 Molar masses were estimated as average 24 - 28 carbons for the fatty acid except for [EO]-CER where 28 to 34 carbons and a C18 di-unsaturated ω -acyl-chain were assumed and 18 carbons for the base

*2 Including both datasets which are shown separately in the original work.

*3 Ratios may not necessarily be representative, since only one studies did analyse these components

It was proposed, that the CER are the main determining factor for the overall lipid matrix structure^[64]. Their long alkyl-chains are very rigid and form highly ordered lamellar systems. However, the variability in the layout of the two chains leads to the possibility of three different basic conformations and as a result different lamellar arrangements. The conformation is dependent on the chain tilt angle α . CER can assume either a hairpin conformation with $\alpha = 0^\circ$ (both chains parallel) the fully extended conformation with $\alpha = 180^\circ$ (both chains directly opposite to each other) or a V-shaped conformation with an angle of $0^\circ < \alpha < 180^\circ$ ^[65,66] (Figure 7).

**Figure 7:** Three basic CER chain conformations depending on the chain tilt angle α .

Depending on the composition and interactions between the CER and the other lipids, the LM can also have a different lateral packing. Generally either a dense orthorhombic chain packing or a slightly less dense hexagonal packing are observed^[67] (Figure 8).

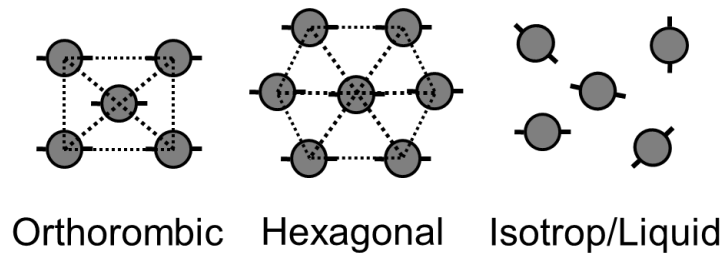


Figure 8: Lateral chain packing of CER in the SC lipid matrix.

The difference in acyl-chain length mainly between C16-18 and >C20 carbon atoms however, was mostly cast aside so far. However, this difference can show an important influence on the LMs lamellar structure. For the C16-18 CER the chain lengths of both the amide bound FA and the sphingoid base are about equal, since most sphingoid bases consists of about 18 carbon atoms with one arranged higher up in the HG. The resulting CER molecules are thus symmetric. For the >C20 CER which represent the main proportion of SC CER however^[25,26], the difference in chain lengths leads to an asymmetrical build. A 2012 study proposed a very important function for these asymmetric C24 CER. This study used a special combination of applications, a very high magnification cryo-electron microscopy (-eM) of vitreous skin sections, combined with defocus series, molecular modelling, and eM simulations. It was found that reconstructed almost native SC shows a very specific electron density band pattern. Using eM simulation it was concluded, that the spacing as well as electron density distribution of this pattern most likely hint towards an arrangement of stacked layers of fully extended CER molecules. The long amide bound fatty acid chain at one side of the lamellae would be associated with the long chain FFAs and opposed by the short sphingoid base chain associated with the CHOL molecules, forming asymmetric monolayers^[66]. This preference in interaction was already observed in previous studies^[68]. Other studies also discussed a possible important function for this asymmetric build. Due to this asymmetry, the longer bound FA chains would be able to overlap in the lamellar mid-plane. In this middle layer a lower chain density would be expected. This would allow for a higher chain mobility and thus a much more fluid phase behaviour than for the outer lamellar regions^[69-71]. This liquid-like layer could have various important functions including for example stability against sheer-stress or compression.

2.1.4 Asymmetric Long-Chain Ceramide [NP] and [AP]

2.1.4.1 CER[NP]

As shown above, the CER[NH] with 21.64 mol% of the total CER is the overall most abundant CER within the LM. It is followed by the CER[NP] with 20.48 mol%, [AP] with 15.84 mol% and [AH] with 15.42 mol%. These four CER would thus be the most interesting to study, since their impact on the native LM can be expected to be most substantial. However, no synthetic CER[NH] and [AH] were available. For this reason, the two phytoshngosine type CER[NP] and [AP] are currently the most attractive targets for

research on the lamellar matrix. This is especially true, since most studies so far focused on the sphingosine based CER, especially on the CER[NS], even though it only has a content of about 5.95 %. For that reason much is already known about the sphingosine CER but not much is known about phytoshingosine CER, especially not about the asymmetric long chain variants. The phytoshingosine CER in comparison are more polar, without the double bond and with an additional hydroxyl-functionality in their HG. In general, they show a much stronger HG interaction, but typically a poorer, hexagonal chain packing, in contrast to the sphingosine type CER with a mostly orthorhombic chain packing^[72–74]. As mentioned above, most of the biophysical studies on ceramides that were conducted up to now, focused on short chain C18 CER. Long chain C24 CER, even though they are far more abundant in the SC, were used only in very few studies, or more recently as part of complex CER mixtures^[69], not allowing the assessment of the influence of the individual CER.

The CER[NP] is constructed from a phytosphingosine base and a non-hydroxylated FA chain. The phytosphingosine HG has no double bond but a C4-OH group. For crystalline CER[NP] C18 and mono- and di-unsaturated 18:1 and 18:2 variants of it were investigated and shown to be polymorphic, strongly depending on the crystallization conditions. Various different properties were reported for the different crystalline phases. The influence of hydration ranged from non-existent to a strong influence on the lamellar thickness. The thickness varied from 3.57-8 nm with mono- as well as bilayer arrangements. For temperatures of 32-37 °C often some phases disappeared^[75–81]. For the unsaturated variants, the fluidity was enhanced^[78,81–83]. Also a CER[NP] C18 monolayer arrangement was investigated and showed a notably less dense chain packing than the compared sphingosine CER^[84]. One study also investigated the C24 crystalline CER[NP]. Six different crystalline modifications were found, with five of them being stacked monolayer systems with either fully extended or V-shaped chains. One crystal state was a bilayer with a hairpin conformation. Due to the chain asymmetry, the longer C24 chains were overlapping in the lamellar mid-plane^[85,86]. In simple CER[NP] C18/CHOL/FFA mixtures often partial phase separation was reported. One of the phases did not absorb any water. However this effect could be partially avoided by heating to skin temperature^[87,88]. For the CER[NP] C24 in a simple mixture with CHOL and palmitic acid (PA) no phase separation was reported^[89]. For a mixture with CHOL and LA on the other hand, besides the main phase with proposedly hairpin folded CER, a second phase was observed. This phase with proposedly V-shaped CER showed absolutely no water uptake. Both phases showed a mainly crystalline-like phase behaviour^[21]. Many of the features of these additional phases resemble that of pure crystalline CER[NP] as discussed above and are thus most likely phase separated [NP]. Using a molecular modelling approach, for the C16 CER[NP] it was concluded, that the C4 OH redirects the C2 OH to a horizontal instead of a perpendicular position as seen for the [NS]. This strengthens the in-plane H-bonding properties but inhibits any intra-lamellar H-bonding, as reported for the [NS]^[90–92].

2.1.4.2 CER[AP]

The CER[AP] differs from the [NP] only by a single OH-group at the bound FA α /C2-position^[92]. However, this small chemical difference yields a variety of distinct properties. The first is a D/L (R/S)-isomerism at this additional optical centre. Although naturally only the D-isomer is found, by chemically synthesizing the [AP], also the L-isomer was obtained. In fact so far all studies investigating model systems with synthetic CER[AP] used a racemic mixture of both isomers (RacCER[AP]). The isomers can however be separated, using thin layer chromatography, which was done for this thesis. Studying crystalline CER[AP] C18, for the L-Isomer three and for the D-Isomer two crystalline states could be shown. All states exhibited a lamellar crystalline structure with different lamellar periodicities. Neither the addition nor the freezing of water altered the lamellar repeat distance, showing that no water is located in between the lamellar sheets^[23]. For the L-Isomer an increase in lamellar spacing could be observed with rising temperature, suggesting a V-shaped conformation. In contrast to this, for the D-isomer, the lamellar repeat distance was noticeably larger, at low temperatures, suggesting a full extended conformation^[93]. The D-CER[AP] showed a strong H-bonding network, hexagonal chain packing and a slightly higher permeability for water, than the [NP]^[76]. In a monolayer, the D-CER[AP] C18 has a Less tight chain packing than the [NS] but about the same as [NP]^[84]. For CER[AP] several mixtures were investigated before. It could be shown, that the CER[AP] C18 shows a strong influence on the lamellar structure with a minimal water content. It is almost uninfluenced by several factors like different chain length of the FFAs, ranging from C16 to C26, presence of ChS or the much longer C30+16 CER[EOS]. The additional lipids were simply force-fitted into the arrangement or partially phase separated if the miscibility was too low^[64,94,95]. Even the well-studied penetration enhancer Isopropyl myristate could hardly influence the CER[AP] based structure as it was simply excluded into a separate isotropic phase^[20]. Together with the CER[AH], the [AP] HG has the most OH-groups (not considering possible [NT] or [AT]) which possibly can explain this strong influence on the lamellar structure attributable to the resulting high H-bonding potential.

2.1.5 The Very Long ω -Hydroxy-Ceramides

The ω -hydroxy FAs are typically very long \geq C27, if bound to a sphingoid base, they form the very long ω -hydroxy CER. These CER are also the ones forming the lipid envelope. In this structure, their ω -hydroxy-group is covalently bound to the cornified-envelope-protein-structure. As mentioned above, in LM lipids in most cases, this ω -hydroxy group is esterified with an additional fatty acid. Typically, the additional fatty acid has between 16 and 20 carbon atoms and is at least mono- or poly-unsaturated. The most common variants are di-unsaturated, especially the linoleic acid. Furthermore, only very few uneven ω -OH-FAs are found^[96]. This group of CER includes the CER[EOS] which is the most abundant^[25] and most studied, the [EOP] which was only used in a couple of studies so far and the [EOH] and [EODS] which were so far not investigate at all. The natural ratio of ω -hydroxy-CER to total CER is about 4.6-9.6 %, with the CER[EOS] being the most

common with an [EOS] to total CER ratio of 2.9-4.6 %^[25,50,51]. These CER, because of their unique structure are discussed, to serve several important purposes. Their possibly most important and definitely most discussed function is their potential to form a special phase arrangement, the long periodicity phase (LPP). This phase will be discussed in detail below^[97]. Only these long CER are able to form this special structure and especially the CER[EOS] is thought to be a prerequisite for its formation^[98]. However, it was shown that also other ω -hydroxy-CER can form it under certain conditions^[97,99,100]. Another proposed function of the very long ω -hydroxy-CER is to crosslink multiple lamellar leaflets, stabilizing the lamellar structure^[95,101]. The unique structure of the LPP especially the unsaturated ω -hydroxy-FAs are also proposed, to be a main contributing factor for the LPPs nanostructure, which will be explained in more detail below.

2.1.6 The Molecular Nanostructure of the Lipid Matrix

2.1.6.1 The Lamellar Structure

Macroscopically, the LM was shown to feature a multilamellar arrangement. This lamellar organisation was first observed in 1973 by freeze-fracture-eM^[102]. The most frequently observed lamellar patterns were 3, 6 or 9 stacked lamellae^[103]. In the later seventies, RuO₄ staining made it possible to observe not only the contrast rich HG regions but also the normally invisible tail regions within the electron micrographs. This led to the discovery of the lamellae, being arranged approximately parallel to the cell surface^[104-108]. At room temperature, an organized dens orthorhombic lipid chain packing was shown. At higher temperatures of 32 °C, which is about the natural skin temperature, the organisation changes to a slightly less dense hexagonal chain packing^[109]. However the native skin is much too complex, to obtain any detailed information on the influence of single lipid species. It is also very difficult to gain any detailed information on the complex LM nanostructure, underlying the macroscopic lamellar arrangement. Because of this newer studies started focusing more and more on model system approaches, containing isolated lipid species. These had however still mixed chain length as well as impurities like other lipids, mainly other CER^[110,111]. Since this left many results open for speculation, the current method is to use defined simplified mixtures with only few synthetic single lipid species with defined acyl chains and HG^[8]. The simplicity of these mixtures allows to gain specific information on the underlying nanostructure of a given system and consequently the biophysical properties of single lipid species and even variants. This makes it possible to learn about the complex native LM step by step and reconstruct its detailed structure and function. Some experiments also use slightly more complex mixtures, to determine the influence of certain lipid fractions, lipid ratios or to learn more about macroscopic interactions and the barrier function in general^[69]. These experiments are equally important to learn about macroscopic effects, but aren't able to extract nearly as much detail.

2.1.6.2 The Short Periodicity Phase

The short periodicity phase (SPP) describes the basic structure found in the SC LM. It is an array of multiple stacked typically 5 - 6 nm thick lamellae^[104]. However, eM experiments also found, that not all lamellae have the same thickness, observing for example 4.5, 5 but also 6.5 nm arrangements side by side^[66]. This could have two possible reasons. The CER could be unevenly distributed, with shorter symmetric C16-18 CER forming lamellae with 4 - 4.5 nm and longer >C20 CER forming lamellae with 5 - 6.5 nm. This could very well be possible, since short symmetric and long asymmetric CER show different mixing behaviours^[112,113]. The other possibility would be an asymmetric nanostructure consisting of stacked monolayers of fully extended CER with the short and the long chains of the mostly asymmetric CER arranged in different bilayers^[66]. However, at the current state it is still unclear, which conformation is found within the native LM. At least most model systems hint towards the preference for the CER to form a hairpin folded arrangement^[69,114-116]. Model systems using short chain symmetric C16 - C18 CER showed a centrosymmetric arrangement with a typical thickness of about 4 - 4.5 nm. Their chains are highly ordered and their terminal CH₃-groups are all located in the same plane^[95,115,116]. CHOL was also determined to be distributed symmetrically, with its OH-Group slightly inward from the CER HG-region^[115]. The FFAs are arranged alongside their acyl-chains^[95]. Preferentially chains with about the same length are associating with each other^[113]. The high rigidity of these symmetric CER often led to low miscibility with other lipids and the formation of laterally separated FFA and CER-rich domains^[117]. However short chain CER are by far the minority within the native SC and a high ratio of them can even negatively influence the barrier function as observed for some skin conditions^[118]. For asymmetric long chain CER with >C20 acyl-chains, the observed nanostructure is very different in many aspects. The CHOL is distributed about the same as in the shorter system^[114]. However, the long chain FFAs and long CER-acyl chains were shown to promote a region in the lamellar mid-plane, where these chains overlap as mentioned above^[69,70,114]. This area containing the less tightly arranged overhangs has different fluidity and solubility properties than the rest of the lamellae. This could proposedly have an important influence on the barrier function as well as the LMs mechanical stability^[70]. This system thus shows an arrangement consisting of several layers with different rigidity and different solubility properties, the rigid polar HG, the rigid non-polar tail region and the more fluid non-polar middle layer. The asymmetry of the molecule reduces its rigidity and due to the association of long FFAs together with long acyl-chains and short FFAs and CHOL together with the shorter acyl chains, the miscibility is enhanced and lateral domain formation is reduced^[112,113].

2.1.6.3 The Long Periodicity Phase

With the RuO₄ staining method as described above, it became possible for the first time, to visualize the tail regions and observe differences within these regions. This led to the discovery of the 12 - 14 nm thick LPP since its main difference to the SPP is the tail arrangement^[104,119,120]. An analogue long phase was also reported for porcine^[121] and murine

skin^[122]. However, even less is known about its detailed structure than for the SPP and it is heavily discussed. Some even argue it to be nothing but an experimental artefact. Originally, in the stained electron micrographs, a 5 - 3 - 5 nm pattern of electron dense (HG) and electron lucent bands (acyl chains) was described^[104,123]. A different study however rather claimed a uniform 4.3 - 4.3 - 4.3 nm stacked SPP-like arrangement^[101]. Integration of CER[EOS] into the 4 - 4.5 nm SPP was observed before^[116,124]. The Observations of the LPP in this case is attributed solely to the properties of the RuO₄ which preferentially stains the unsaturated linoleic acid moieties found in the middle layer, falsely indicating the arrangement^[125]. A uniform arrangement was also supported by observations made using cryo-eM^[126]. However, a variety of other studies also observed similar long 12 - 13 nm long phase arrangements, using for example X-ray or neutron diffraction which are not dependent on staining to determine the length of a lamellar phase^[99,110,111,127-133]. This makes it harder to simply dismiss the LPP as nothing but an experimental artefact caused by a certain staining method. However, there is also a valid complaint about the significance of these results, since almost all studies used an amount of ω -esterified CER far greater than the natural maximum of about 10 mol%. This could possibly have artificially induced the formation of these longer phase arrangements. So far no study was able to induce the formation of a native-like LPP using only a native ratio of about 10 % ω -esterified CER. Since so many studies observed an LPP, sometimes with only a slightly higher than native amount of ω -esterified CER for example 15 %^[97], it is most likely that the LPP is not a mere experimental artefact. However more complex conditions than simply the presence or absence of the ω -esterified CER seem to be relevant. The oldest and most well-known model describing the LPP nanostructure is the sandwich model. This model describes the LPP with two thicker rigid outer bilayers, where the long chains of the ω -hydroxy-CER, the FFAs and other CER are located. Within the thinner middle layer, the unsaturated ω -FAs, the CHOL and short and unsaturated FFAs are found in a single layer^[134-137]. Contrary to that, using neutron diffraction a recent study observed an arrangement with three about uniform layers. While the outer layers are still constructed of the very long chains of the ω -esterified CER, the middle layer in this arrangement in contrast to the sandwich model mainly contains rigid CER and FFAs. It is thus not to be assumed, to have any fluid properties as proposed for the sandwich model^[138]. A follow-up study on this system determined the positions of water, CHOL and the ω -FAs within this system. Water in this system was not only found within the outer but also within the inner ω -HG-regions. The water content however was much less than within the outer HG-region which is to be expected, since the inner regions are largely constructed from less polar acyl groups. The omega-acyl chains of the CER[EOS] were found slightly outward from the lamellar centre. The CHOL was found slightly outward from the ω -HGs with the CHOLs OH in direct proximity to them. This arrangement would allow for H-bonding of the CHOL OH with the ω -HGs^[139]. At this point it is not completely clear, which arrangement if any of the observed ones are really corresponds to the native LPP. So far the influence of other CER species than the [EOS] itself on the LPP nanostructure was not also investigated much.

3. Materials and Methods

3.1 Materials

Table 3: Used Chemicals

Solvents	Source	Purity
Chloroform	Sigma-Aldrich Chemie GmbH (München), Ger.	≥99.9 %
Methanol	Sigma-Aldrich Chemie GmbH (München), Ger.	≥99.9 %
Salts		
K ₂ SO ₄	Sigma-Aldrich Chemie GmbH (München), Ger.	≥99 %
NaBr	Sigma-Aldrich Chemie GmbH (München), Ger.	≥99 %
Ceramides		
[NS] C18; N-(Stearoyl)-sphingosine	Synthesis* ¹	≥95 %
[NS] C18-D ₃ ; N-18,18,18-D ₃ -(Stearoyl)-sphingosine	Synthesis* ¹	≥95 %
[NS] C24; N-(Tetracosanoyl)-phytosphingosine	Synthesis* ¹	≥95 %
[NS] C24-D ₃ ; N-24,24,24-D ₃ -(Tetracosanoyl)-phytosphingosine	Evonik Goldschmidt AG (Essen)/ Synthesis* ¹	≥95 %
[NP] C18; N-(Stearoyl)-phytosphingosine	Evonik Goldschmidt AG (Essen)/ Synthesis* ¹	≥95 %
[NP] C18-D ₃ ; N-18,18,18-D ₃ -(Stearoyl)-phytosphingosine	Synthesis* ¹	≥95 %
[NP] C24; N-(Tetracosanoyl)-phytosphingosine	Synthesis* ¹	≥95 %
[NP] C24-D ₃ ; N-24,24,24-D ₃ -(Tetracosanoyl)-phytosphingosine	Synthesis* ¹	≥95 %
D-[AP]; N-(D-α-Hydroxytetracosanoyl)-phytosphingosine	Synthesis* ¹	≥95 %
D-[AP]-D ₃ ; N-24,24,24-D ₃ -(D-α-hydroxytetracosanoyl)-phytosphingosine	Synthesis* ¹	≥95 %
L-[AP]; N-(L-α-Hydroxytetracosanoyl)-phytosphingosine	Synthesis* ¹	≥95 %
L-[AP]-D ₃ ; N-24,24,24-D ₃ -(L-α-Hydroxytetracosanoyl)-phytosphingosine	Synthesis* ¹	≥95 %
[EOS]-br; N-(30-(10-Methyl-hexadecanoxy)-tricontanoyl)-sphingosine	Synthesis* ¹	≥95 %
[EOS]-br-D ₃ ; N-(30-(10-Methyl-16,16,16-D ₃ -hexadecanoxy)-tricontanoyl)-sphingosine	Synthesis* ¹	≥95 %
[EOS]-D ₃ -br; N-(30-(10-D ₃ -Methyl-hexadecanoxy)-tricontanoyl)-sphingosine	Synthesis* ¹	≥95 %
Other Lipids		
Stearic acid (Hexadecanoic acid) C18	Sigma-Aldrich Chemie GmbH (München), Ger.	≥99 %
Lignoceric acid (Tetracosanoic acid) C24	Sigma-Aldrich Chemie GmbH (München), Ger.	≥99 %
Cholesterol	Sigma-Aldrich Chemie GmbH (München), Ger.	≥99 %

*1: These substances were kindly provided by the group of Prof. Bodo Dobner from the department of Biochemical Pharmacy of the MLU-Halle-Wittenberg which synthesized and purified them.

Table 4: Used Instruments and Utensils

Description	Manufacturer
HANSA 281 gravity feed airbrush (Nozzle: 0.2 mm)	Harder & Steenbeck, Norderstedt, Ger.
Olympus microscope BH2 with modules:	Olympus Deutschland GmbH (Hamburg) Ger.
<ul style="list-style-type: none"> • MTV-3 Camera, MA-2 Shutter system, TGH power source • Objectives IC 20, ZEISS 40 mm 	
X-ray powder diffractometer Bragg-Brenanto D8	Bruker AXS GmbH (Karlsruhe), Ger.
Membrane Diffractometer V1:	Helmholtz-Zentrum (Berlin), Ger.
<ul style="list-style-type: none"> • Neutron cold source: H₂ • Collimation: $\alpha_0 = 1^\circ$ at 0.45 nm (result of ⁵⁸Ni-neutron guide) • α_1: defined by two slit systems 	
Monochromator:	
<ul style="list-style-type: none"> • Highly ordered poyrolytic graphite (002), vertically focusing • N₂ cooled Be-Filter • Wave length: $\lambda = 4\text{-}6 \text{ \AA}$ • Flux: $1 \times 10^7 \text{ n}\cdot\text{cm}^{-2}\cdot\text{s}^{-1}$ • Range of scattering angles: $-10^\circ < 2\Theta > 120^\circ$ • Take off angle: $2\Theta_M = 60^\circ\text{-}120^\circ$ (not alterable during experiment) • Sample distance: 0.8 m - 1.5 m (extendable) 	
Detector:	
<ul style="list-style-type: none"> • ³He, 19 x 19 cm², Pixel size: 1.5 x 1.5 mm² (Height and inclination adjustable) • Sample-to-detector distance: 0.8 m-2.0 m 	
Sample environment:	
<ul style="list-style-type: none"> • Aluminium containers with humidity and temperature control (Humidity control via saturated salt solutions) • Software: CARESS 	
Small-angle diffraction instrument D16	Institut-Laue-Langevin (Grenoble), France
<ul style="list-style-type: none"> • Neutron cold source: H₂ • Neutron guide: 120 x 60 mm² 	
Mnonochromator:	
<ul style="list-style-type: none"> • 7 vertically bending Pyrolytic graphite (002), + N₂ cooled mosaic crystals $d=3.355 \text{ \AA}$ • Area per element: 17 x 80 mm² • Total area: 122 x 60 mm² • Aavelength 4.55 Å, 7.5 Å, 5.6 Å and 9 Å (cut-off 3.95 Å) • Distance to Sample: 2.8 m 	
Be-filter	
<ul style="list-style-type: none"> • Mosaicity: 0.7° • Path length: 100 mm • Efficiency: $\lambda/2 < 0.1 \%$ 	
Slits:	
<ul style="list-style-type: none"> • S1 (Monochromator) max. 150 x 40 mm² • S2 (sample) max. 150 x 40 mm² 	
Sample	
<ul style="list-style-type: none"> • Max flux at sample: $107\text{cm}^{-2}\cdot\text{s}^{-1}$, 7 x 7 mm² • Sample rotation (ω): $-180^\circ \dots +180^\circ \pm 0.002^\circ$, ($\varphi$): $-180^\circ \dots +180^\circ$, • ($\chi$): $-180^\circ \dots +180^\circ$ • Aluminium containers with humidity and temperature control (humidity control via reservoir temperature) 	
³ He detector (MILAND)	
<ul style="list-style-type: none"> • Distance to sample: 0.3 to 1.0 m • detector rotation (2Θ) $-5^\circ \dots +130^\circ \pm 0.01^\circ$ • Area: 320 x 320 mm² • Resolution (pixel size): 1x1 mm² • Max. counting rate 100 kHz (less than 1% dead time) 	

Table 5: Used software

Name	Version	Programmer/Organisation
Igor Pro	6.3.7.2	Wavemetrics
• HFIT	3.4	Thomas Hauss (Helmholtz-Zentrum, Berlin, Ger)
• mmPanel	0.8	
LAMP	8.5	D. Richard, M. Ferrand, G. J. Kearley (Institute-Laue-Langevin, Grenoble, France)
Alpha	2.3	Thomas Hauss (Helmholtz-Zentrum, Berlin, Ger)
Omega	0.99d	Thomas Hauss (Helmholtz-Zentrum, Berlin, Ger)

3.2 Sample Preparation

For the experiments performed for this thesis, CER/CHOL/FFA model systems with a 1/0.7/1 molar ratio were prepared. Each Lipid component was prepared in a sufficient amount to produce 1500 μL of lipid solution with a concentration of $10 \text{ mg}\cdot\text{ml}^{-1}$. For components with low solubility, the concentration was lowered to $5 \text{ mg}\cdot\text{ml}^{-1}$, adapting the total volume of the solution accordingly. Each Lipid was solved individually with a mixture of chloroform and methanol in a ratio of 2:1 in glass tubes with a lid. Defined volumes of each individual solution were combined, to achieve the desired ratio for each component. For each lipid mixture, a 60 mm x 15 mm x 0.05 mm quartz-glass slide (Spectrosil® 2000, Saint-Gobain, Wiesbaden, Germany) was preheated to a temperature between 70 and 85 °C, depending on the mixture of lipid components (higher temperatures for shorter CER). The slides were kept at the individual temperature while the sample was sprayed onto to the surface, using an airbrush instrument, under a fume cupboard. During this process, the solvent mixture quickly evaporated, leaving the lipids behind as a thin solid film. To remove all possible remnants of the solvent mixture, the samples were dried overnight under vacuum in a desiccator. To induce the formation of a native-like multilamellar lipid structure, the dried samples were annealed. This was performed by repeated cycles of heating to a temperature about 5 °C below the spraying temperature, at high humidity, generated by a small water reservoir inside a closed Petri dish. The heating was always followed by cooling at room temperature (RT) and ambient conditions. For long chain systems 2 h $\vartheta\uparrow$, 1 h RT 1 h $\vartheta\uparrow$, for short chain systems 1 h $\vartheta\uparrow$, 1 h RT, 30 min $\vartheta\uparrow$, 30 min RT, 30 min $\vartheta\uparrow$, 30 min RT, 15 min $\vartheta\uparrow$. A detailed table showing the composition of each sample as well as the individual spraying and annealing temperatures are given under results for each experiment individually. With this method, due to the spraying by hand, common sample thicknesses can only be estimated with about 5 - 10 μm and between 1000 and 1500 bilayers. This preparation method is modified according to Seul et al.^[140].

3.3 Neutron Diffraction Experiments

3.3.1 General Principles of Neutron Diffraction

Neutron diffraction describes the process of neutrons being coherently scattered by a medium with a well ordered structure, like a crystal or a lamellar system. Because of this order, the sum of the scattering can yield a defined diffraction pattern, which can be recorded. This method can be used as a tool for a wide variety of different applications, including non-invasive probing, structural and even structure dynamics investigations^[27]. Scattering is a physical process, which as a result of a wave hitting a target generates a spherically scattered wave around the scattering centre. This scattering can be either coherent or incoherent, depending on the scattering properties of each individual scattering centre. For neutrons these scatterings centres are the atomic nuclei with which they interact. This property is described as the scattering length and is an intrinsic and non-systematic property of each individual element/isotope. For some elements/isotopes, resonance effects can lead to a 180° phase shift of the incoming neutron wave, due to the formation of a transition state, leading to a negative coherent scattering length. In a complex system, with more than one scattering centre close enough to each other, basically forming a grid, these scattered waves interfere with each other. This interference can occur in several different ways. For two completely coherent waves, which are in phase and spread in the same direction, the interference is constructive. This results in the summation of the amplitudes, leading to a higher total amplitude. If the phase is shifted by exactly half of the wavelength, a destructive interference takes place, reducing the amplitude of the wave. If both waves have the same amplitude, the total amplitude becomes zero^[141]. If the waves are not completely in phase, have a different wavelength or spread in different directions, the interference is partially destructive, partially reducing the total amplitude (Figure 9).

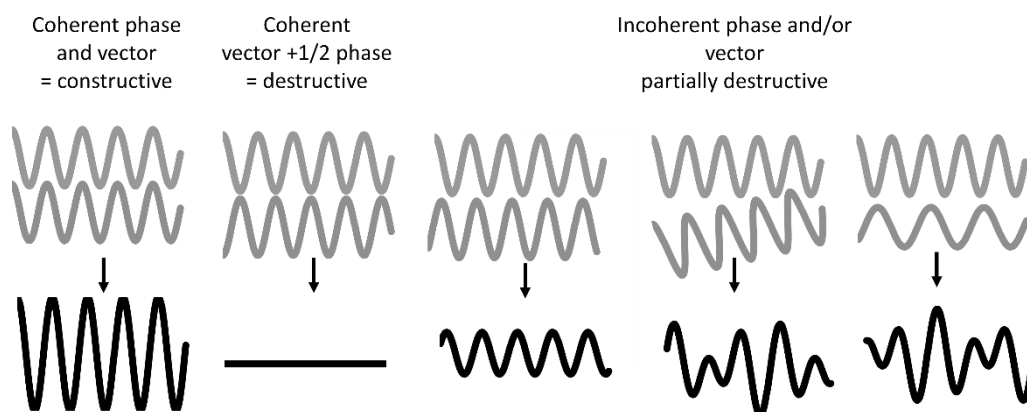


Figure 9: Different cases of interference of two waves.

The interference of multiple waves depends on the scattering properties of the target structure (size, shape, topology, etc.). In complex systems without an ordered structure, the individual scattering centres are distributed randomly and the mean of the total amplitude becomes about zero, since for many incoherently interfering waves, the overall

interaction is destructive. For ordered systems, the waves are consistently scattered, resulting in specific waves always interfering at the same position. The result is a specific combination of local maxima and minima, the diffraction pattern. This pattern is dependent on the position of each scattering centre relative to the incoming wave^[27]. The observed pattern is thus an indication for the structure of the system (Figure 10).

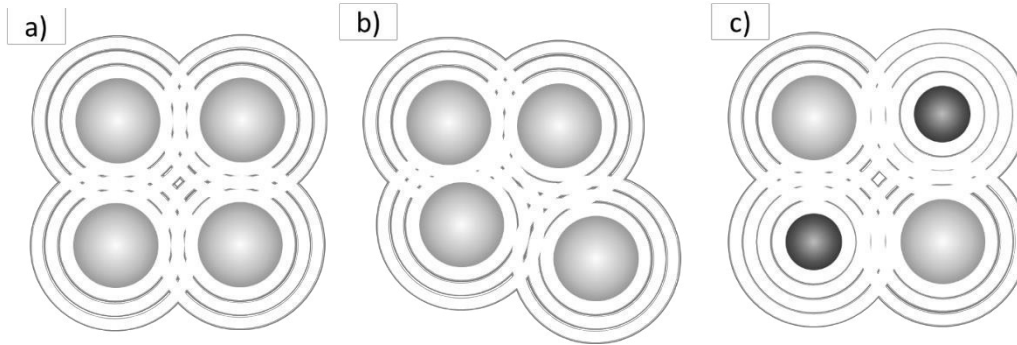


Figure 10: Diffraction in different complex systems. a: Homogenous highly ordered system. b: Homogenous disordered/partially ordered system. c: Inhomogeneous highly orders system

3.3.2 Diffraction in Ordered Multilamellar Systems

Besides the samples characteristics, the neutron wavelength influences the appearance of the diffraction pattern. The neutron wavelength is defined as:

$$\text{EqI: } \lambda_n = \frac{h}{\vec{p}_n} = \frac{h}{m_n \cdot \vec{v}_n}$$

h : Plancks constant, \vec{p}_n : Neutron momentum vector, m_n : Neutron mass and \vec{v}_n : Neutron velocity vector. As explained above, the wavelength can be exactly predetermined by cooling the neutrons to about the desired wavelength and filtering the exact one using a monochromator and a suitable filter medium for secondary harmonic wavelength. For diffraction experiments cold neutrons with a wavelength range of 2 - 30 Å and an energy of 0-0,025 eV are used. The energy of the neutron is dependent on its momentum, with the neutrons momentum vector being defined as:

$$\text{EqII: } \vec{p}_n = \hbar \cdot \vec{k}$$

With the reduced Plancks constant $\hbar = h:2\pi$, and $\vec{p}_n = h:\lambda_n$ as shown in Eq I, the absolute value of the neutron wave vector \vec{k} can be calculated from the predefined neutron wavelength as follows:

$$\text{EqIII: } |\vec{k}| = 2\pi : \lambda_n$$

When interacting with the sample, the neutrons experience a change of direction and/or velocity, depending on the atoms and their arrangement found within the sample. Monitoring the neutrons momentum thus provides information about these factors. To describe this change in momentum the relation of momentum vectors before and after, a momentum transfer vector \vec{Q} , is introduced. This vector is defined as follows.

$$\text{EqIV: } \vec{Q} = \Delta\vec{k} = \vec{k}_1 - \vec{k}_2$$

With \vec{k}_1 as neutron wave vector before the interaction with the sample and \vec{k}_2 as neutron wave vector after interaction with the sample. Due to a possible partially elastic collision, the neutrons wave vector may change due to energy loss ΔE , which can be described as:

$$\text{EqV: } \Delta E = E_1 - E_2 = \hbar^2 \cdot \frac{\vec{k}_1}{2m_n} - \hbar^2 \cdot \frac{\vec{k}_2}{2m_n}$$

Only if the collision is completely elastic, $\Delta E = 0$, no change of the wave vector takes place $|\vec{k}_1| = |\vec{k}_2|$. \vec{Q} can then be simplified to:

$$\text{EqVI: } \vec{Q} = 2\vec{k}_1 \cdot \sin(\theta_s)$$

Relating it to the scattering angle θ_s . For a regular repeating structure like the multiple lamellae of CER systems, a Bragg diffraction pattern can be concluded. For a Bragg diffraction the vector is defined as:

$$\text{EqVII: } \vec{Q} = 2\pi : d$$

With d as the spacing between two sets of equidistant structurally organized planes. Within the investigated multilamellar systems, this lamellar repeat distance is about equal to the thickness of a single lamellae, if these lamellae are clearly separable at their border regions. Since $|\vec{k}| = 2\pi : \lambda_n$, through transformation of \vec{Q} , we can get the Braggs equation.

$$\text{EqVIII: } \lambda_n = 2d \cdot \sin(\theta_s)$$

From the Braggs equation, the lamellar repeat distance can be calculated as:

$$\text{EqIX: } d = \frac{\lambda_n}{2\sin(\theta_s)}$$

With this equation, given the condition of a completely elastic collision, the lamellar repeat distance can be calculated from the predefined neutron wavelength λ_n and the observed scattering angle θ_s . The so called Bragg-maxima which give an ordered diffraction pattern with single defined diffraction peaks (reflexes) result from the coherent scattering at each crystal layer which leads to a constructive interference. This is a result of the waves staying in phase because the path length dependend on the, for an ordered system constant repeat distance, is a multiple of the neutron wavelength λ_n .

3.3.3 Membrane Diffraktometer V1

The V1 is located at the Lise-Meitner campus of the Helmholtz Zentrum Berlin. Neutrons for its measurements are generated by the research reactor BER II. The V1 is conceptualized as a diffraction instrument mainly for biological samples. It is optimized for samples with unit-cells between 5 and 10 nm. The Neutrons are cooled by an H₂ cold source. With the adjustable highly ordered graphite monochromator, the neutron wavelength can be adjusted between 4 and 6 Å, fully utilizing the 3 cm x 12.5 cm neutron guide NL1A (Figure 11 b). An additional Be-filter is used, to suppress second order and wavelength below 3.9 Å (Figure 11 b). For the experiments performed during this thesis, a wavelength of 4.567 Å was chosen. The samples were placed at a distance of 101.8 cm

to the two dimensional ^3He detector (Figure 11 a,b). Using the V1 for CER-based multilamellar model membrane systems, because of the relatively small detector surface, an ω - 2Θ -scan is performed. For this scan, the sample is rotated around the axis parallel to the detector surface. At the same time, the detector angle Θ parallel to but double the value of the sample angle 2Θ . The collected intensity of the scattered neutrons is integrated over the detector y axis for each Θ position (Figure 11 c). Furthermore, depending on the step width, for each Θ position multiple datasets are collected and also summated, to obtain a final Intensity- 2Θ diffractogram (Figure 12). To simulate natural conditions as closely as possible, three chambers for the control of humidity and temperature are available^[142]. The temperature is regulated via a water flow based heating/cooling system while the humidity is regulated using saturated salt solutions^[143,144] (Figure 11 b).

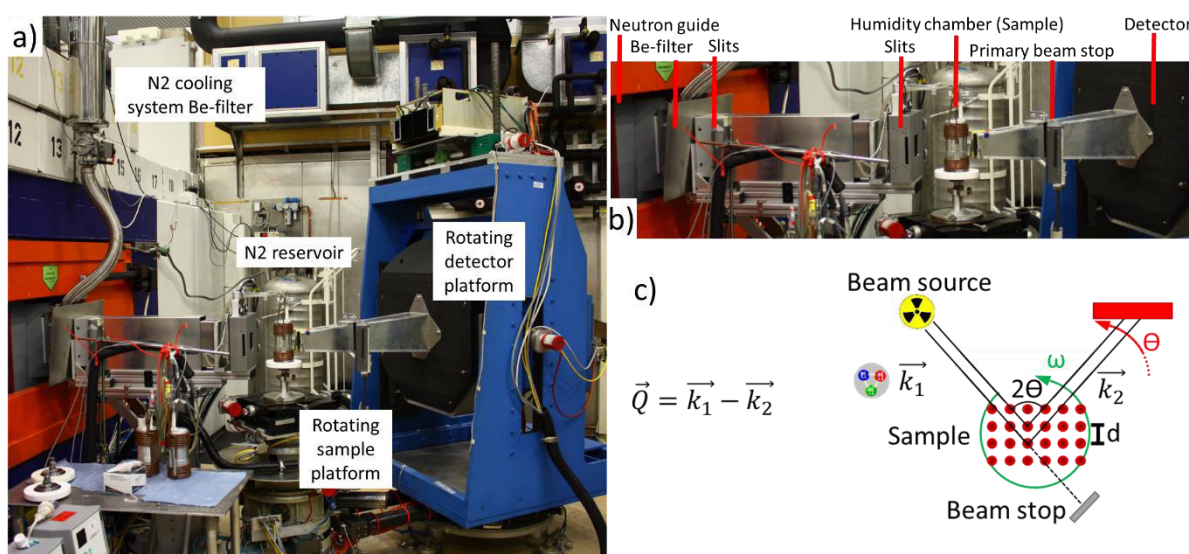


Figure 11: The V1 and the beam path at this Instrument^[142].

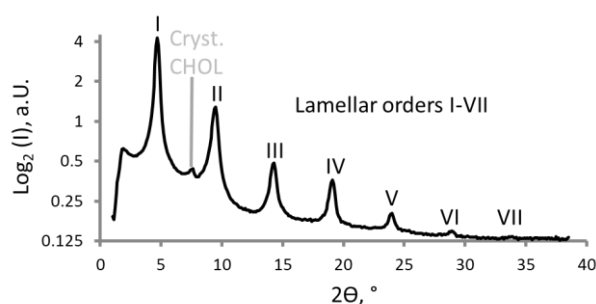


Figure 12: Representative diffraction pattern for a sample measured at the V1 (CER[NP] C24 / D-[AP] C24 / CHOL / LA, 0.33 : 0.66 : 0.7 : 1, 100% D₂O, 98 % R.H.).

3.3.4 Small Momentum Transfer Diffractometer D16

The D16 small momentum transfer diffractometer is conceptualized for the investigation of partially ordered structures, as they are found in stacked biological membranes, with a unit cell size of about 5 nm. Large vertically oriented samples profit the most from the instrument scattering geometry, because of the large neutron beam vertical cross-section. A real space resolution up to the fraction of a nanometre can be achieved with this

Instrument. Neutrons are generated by the Institut Laue-Langevins high flux reactor and are moderated using a liquid H₂-cold source. The neutrons are then transported through a cold neutron guide to the instrument (Figure 13 a,c). A highly ordered pyrolytic graphite monochromator can reflect 4 different wavelength 4.55 Å, 7.50 Å, 5.60 Å and 9.00 Å. (Figure 13 c). A N₂ cooled Be-filter suppresses higher harmonic wavelength (Figure 13 c). For the experiments performed for this thesis, the wavelength was adjusted to 4.55 Å. The position sensitive ³He detector (Figure 13 a – c) was placed at a 950 cm distance from the sample. The detector has a relatively large area of 32x32 cm² and a high 1x1 mm² resolution. Using the D16 for CER-based multilamellar model membrane systems, because of the large detector surface, a quasi-one-axis-rocking-scan is performed. For this scan, the sample is rotated around the axis parallel to the detector surface. The detector stays stationary, collecting the intensity over a wide 2 Θ range. The detector is only rotated, if the detector area does not cover all detectable reflections (Figure 13 c). The 3-dimensional (2 Θ -y-Intensity) raw data are processed, using the in-house developed LAMP program. The detector area which is integrated is chosen after the scan, depending on the actual Bragg reflection position. To determine the ω -angle dependent Bragg reflection maximum, the intensity is integrated over the selected y-axis region. A three dimensional (2 Θ - ω -Intensity) matrix is obtained (Figure 13 d). Images for $\pm 1.5^\circ \omega$ around the Bragg reflection maximum are integrated for each reflex. Finally a 2-dimensional (2 Θ -Intensity) diffractogram is obtained (Figure 14). To simulate natural skin conditions as closely as possible, three temperature and humidity chambers are available. The temperature is regulated via a water flow based heating/cooling system. The humidity is controlled by setting a separate temperature for an internal water reservoir, controlling the equilibrium of evaporation and condensation^[145].

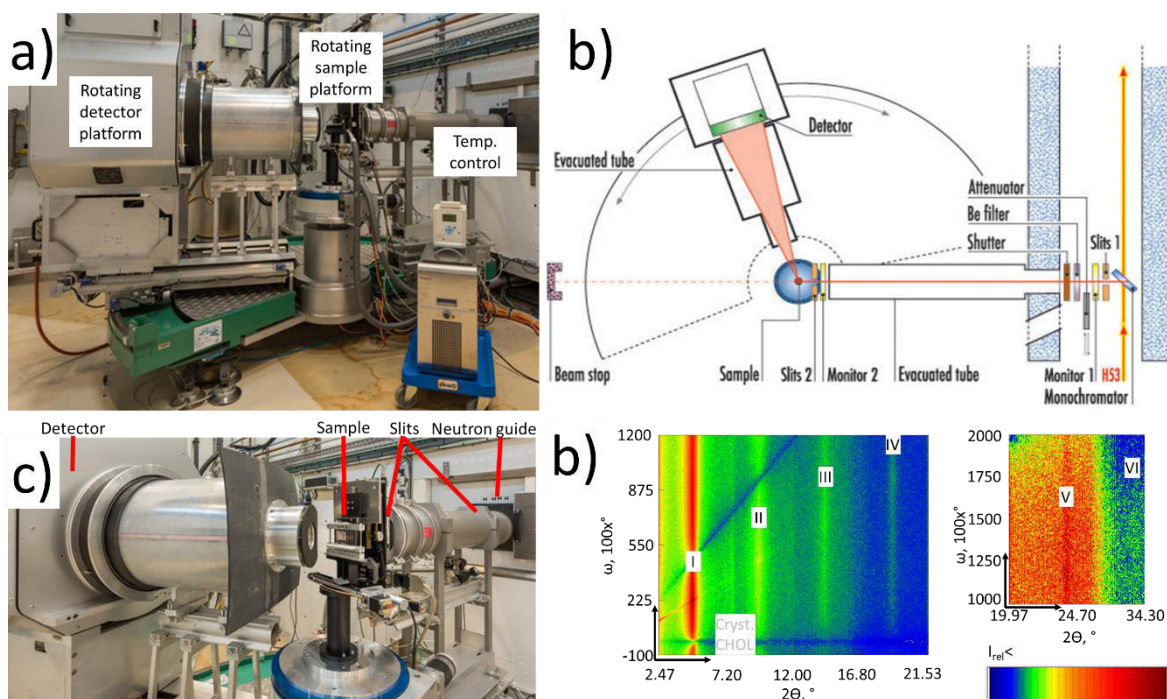


Figure 13: Specifications of the D16 a) constructional details. b) beam path. c) Typical 3 dimensional data array as obtained from a D16 rocking scan (Sample: CER[NP] C24 / [AP] C24 / [EOS]-br / CHOL / LA, 0.6 : 0.3 : 0.1 : 0.7 : 1, 100 % D₂O, 98 % R.H.).

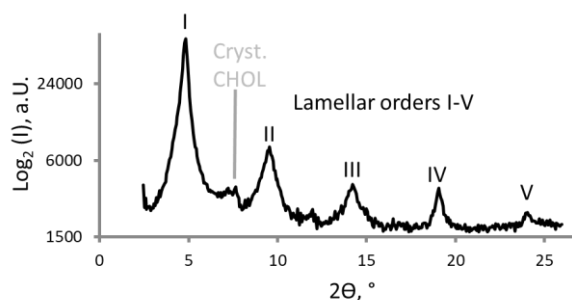


Figure 14: Representative diffraction pattern for a sample measured at the D16 (Sample: CER[NP] C24 / [AP] C24 / [EOS]-br / CHOL / LA, 0.6 : 0.3 : 0.1 : 0.7 : 1, 100 % D₂O, 98 % R.H.).

3.3.5 Evaluation and Implications of Diffraction Data

For the scattering of neutrons, at a single fixed scattering centre (single nucleus), the incoming neutron wave can be regarded as a plane wave ψ_- while the scattered neutron wave, has a spherical shape ψ_o . The characteristics of the scattered wave ψ_o are dependent on the scattering power b and scattering properties, either coherent b_{coh} or incoherent b_{inc} . As explained in 3.3.1, the coherent scattering length can either have a positive or a negative value. They are typically in the range of 10^{-13} cm. The scattering cross-section σ_s is calculated as $\sigma_s = 4\pi b_{coh}^2$ and represents a nucleus's effective collision area with an incoming neutron. Important for the collection of diffraction profiles is the coherent scattering. This value differs for different elements but also for different isotopes of the same element. There is an especially strong difference between the Hydrogen ^1H ($-3.74 \cdot 10^{-13}$ cm) and Deuterium $\text{D}/^2\text{H}$ ($6.67 \cdot 10^{-13}$ cm), with even a different algebraic sign (Table 6). As mentioned above, this makes it possible to use deuterium as a distinguishable label for biological molecules, without strongly altering their chemical and biophysical properties, as would be the case with most other labels.

Table 6: Overview of the scattering length of elements found in biological molecules^[28].

Element	Scattering length b_{coh} , 10^{-13} cm
Hydrogen ^1H	-3.7406
Deuterium $^2\text{H}/\text{D}$	6.671
Carbon ^{12}C	6.6511
Carbon ^{13}C	6.19
Nitrogen ^{14}N	9.37
Nitrogen ^{15}N	6.44
Oxygen ^{16}O	5.803
Oxygen ^{17}O	5.78
Oxygen ^{18}O	5.84

Within the Intensity-2 θ -diffractograms, collected as described above, the integral intensity of each diffraction peak holds information on the sum of scattering of a layer and thus the neutron scattering length density (NSLD) in each region. This relation can be used, to assess the lamellar micro- and molecular nanostructure of the system. The software

IGOR Pro was used to extract information about the NSLD and calculate corresponding profiles. These profiles are basically a virtual representation of the differences in the sum of scattering length properties along the lamellar unit cell. First the integral of each lamellar reflex was determined by fitting the peaks with 1 - 4 Gaussian functions.

$$\text{EqX: } I_{Ln} \int_{\theta_0}^{\theta} g(\theta) = a + b \cdot \theta + \sum_{m=1}^{m_{max}} I_m \cdot e^{\left(-\frac{\theta-\theta_0}{w_n}\right)^2} d\theta$$

With I_{Ln} : Integral intensity area under the n^{th} lamellar order peak, a and b are coefficients approximating a linear background, I_n : ω Integral intensity along the 2θ -axis of the n^{th} Gauss peak, w_n width of the n^{th} Gauss-peak. The Integral intensity along the 2θ -axis is proportional to the squared number of diffracting lamellar layers N_L^2 . From the integral intensities I_{Ln} for each diffraction order n , a structure factor F_n , representing the structure properties of each layer is calculated. The absolute values of each F_n is calculated as ^[146]:

$$\text{EqXI: } |F_n| = \sqrt{L_n \cdot A_n \cdot I_{Ln}}$$

With L_n the Lorentz-correction factor

$$\text{EqXII: } L_n \sim \sin(\theta) \sim n$$

and the absorption correction A_n which can be calculated as:

$$\text{EqXIII: } A_n = \frac{\sin(\theta)}{2\mu h} \cdot \left(1 - e^{-\frac{2\mu h_s}{\sin(\theta)}}\right)$$

With the linear absorption coefficient μ and the thickness of the sample h_s . Since both the absorption as well as the number of diffracting layers rise with the samples thickness, there is a certain optimal range of sample thickness with minimal absorption but still enough layers to yield good diffracting properties. From the structure factors and the lamellar thickness, the NSLD-profile as function $\rho(x)$ can be calculated as a combination of wave functions, by Fourier synthesis of the structure factors F_n according to:

$$\text{EqXIV: } \rho(x) = a + b \frac{2}{d} \sum_{n=1}^{n_{max}} F_n \cos\left(\frac{2\pi n x}{d}\right)$$

The coefficients a and b are approximating a linear background of $\rho(x)$. However, for the Fourier transform, both the absolute value as well as the phase sign of each structure factor F_n are required. Determining the phase of the structure factor however is no trivial problem. Fortunately, assuming a centrosymmetric arrangement, typical for CER-based systems and a Gaussian water distribution with a maximum position $x = \frac{d}{2}$ within the hydrophilic head groups, the phase problem can be simplified to either $+$ or $-$ for each F_n . By applying different $\text{H}_2\text{O}/\text{D}_2\text{O}$ contrasts, representing an *isomorphous* replacement, the absolute value of the structure factor can be influenced. A three point measurement with three different $\text{H}_2\text{O}/\text{D}_2\text{O}$ contrasts is thus sufficient for the calculation of the phase of each structure factor shown in Figure 12^[146-149].

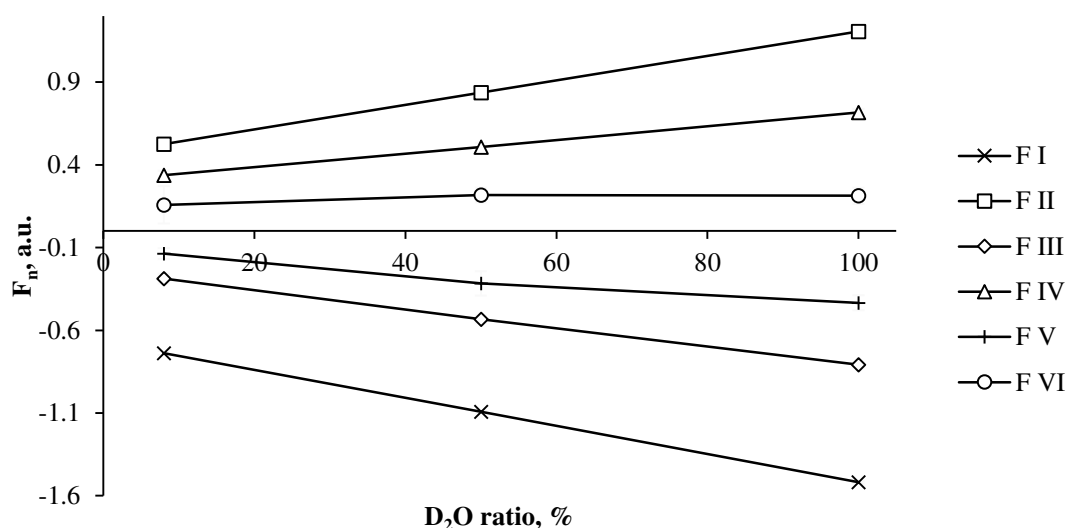


Figure 15: Example for the determination of the F_n using a three point measurement (CER[NP] C24 / D-[AP] C24 / CHOL / LA, 0.33 : 0.66 : 0.7 : 1, 98 % R.H.). *Error bars are shown but are too small to be visible.

A higher D₂O content also generates a higher signal-to-background ratio, which allows for detection of peaks of higher diffraction orders with high precision. These higher order peaks are very important for the calculation of a detailed NSLD-profile. From these profiles, many structural details can be observed. In the outer regions, the CER and FFA HGs are located. These show a higher scattering (Figure 16 a, c red), which is a result of the contained elements with a stronger positive scattering length like C, N and O as well as the lower content of H, which has a negative scattering length (Figure 16). The CHOLs structure with less H leads to a small peak, slightly inward from the head groups region (Figure 16 a, c yellow). The rest of the profile, representing the part of the unit cell, where the aliphatic chains are located is rather flat, since the sum of scattering lengths for the CH₂-groups is $-0.830 \cdot 10^{-13}$ cm and thus near 0 (Figure 16 a, c blue). For symmetric CER, all the CER and FFA CH₃-groups are in the same plane in the lamellar centre. The result due to the negative sum of $-4.571 \cdot 10^{-13}$ cm for the scattering length is a minimum in the lamellar mid-plane. Such a minimum is not observed for the asymmetric CER (Figure 16 a, c green). For these, the two chains have different lengths (C24 FA and C18 base). The longer chains overlap in the lamellar mid-plane, dispersing the terminal CH₃ groups to two different locations. An estimated localization of the lipids within the unit cell is given in Figure 16 b for C18 systems and Figure 16 d for >C20 systems.

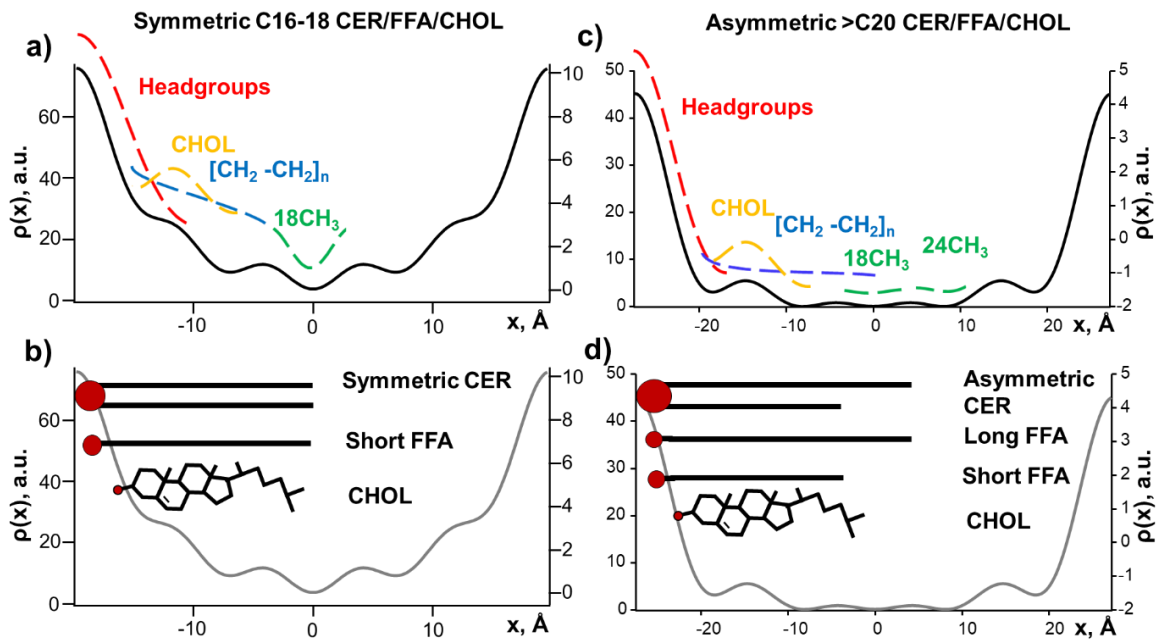


Figure 16: NSLD-profiles for multilamellar lipid model systems (98 % R.H. 100 % D₂O), based on symmetric C18 CER left (CER[NS]C18/[EOS]-br/CHOL/FFA, 0.8 : 0.2 : 0.7 : 1) and on asymmetric >C20 CER (CER[NP]C24/D-[AP]C24/CHOL/FFA, 0.33 : 0.66 : 0.7 : 1) on the right.

As described above, due to the difference in scattering length for different isotopes, especially H and D, they can be used as distinguishable labels, without strongly altering the molecules chemical and biophysical properties. By comparing the profile calculated for the base system with the corresponding system, containing a deuterated lipid, the position of the deuterated group within the unit cell can be located (Figure 17).

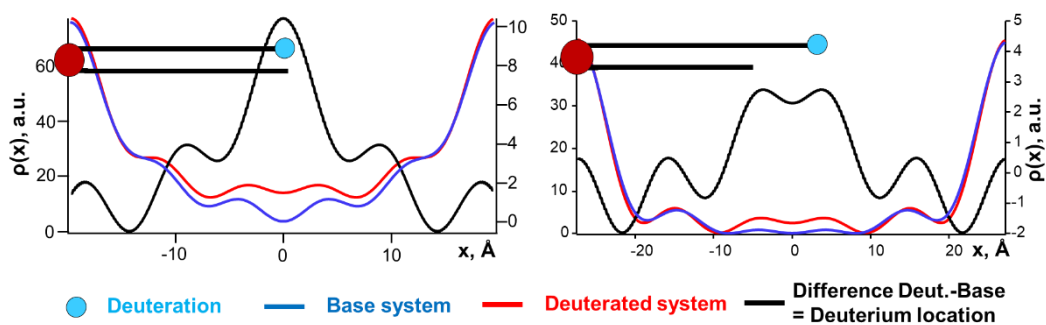


Figure 17: Comparison of the NSLD-profiles for multilamellar lipid model systems (98 % R.H. 100 % D₂O), based on symmetric C18 CER left (CER[NS]C18/[EOS]-br/CHOL/FFA, 0.8 : 0.2 : 0.7 : 1 ±[NS] C18-D₃) and on asymmetric >C20 CER right (CER[NS] C24/D-[AP]C24/CHOL/FFA, 0.33 : 0.66 : 0.7 : 1 ±D-[AP] C18-D₃) each compared to systems containing a deuterated Lipid.

Due to the contrast variation it also becomes possible to locate the water within the unit cell. The sum of coherent scattering of H₂O ($b_{coh}(\sum H_2O) = -1,678 \cdot 10^{-13} \text{ cm}$) and D₂O ($b_{coh}(\sum D_2O) = 19.105 \cdot 10^{-13} \text{ cm}$) have an opposite sign. At the D₂O/H₂O contrast of 8:92, the sum of the relative scattering values of H₂O ($b_{coh}(\sum H_2O) \cdot 92\%$) = $-1.544 \cdot 10^{-13} \text{ cm}$ and D₂O ($b_{coh}(\sum H_2O) \cdot 8\%$) = $1.530 \cdot 10^{-13} \text{ cm}$ becomes zero, eliminating any contribution to the diffraction profile. Consequently 100 % of the signal is a result of the lipid system. At 100 % D₂O, the signal contribution is maximal. Subtracting the 8 % profile from the 100 % profile, leaves only the contribution of the D₂O, showing where water is located Figure 18.

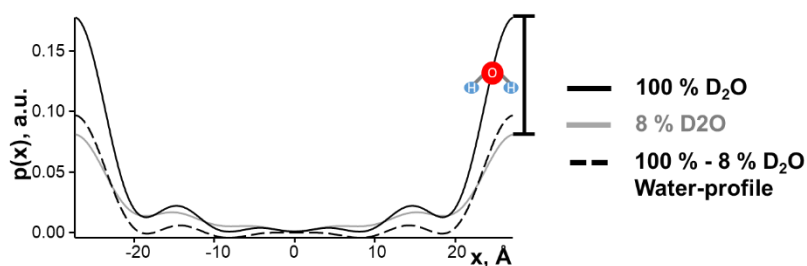


Figure 18: Comparison of the NSLD-profiles at 8 % D₂O and 100 % D₂O for a multilamellar lipid model system (CER[NP] C24/D-[AP] C24/CHOL/FFA, 0.33 : 0.66 : 0.7 : 1, 98 % R.H.). The localization of water in the unit cell is determined by subtraction of both.

To gain information on the relative water content within the different systems, the difference between the minimum and maximum point of the water profile (100 % D₂O - 8 % D₂O) at 98 % R.H. was determined. It was normalized to the difference between the minimum and maximum point of the corresponding 100 % D₂O 98 % R.H. NSLD. For C18 instead of the absolute minimum, a local minimum in the CH₂ region has to be determined.

3.4 X-ray Diffraction

X-ray diffraction was performed in preparation for the neutron diffraction experiments. This was done, to check if the sample shows repeated Bragg-peaks, indicating the correct formation of a multilamellar structure. It was furthermore possible, to obtain an estimation of the lamellar repeat distance and expected diffraction peak intensity in the neutron diffraction experiments. The general principles of scattering and diffraction, which were already explained above for neutrons are basically the same for X-rays. These measurements also yield comparable diffraction profiles with intensity-2 θ -diffractograms as shown in Figure 19.

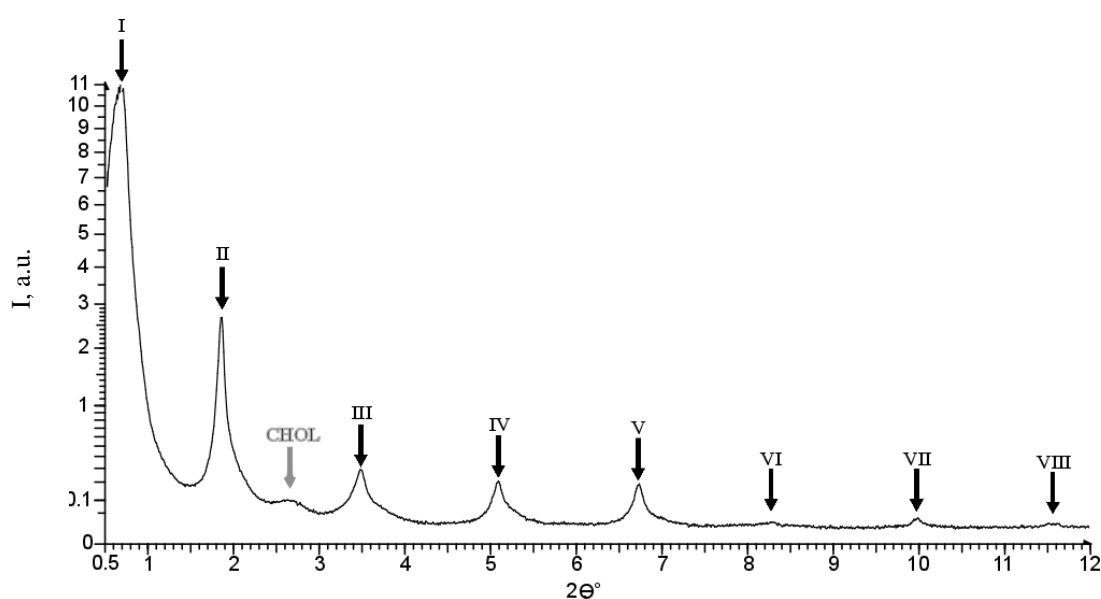


Figure 19: Example for a typical diffractogram as observed using X-ray diffraction (sample: CER[NP]/[AP]-D₃/CHOL/LA, dry ambient conditions, $\lambda_{\text{Cu-K}\alpha} = 1.5406 \text{ \AA}$).

Since the X-ray measurements served mainly as a reference measurement, this section will give a short overview of the main differences between the interactions of neutrons and X-rays with matter. It will furthermore explain the advantages of neutrons over X-rays and demonstrate why ultimately neutron diffraction was chosen as the preferred method for these investigations. Additionally, a few effects that also take place for the interaction of neutrons with matter but are far less relevant in this context will be highlighted.

First of all, the peak intensities in X-ray diffraction-experiments are not equivalent to the intensities measured using neutron diffraction. The X-ray scattering is dependent on the number of electrons in the electron shell. Neutron scattering is instead dependent on the properties of the atomic nuclei, as described above. X-rays are electromagnetic waves which's wavelength for diffraction experiment is typically between 0.05-2.50 Å. For the measurements for this thesis, the X-rays were generated using a Cu-K beam source, which generated Cu-K α X-rays with a wavelength of $\lambda_{\text{Cu-K}\alpha} = 1.5406 \text{ \AA}$. As an electromagnetic wave, they are strongly influenced by electromagnetic fields as they are generated by electrically charged particles. Their main interaction with matter as waves is thus with the electrical field generated by the electrons, by which they can get scattered. In contrast to that, the neutrons as neutral particles interact very little with electric fields. Their interaction with the nuclei allows for the detection of small atoms like hydrogen, which are almost invisible to X-rays because of their few electrons. Neutron waves furthermore can distinguish different isotopes, which is impossible for X-rays, since the electron shell is basically uninfluenced by additional neutrons in the nucleus. Due to a generally lower scattering and absorption cross-section for neutrons, they can penetrate deeper into many -especially organic- materials even at low energy.

X-rays, as all electromagnetic waves due to the wave particle dualism however can also be described as particle beams, consisting of photons, which are mass-less subatomic elementary particles. Viewed as particles they can feature additional interactions. X-ray photons due to their high energy are an ionizing radiation. They can be absorbed, transferring all of their energy to an electron. If it is an electron from an inner shell, it can get elevated into an outer free shell or punched out completely, either way can another electron from a higher shell fill in the empty position in the lower one. Since the electron is in a lower energy state now, the excess energy is emitted as a photon. In contrast to X-rays, neutrons are not elementary but composite particles constructed from three quarks. This makes neutron expanded particles with a mass of $1.675 \cdot 10^{-27} \text{ kg}$. This consequently changes the way they physically interact with matter in comparison to the mass-less photons, especially concerning collision processes. Because in contrast to X-rays, neutrons have a magnetic moment, magnetic properties can easily be investigated. The relevant interactions of X-rays with matter are shown in Figure 20.

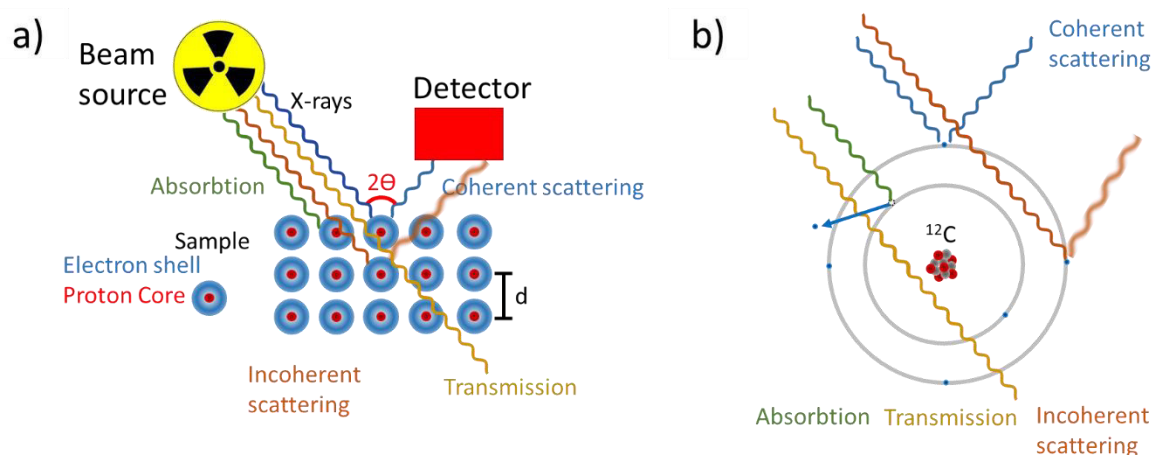


Figure 20: Relevant interactions of X-rays with matter

Overall, neutron diffraction is in many aspects more versatile for the investigation of biological structures than X-rays are. Hydrogen, carbon and other atoms present in organic molecules have low absorption cross-sections, leading to absorption effects playing a very minor role for such experiments. The lower absorption and scattering cross-sections also allow for a much higher penetration depth of even lower energy neutrons into the material, providing better structural information with minimal damage to the sample. The possibility to label molecules with isotopes like deuterium, allowing to locate the labeled group exactly, without strongly changing the biophysical and chemical properties of the molecule is possibly the greatest advantage.

4. Results and Discussion

The results and discussion in this thesis will be presented in the form of the manuscripts published as a result of the work for this thesis. The manuscripts are given in the state as of the time, they were accepted for publication*.

* The used abbreviations, nomenclature, units and formatting are used as they were in the original manuscript and may vary slightly from the introductory part of this thesis. This was done, to give an unadulterated representation of the original published work. The used different abbreviations are not shown in the table of abbreviations if only use of capital letters or brackets changed. The introductory part for each of the manuscripts is omitted, to limit redundancy.

4.1 Investigation of a CER[NP] and [AP]-Based *Stratum Corneum* Modelling Membrane System: Using Specifically Deuterated CER Together with a Neutron Diffraction Approach

LANGMUIR

Cite This: *Langmuir* XXXX, XXX, XXX-XXX

Article

pubs.acs.org/Langmuir

Investigation of a CER[NP]- and [AP]-Based *Stratum Corneum* Modeling Membrane System: Using Specifically Deuterated CER Together with a Neutron Diffraction Approach

Thomas Schmitt,^{*,†,Ⓜ} Stefan Lange,[‡] Bodo Dobner,[§] Stefan Sonnenberger,[§] Thomas Hauß,^{||} and Reinhard H. H. Neubert[†]

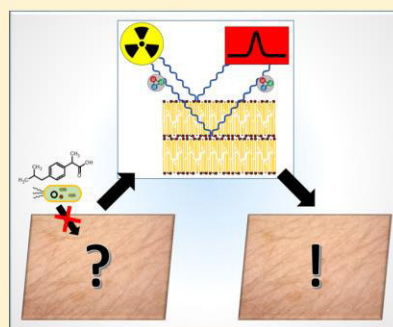
[†]Institute of Applied Dermatopharmacy, Martin Luther University Halle-Wittenberg (IADP), Weinbergweg 23, 06120 Halle/Saale, Germany

[‡]Institute of Medical Physics and Biophysics, University of Leipzig, Härtelstraße 16-18, 04107 Leipzig, Germany

[§]Institute of Pharmacy, Martin Luther University Halle-Wittenberg (MLU), Wolfgang-Langenbeck-Str. 4, 06120 Halle/Saale, Germany

^{||}Helmholtz-Zentrum Berlin für Materialien und Energie (HZB), Hahn-Meitner-Platz 1, 14109 Berlin, Germany

ABSTRACT: Neutron diffraction was used as a tool to investigate the lamellar as well as molecular nanostructure of ceramide-[NP]/ceramide-[AP]/cholesterol/lignoceric acid model systems with a nativelike 2:1 ratio and a 1:2 ratio to study the influence of the ceramide-[AP]. By using mixtures together with cholesterol and free fatty acids as well as a humidity and temperature chamber while measuring, natural conditions were simulated as closely as possible. Despite its simplicity, the system simulated the native *stratum corneum* lipid matrix fairly closely, showing a similar lamellar thickness with a repeat distance of 5.45 ± 0.1 nm and a similar arrangement with overlapping long C24 chains. Furthermore, despite the very minor chemical difference between ceramide-[NP] and ceramide-[AP], which is only a single OH group, it was possible to demonstrate substantial differences between the structural influence of the two ceramides. Ceramide-[AP] could be concluded to be arranged in such a way that its C24 chain in both ratios is somehow shorter than that of ceramide-[NP], not overlapping as much with the opposite lamellar leaflet. Furthermore, in the unnatural 1:2 ratio, the higher ceramide-[AP] content causes an increased tilt of the ceramide acyl chains. This leads to even less overlapping within the lamellar midplane, whereas the repeat distance stays the same as for the ceramide-[NP]-rich system. In this nativelike 2:1 ratio, the chains are arranged mostly straight, and the long C24 chains show a broad overlapping region in the lamellar midplane.



<http://pubs.acs.org/doi/abs/10.1021/acs.langmuir.7b01848>

4.1.1 Materials and Methods

4.1.1.1 Ceramide Mixtures

For the experiments described in this study, mixtures of CER, CHOL and lignoceric acid (LA) were prepared. The used CER[NP] (N-(tetracosanoyl)-phytosphingosine) and CER[AP] (N-(α -hydroxytetracosanoyl)-phytosphingosine) were obtained from synthesis and purified to ≥ 95 % (soon to be published elsewhere). CHOL and LA were purchased from Sigma Aldrich GmbH (Taufkirchen, Germany). The chemical structures of the used molecules are displayed in Figure 21.

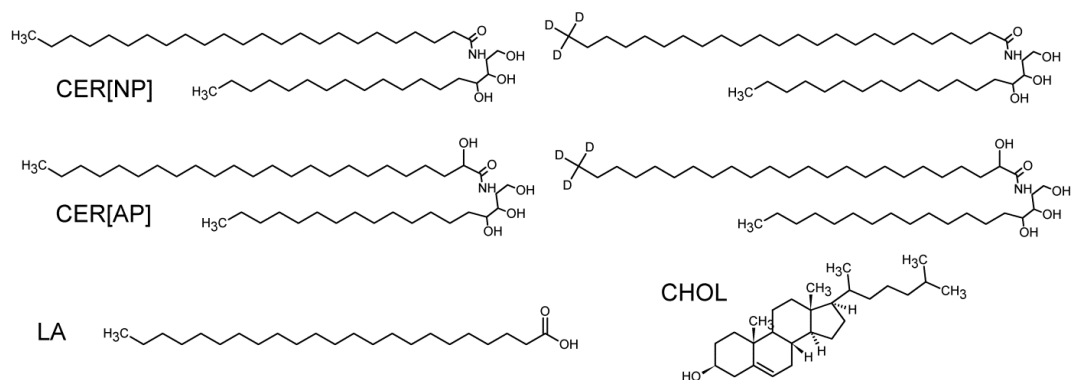


Figure 21: Structures of the lipids used for these experiments.

4.1.1.2 Sample preparation

The SC model membranes were prepared on quartz glass slides. For sample application, the pure substances were solved in a 2:1 mixture of chloroform and methanol (analytical grade, by Sigma Aldrich) with a concentration of 10 mg/ml. These solutions were then combined to generate CER/CHOL/CHOL mixtures with molar ratios of 1/0.7/1 and varying CER[NP]/[AP] distribution, according to Table 7. For each molar ratio, three mixtures with either CER[NP]/[AP], CER[NP]-D₃/[AP] or CER[NP]/[AP]-D₃ were prepared for use in neutron scattering experiments. For deposition, the mixtures were sprayed onto the surface, using an airbrush instrument (Harder & Steenbeck, Norderstedt, Germany).

Table 7: Used mixtures of CER[NP]/CER[AP]/CHOL/LA

Mixture	Molar ratio (n/n)
CER[NP]/CER[AP]/CHOL/LA	0.66 / 0.34 / 0.7 / 1
CER[NP]-D ₃ /CER[AP]/CHOL/LA	0.66 / 0.34 / 0.7 / 1
CER[NP]/CER[AP]-D ₃ /CHOL/LA	0.66 / 0.34 / 0.7 / 1
CER[NP]/CER[AP]/CHOL/LA	0.34 / 0.66 / 0.7 / 1
CER[NP]-D ₃ /CER[AP]/CHOL/LA	0.34 / 0.66 / 0.7 / 1
CER[NP]/CER[AP]-D ₃ /CHOL/LA	0.34 / 0.66 / 0.7 / 1

Using an optimized and well-established preparation method, the samples were sprayed at a temperature of 70.5 °C which is just below the melting point of the mixture. Afterwards the samples were annealed, to form the multi-lamellar structure by heating to 65 °C under high humidity for 2 h, cooling at room temperature for 1 h and again heating under high humidity for 1 h. This method did show the best crystallisation conditions and thus optimized formation of the macroscopic multilamellar structure.

4.1.1.3 Neutron diffraction experiments

For the neutron diffraction experiments the SC model membranes prepared on quartz glass slides were used. Diffraction data were collected at the Membrane Diffractometer V1 located at the Lise-Meitner campus of the Helmholtz-Zentrum Berlin. Neutrons generated by the research reactor BER II were cooled using an H₂ cold source to increase the flux of neutrons around 4 Å wavelength. A pyrolytic graphite monochromator was utilized to diffract neutrons with a wavelength of $\lambda = 4.567$ Å. The distance between sample and detector was 101.8 cm. While rotating the sample angle ω and the detector angle θ in an ω -2 θ -scan, the intensity of the scattered neutrons was recorded as a function of the scattering angle 2 θ . For contrasting against the water background the three different H₂O/D₂O ratios of 0:100, 50:50 and 92:8 (w/w) were applied. A higher D₂O content also generates a higher signal-to-background ratio, which allows for detection of peaks of higher diffraction orders with high precision. These higher order peaks are very important for calculation of a detailed neutron scattering length density profile (NSLD). Conditions according to Table 8 were applied to all mixtures. The temperature for contrast variation was kept at 37 °C, and the relative humidity at 98 %. For the 92:8 H₂O/D₂O ratio, additionally

first the humidity was lowered to 57 % and second the temperature was lowered to 32 °C, to better represent physiological conditions (Table 8). Since it could be observed that no more changes in the diffraction signal occurred after about 6 h of equilibration, samples were given a period of at least 7 h after any change of either temperature, humidity or H₂O/D₂O ratio. The membrane spacing was determined according to Bragg's law $n\lambda = 2d \sin(\theta)$. The NSLD $\rho(x)$ was calculated by Fourier synthesis of the structure factors F_n according to:

$$\rho(x) = a + b \frac{2}{d} \sum_{n=1}^{n_{max}} F_n \cos\left(\frac{2\pi nx}{d}\right)$$

The coefficients a and b are for relative normalisation of $\rho(x)$, d is the lamellar periodicity and n the order of diffraction. The absolute values of the structure factors could be calculated as $|F_n| = \sqrt{hA_nI_n}$, with h as the Lorentz correction, A_n as absorption correction^[146] and I_n as Intensity of the nth peak. The integration of the Bragg's peak intensities was performed using the IGOR Pro 6.1 software (WaveMetrics Inc., Portland, OR, USA). For the Fourier transform, both the absolute value as well as the phase sign of each structure factor F_n is required. Assuming a Gaussian water distribution with a maximum position $x = \frac{d}{2}$ within the hydrophilic head group region, allows determination of the F_n by application of different H₂O/D₂O contrasts, representing an *isomorphous* replacement^[146,149]. The centro-symmetric lipid arrangement which is to be expected of CER-membranes leads to a phase of either + or – for each F_n . A three point measurement with three different H₂O/D₂O contrasts is thus sufficient for the calculation of the phase of each structure factor. A detailed description of this can be found elsewhere^[146–148].

Table 8: Different conditions, applied for all mixtures.

H ₂ O/D ₂ O (w/w)	ϑ [°C]	R.H.[%]
0:100	37	98
50:50	37	98
92:8	37	98
92:8	32	98
92:8	32	57

4.1.2 Results

Due to the spraying process by hand, common sample thicknesses can only be estimated with about 5-10 μm and between 1000 and 1500 bilayers. From these layers however only a few hundred contribute to the signals of the diffraction profiles due to technical limitations of the method. From the generated diffraction profiles, it could be shown, that the CER[NP] and [AP] form a continuous multilamellar system with a lamellar repeat distance of 5.45±0.1 nm in both applied ratios of 1:2 and 2:1 with the latter as the more native-like ratio^[25,26]. The observed membrane thickness is equal to the observed short periodicity phase (SPP) in the mammalian SC^[104]. Without the addition of any very-long-ω-acyl-CER no long-periodicity phase (LPP) with a 12-13 nm repeat distance was observed, as expected. Furthermore, no other phases with a distinctly different repeat distance like for example a FFA enriched phase as often reported for symmetric short-chain C16 or C18 CER was found^[150–152]. The observed repeat distance was slightly shorter than two full length C24 CER chains opposing each other would be. It is however about equal to an arrangement with hairpin folded CER, with the long C24 chains interdigitating within the lamellar mid-plane. By calculating a NSLD as described above, additionally to the lamellar arrangement, the molecular nanostructure could be assessed. Representative diffraction data are given in Figure 22a.

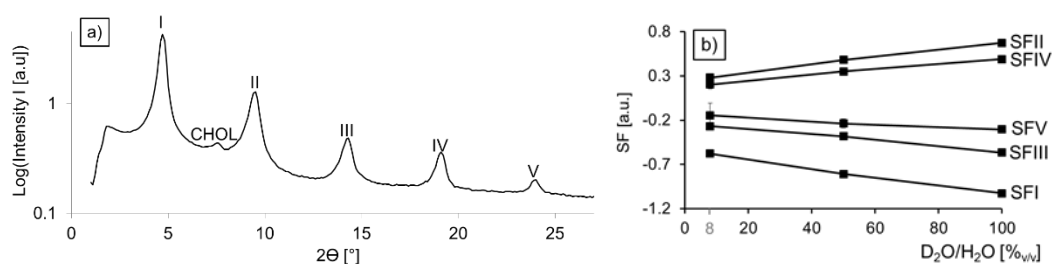


Figure 22: Representative physical data for the CER[NP]-D3/[AP]/CHOL/LA system. a) diffraction data at 100 % D₂O/H₂O and 98 % R.H. with five clearly observed diffraction orders and a smaller reflex, indicating phase separated CHOL. b) phasing plot with the calculated structure factors for orders I-V at 8, 50 and 100 % D₂O/H₂O ratio and 98 % R.H.

All structure factors that could be determined by the D₂O/H₂O-contrast variation were in phase with uneven factors with a negative and even factors with a positive sign Table 9. A representative phasing plot is given in Figure 22b.

Table 9: Structure factors F_n for diffraction orders 1-5 at 100 % D₂O and 98 % R.H.

	CER NP/AP (2:1)	CER NP-D3/AP (2:1)	CER NP/AP-D3 (2:1)
F ₁	-0.335 ± 0.001	-0.331 ± 0.002	-0.287 ± 0.001
F ₂	0.220 ± 0.002	0.229 ± 0.003	0.244 ± 0.006
F ₃	-0.185 ± 0.003	-0.216 ± 0.006	-0.192 ± 0.006
F ₄	0.160 ± 0.005	0.127 ± 0.008	0.151 ± 0.012
F ₅	-0.100 ± 0.006	-0.097 ± 0.023	-0.126 ± 0.013
	CER NP/AP (1:2)	CER NP-D3/AP (1:2)	CER NP/AP-D3 (1:2)
F ₁	-0.371 ± 0.002	-0.324 ± 0.324	-0.331 ± 0.001
F ₂	0.239 ± 0.002	0.258 ± 0.258	0.262 ± 0.002
F ₃	-0.180 ± 0.002	-0.173 ± 0.173	-0.153 ± 0.004
F ₄	0.143 ± 0.004	0.153 ± 0.153	0.159 ± 0.004
F ₅	-0.067 ± 0.006	-0.093 ± 0.093	-0.095 ± 0.008

The head groups, located within the outer regions of the lamellar structure, can be easily identified by the high scattering length density. No noticeably higher scattering length densities are observed within the unit cell. The contrast variation shows minimal water content, with the water located solely within the head group region. At a D₂O/H₂O ratio of 8/92 the water becomes invisible for the neutron beam because positive D and negative H coherent scattering length silence each other. The profile with 8 % D₂O thus only shows the diffraction signals for the lipids themselves. The profile at 100 % gives a maximum water signal. The difference between both, shown in Figure 23 a) and b), indicates the position of any water molecules. This difference in signal can only be observed within the two outer head group regions. The change in relative humidity (R.H.) from 57 % which is about the natural moisture content of the skin^[38] to 98 % R.H. did not show a change in absolute signal intensity so no change in water content (Figure 23 c)).

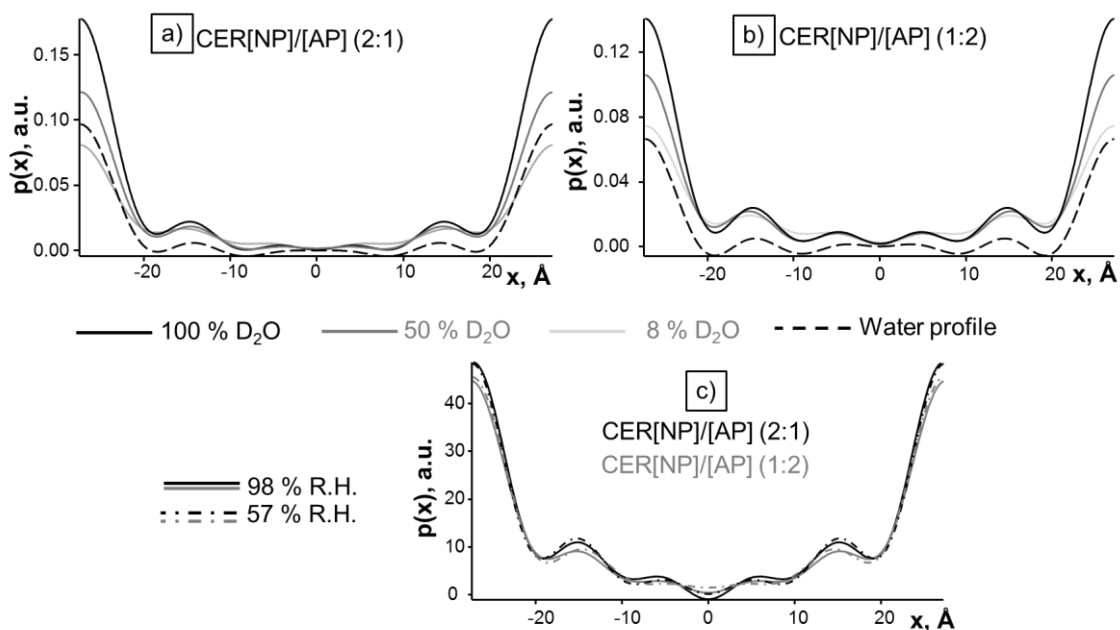


Figure 23: NSLD for the three different H₂O/D₂O contrasts a) for the non-deuterated CER[NP]/[AP] (2:1). b) for the non-deuterated CER[NP]/[AP] (1:2). And c) for both non-deuterated systems at the two different humidities 98 % and 57 %.

Also no change in spacing, thus no swelling by any kind of structural change affecting the lamellar structure was observed. This shows that the water molecules are pretty tightly bound to the head groups and no additional water can penetrate even at very high moisture. This water fixation is due to a strong H-bonding network within the head group region^[153–155]. This is in accordance to the observation made by Gruzinov et al. that the SPP does not change under the influence of excess hydration^[155]. The same was true for the change of temperature from 37 °C to 32 °C which did not yield any noticeable structural change.

Within the middle area of the lamellar structure, the long acyl-chains are located. These are showing only very weak diffraction signals, due to the coherent scattering length b_c of the carbon ($b_c=6.64$ fm) and hydrogen ($b_c=-3.74$ fm) which overall results in a signal that is around zero. This results in a minimum for the NSLD within the lamellar mid-plane. For the systems consisting of symmetric short-chain CER this minimum is very pronounced. This is due to the more negative scattering length density caused by the terminal CH₃ group. In contrast to this, the minimum for the long-chain CER is much less distinct, which further hints to an overlapping arrangement with the CH₃-groups not located in the same region of the lamellae^[156].

By using specific partially deuterated CER, the position of the CER methyl groups within the lamellae and thus the nanostructure could be investigated in even more detail. Due to the positive difference in neutron scattering length with the deuterium atoms ($b_c = 6.67$ fm), much like for the head group, the position of the terminal end of the C24 chain of the CER could be determined. For both CER two deuteration positions located slightly outward from the lamellar centre were determined for the two ratios 1:2 and 2:1 respectively. Since the deuteration is located at the terminal end of the long chain, the only possible way to achieve two deuteration positions is an arrangement with overlapping long chains. Each of the two deuteration positions thus belongs to the tail of the CER with its head group located in the head group region further away from it. The deuteration position closer to the head group is the one that belongs to the CER of the opposite lamellar leaflet (Figure 24).

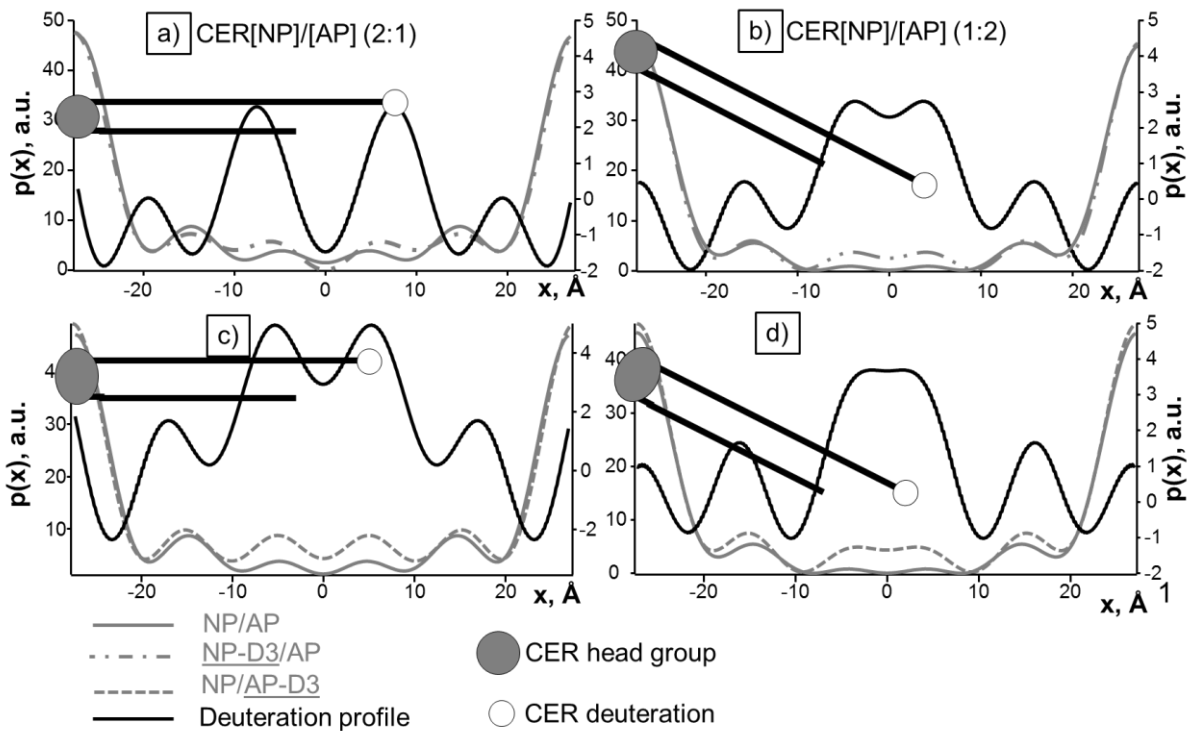


Figure 24: NSLD for the two investigated model systems CER[NP]/[AP] 2:1 a) and c) and 1:2 b) and d). The profiles of the deuterated and non-deuterated samples are compared. For the deuterated CER[NP] a) and b) and for the deuterated CER[AP] c) and d). A possible arrangement of the investigated CER within each lamellar system is indicated by a stylized CER molecule.

Most interesting however was the difference within the nanostructural arrangement of the lipid tails between the CER[NP] and [AP] as well as between the two different ratios. Due to the as described otherwise overall very low and uniform neutron scattering profile of the lipid tails, this difference could only be observed using the specifically deuterated lipids. Two factors were notable, the first is the difference between the two systems, which is the position of the terminal end of both the CER[NP] and [AP] within the different systems. For the system with the [NP]/[AP] ratio of 1:2 which's properties are mainly determined by the CER[AP], both deuteration peaks are located closer to the lamellar mid-plane. Since, as already shown above, the arrangement is most likely one with overlapping long acyl-chains, this would mean, that the terminal ends are located closer to the corresponding head group region than for the native-like 2:1 system. Both systems however show the same repeat distance and thus lamellar thickness. Energetically the most likely cause for this is a slightly tilted arrangement of the CER chains. This could also explain the identical repeat distance, since otherwise the overall lamellar thickness would also decrease with chains arranged in a tilted fashion. The chains of the native-like 2:1 system on the other hand would be arranged mostly straight causing the observed broader overlapping area and CD_3 positions further away from the lamellar mid-plane.

The second notable observation is the difference between the deuteration positions of the CER[NP] and [AP] that can be detected in both systems. It is thus contributed to the difference between the CERs themselves. For the CER[AP] the deuteration positions are always located further towards the lamellar centre and thus also the corresponding head group region than observed for the CER[NP]. This effect could also be a result of a changed tilt, since however two different tilts within the two CER in the same lamellar system would be geometrically unfavourable. This makes it more likely, that the CER[AP] C24 chain is indeed arranged in a fashion, that in contrast to the CER[NP] C24 chain, somehow shortens it within the lamellar system. Since the only chemical difference between the CER[NP] and [AP] is one additional hydroxyl group at the C2 of the C24 chain of the [AP] this chemical difference has to be the cause.

The additional peaks in the difference (deuteration) profiles slightly inward from the head group region which are observed especially in Figure 24c are mainly a result of the limited number of diffraction peaks. With a finite number of diffraction peaks, only a finite number of wave functions can be calculated, giving the profile a still very wave-like appearance. Due to the differences introduced by the deuteration, the shape of the overall profile was slightly changed, yielding the error especially at this position. Since the observed deuteration peaks however always show about double the intensity of the error peaks they can easily be distinguished from the errors. It has furthermore to be considered, that no normalization of the difference profile to total signal intensity was not performed, thus at the outer borders the error is higher, due to the higher signal.

4.1.3 Discussion

This study was able to show that CER[NP]/[AP] based model systems form a continuous lamellar system in both investigated ratios. Macroscopically, these systems seem to simulate the SC lipid matrix quite well. The lamellar thickness is comparable to observations of the SPP within electron microscopic images of native skin^[104]. It is furthermore very stable under varying hydration, not showing any swelling as observed in other model systems before^[155]. The overlapping long chains within the lamellar mid-plane are also in good agreement with many other studies. One example is a model based study focusing on the C24 CER[NS] that even predicts a kind of liquid like behaviour for this overlapping middle area^[70]. But also more complex mixtures, mimicking the composition of the SC lipid matrix more closely show similar phase behaviour and lamellar arrangement to the basic model investigated here. One study for example performed neutron diffraction experiments on a reconstructed native-like model membrane system, only missing the CER[EOS], which formed an SPP. A CER[NS] with a perdeuterated C24 chain was used to determine its position within the lipid matrix. A symmetric hairpin folded configuration with interdigitating fatty acid tails was concluded as most likely arrangement. The system also had a comparable repeat distance of 5.4 nm. This study calculated that about 2 water molecules are bound per CER indicating minimal hydration and thus minimal effect of hydration on the lamellar structure^[69]. To our knowledge, this makes the model system investigated here the first system, that shows a native-like lamellar structure while containing only so few components. Despite the only small chemical differences between the CER, different mixtures did show a wide variety of different structures and properties in the past. These include variable repeat distances^[64,87,157], in some cases also phase separation^[87] and other distinct effects. As expected, the used two CER as two of the most abundant, especially the asymmetric C24 variants seem to have a very strong influence on the lamellar structure of the SPP of the native SC lipid matrix.

The simplicity of the system used in this study gives it a clear advantage, in terms of general applicability. Within the more complex CER mixtures used before, it was for example not possible to specifically assess the properties of single CER variants^[69,114]. Especially for pharmaceutical and industrial purposes an extremely expensive and complex mixture is no applicable option. A simple four component system with native-like properties on the other hand could possibly be utilized as a simple yet effective tool for various purposes.

As discussed by Das et al., an overlapping middle layer as described for the systems investigated here could very well serve an important biological function. First of all a high resistance against shear stress could be the result, moving the more rigid outer regions against each other, only influencing the flexible middle layer^[70]. Furthermore, it could be possible, that such an interdigitation stabilizes the interaction between both leaflets of the lamellae, improving the overall miscibility of different lipids. These regions with different solubility properties would furthermore enhance the barrier function of the lipid matrix. Most molecules are either polar or non-polar, even amphoteric molecules have regions that are either of these. According to the laws of enthalpy if the molecule or a part of the molecule is not well soluble in

one of the layers it will preferentially be located back to a layer of better solubility and would thus not be able to penetrate deeper into the SC. This works only, if this effect is stronger than the influence of entropy, aiming for a random distribution, thus this strong solubility difference is necessary for a most effective barrier.

The most interesting aspect of the obtained results however is the notably different nanostructure of the CER[NP] and [AP] which was observed. Since chemical differences between CER species are mostly very minor, one could assume that structural differences should also be minor and the CERs may be even mostly redundant. As shown within several studies before however this is not the case. In this study we were also able, to demonstrate a major differences, as a result of a single additional OH-group at the C2 of the C24 chain of the CER[AP]. It led to a shorter C24 chain arrangement within both lamellar systems. An imaginable arrangement that could shorten the CER[AP] chain would for example be one, with the additional OH-group located further within the head group region, due to additional H-bonds. This would pull the C24 chain slightly towards the head group region and due to the overlapping closer to the lamellar centre. For the head group of the CER[NP] it was demonstrated, that all H-donors and acceptors partake in an extended H-bonding network^[75,76,81]. For the head group of the CER[AP] however this seems to be not the case. For this CER a strong H-bonding network could also be observed, however some studies concluded that the additional OH-group does not partake in any H-bonding, but instead disrupts the existing network, due to its unfavourable position. This could possibly also lead to structural changes, somehow shortening the C24 chain.

Most notable is also the difference between the native-like 2:1 ratio which shows a mostly straight chain arrangement, while the higher CER[AP] content in the 1:2 system leads to a chain tilt. The reason why the lamellar thickness does not change, despite the tilted chains would in theory take up less perpendicular space, is most likely the chain tilt itself. Since the chain overhangs within the lamellar mid-plane can move more freely than the rigid chains within the outer region, they would still be arranged straight since they would interact with each other, which would not be possible with a differing tilt. Since the long chains right at the boarder of the middle layer are however tilted, the straight overhangs cannot interdigitate into the opposing layer any further than up to this boarder, preventing a change in lamellar thickness. A geometrical model showing this effect graphically is given in Figure 25.

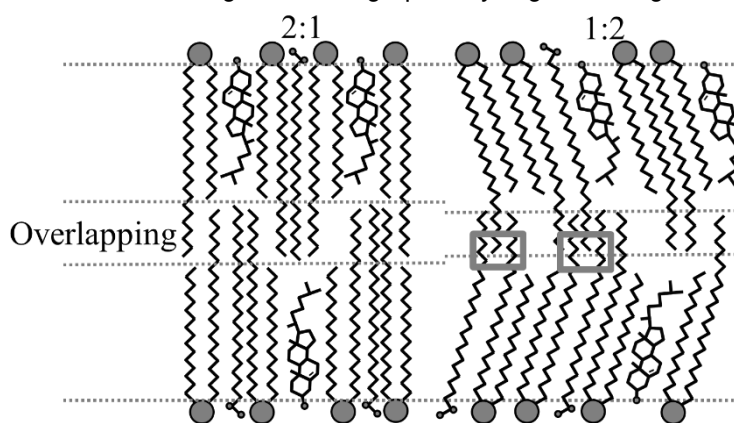


Figure 25: Proposed arrangement for the CER[NP]/[AP] 2:1 and 1:2 ratio model system including CHOL and LA. The grey boxes indicate regions, preventing the loss of lamellar thickness, despite the chain tilt.

These results were never before observed with this amount of detail.

The exact nanostructural difference between the CER[NP] and [AP] leading to their differing length is however not yet clear, since it cannot be determined in any more detail without further investigating this model system and especially the head group architecture and chain conformation. Since only one chain is deuterated at the moment, no finite conclusion on the chain conformation is possible. The observed data however very much suggest a hairpin-folded arrangement as shown in Figure 25, illustrating the proposed arrangement for both systems, assuming the hairpin conformation.

As described above, the CER[NP] and D-isomer of the CER[AP], especially the C24 variants were not much investigated so far and not at all, using neutron diffraction. Also the systems were either short chain or very complex systems. To obtain these results especially with the given amount of detail was only possible, by using the specifically deuterated CER molecules in combination with neutron diffraction as a powerful tool. In side by side comparison to the system, using a perdeuterated CER[NS] to assess the chain arrangement discussed above, the advantages of the specific deuteration in this instance can clearly be demonstrated. While the perdeuterated chain has the advantage that the whole chain is detectable, it is not suitable to show much detail on the nanostructure. For the perdeuterated CER, due to the overall much higher diffraction signal, the whole NSLD profile shows elevated values, even slightly in the head group region. Concerning the nanostructure only the general area where the chains overlap can be estimated^[69]. Using the specifically deuterated CER on the other hand it was possible to determine a distinct single position for each terminal CD₃ group, even if they were in almost direct proximity. This even allowed for the observation of the slightly shorter length of the alkyl chains of CER[AP].

This study demonstrates, that for a thorough investigation of the SCs properties, it is important, to approach it from both sides. To investigate very complex systems for the macroscopic influence of certain factors like pH, ion concentration, fatty acid or CER chain length composition. It is however just as important to investigate the nanoscopic influence of single CER variants on the lamellar structure to understand its properties. In terms of general applicability however, the simpler systems are by far superior due to cost issues, less complex preparation, handling and observable amount detail, especially in combination with specifically deuterated CER.

4.1.4 Conclusion

In this study it was possible to demonstrate that the two CER [NP] and [AP] which are the two most abundant CERs in the SC are also a main determining factors for the typical lamellar structure of the SC lipid matrix. Using these two CER a model system could be realized that was very closely mimicking the native SC lipid matrix. They form a single continuous lamellar phase for both applied molar ratios of [NP]/[AP] = 2:1, which is about the native ratio and 1:2 to study the influence of the CER[AP].

The mixture behaves very much like the native SC lipid matrix. The observed lamellar thickness of 5.45 ± 0.1 nm is about the same as for the native SPP. The long C24 tails of the lipids are overlapping within the lamellar centre which also seems to be a feature of the native SC lipid matrix.

Most intriguing, however, is the difference that was observed between the two CERs with the CER[AP] appearing to be somehow shorter than for the [NP] reducing the overlapping area in the lamellar mid-plane. The unnaturally higher CER[AP] content of [NP]/[AP] 1:2 also led to an arrangement with the acyl-chains having a stronger tilted arrangement which also reduced their overlapping within the mid-plane, without however influencing the lamellar repeat distance. For the native-like [NP]/[AP] 2:1 ratio on the other hand the chains were arranged mostly straight with broad overlapping region in the lamellar mid-plane. Only by using the specifically deuterated CERs it was possible to observe these details.

4.2 Determination of the influence of C24 D/(2R)- and L/(2S)-isomers of the CER[AP] on the lamellar structure of *stratum corneum* model systems using neutron diffraction

Chemistry and Physics of Lipids 209 (2017) 29–36



Contents lists available at ScienceDirect

Chemistry and Physics of Lipids

journal homepage: www.elsevier.com/locate/chemphyslip



Determination of the influence of C24 D/(2R)- and L/(2S)-isomers of the CER[AP] on the lamellar structure of *stratum corneum* model systems using neutron diffraction



Thomas Schmitt^{a,1}, Stefan Lange^{b,c,1}, Stefan Sonnenberger^c, Bodo Dobner^c, Bruno Demé^d, Reinhard H.H. Neubert^{a,*}, Gert Gooris^e, Joke A. Bouwstra^e

^a Institute of Applied Dermatopharmacy at the Martin Luther University Halle-Wittenberg (IADP), Weinbergweg 23, 06120 Halle/Saale, Germany

^b Institute of Medical Physics and Biophysics, University of Leipzig, Härtelstraße 16-18, 04107 Leipzig, Germany

^c Institute of Pharmacy, Martin Luther University Halle-Wittenberg (MLU), Wolfgang-Langenbeck-Str. 4, 06120 Halle/Saale, Germany

^d Institut Laue-Langevin, 71 Avenue des Martyrs, CS 20156, 38042 Grenoble CEDEX 9, France

^e Leiden Academic Centre for Drug Research, Department of Drug Delivery Technology, Gorlaeus Laboratories, University of Leiden, Max Planckweg 8 2333 CE Leiden, The Netherlands

ARTICLE INFO

Keywords:

Ceramides
Stratum corneum
Skin
Membrane
Lipids
Neutron diffraction

ABSTRACT

This study was able to investigate the different influence of the D- and L-ceramide [AP] on the lamellar as well as molecular nanostructure of *stratum corneum* simulating lipid model mixtures. In this case, neutron diffraction together with specifically deuterated ceramide was used as an effective tool to investigate the lamellar and the molecular nanostructure of the mixtures. It could clearly be demonstrated, that both isomers show distinctly different characteristics, even though the variation between both is only a single differently arranged OH-group. The L-ceramide [AP] promotes a crystalline like phase behaviour even if mixed with ceramide [NP], cholesterol and free fatty acids. The D-ceramide [AP] only shows crystalline-like features if mixed only with cholesterol and free fatty acids but adopts a native-like behaviour if additionally mixed with ceramide [NP]. It furthermore demonstrates that the L-ceramide [AP] should not be used for any applications concerning ceramide substitution. It could however possibly serve its own purpose, if this crystalline like behaviour has some kind of positive influence on the SC or can be utilized for any practical applications. The results obtained in this study demonstrate that the diastereomers of ceramide [AP] are an attractive target for further research because their influence on the lamellar as well as the nanostructure is exceptionally strong. Additionally, the results furthermore show a very strong influence on hydration of the model membrane. With these properties, the D-ceramide [AP] could be effectively used to simulate native like behaviour even in very simple mixtures and could also have a strong impact on the native *stratum corneum* as well as high relevance for dermal ceramide substitution. The unnatural L-ceramide [AP] on the other hand should be investigated further, to assess its applicability.

<https://doi.org/10.1016/j.chemphyslip.2017.11.001>

4.2.1 Materials and Methods

4.2.1.1 Preparation and Separation of the CER[AP] Diastereomers

The CER[NP] (N-(tetracosanoyl)-phytosphingosine) and terminally deuterated CER[NP]-D₃ (N-(tetracosanoyl-24,24,24-D₃)-phytosphingosine) was prepared according to Sonnenberger et al.^[158]. The racemic CER[AP] (N-(2R/S-hydroxytetracosanoyl-24,24,24)-phytosphingosine) was kindly provided by Evonic Industries AG and the racemic terminally deuterated CER[AP]-D₃ (N-(2R/S-hydroxy-tetracosanoyl-24,24,24-D₃)-phytosphingosine) synthesized correlative to Sonnenberger et al.^[23].

For separation of the L- and D-diastereomers the racemic CER[AP] and CER[AP]-D₃ were absorbed on a small amount of silica gel (SiO₂:CER 2:1) and separated by column chromatography with fresh distilled chloroform and methanol (SiO₂:CER_{rac} 200:1; CHCl₃:MeOH:0.5%_{v/v} NH₃aq 96.5:3.5 for (L-CER[AP]-D₃))

followed by 95:5 for (D-CER[AP]-D₃). The separation process was followed by thin layer chromatography (CHCl₃:MeOH:NH_{3(aq)} 90:10:0.5 *R_f*= 0.52 (L-CER[AP] and L-CER[AP]-D₃), 0.27 (D-CER[AP] and D-CER[AP]-D₃). The purity of the L- and D-forms were also checked by HPLC (chromatograms: see supporting information). The L-CER[AP]-D₃ and D-CER[AP]-D₃ were also characterised by ¹H-/¹³C NMR and HRMS (spectra and data: see supporting information).

4.2.1.2 Sample PreparationBN

For the performed experiments, mixtures of CER, CHOL and lignoceric acid (LA) were prepared in a 1:0.7:1 ratio. CHOL and LA were purchased from Sigma Aldrich GmbH (Taufkirchen, Germany). The CER[NP], D- and L-CER[AP] as well as their terminally deuterated derivatives were obtained as described above. The chemical structures of the used deuterated CER are displayed in Figure 26.

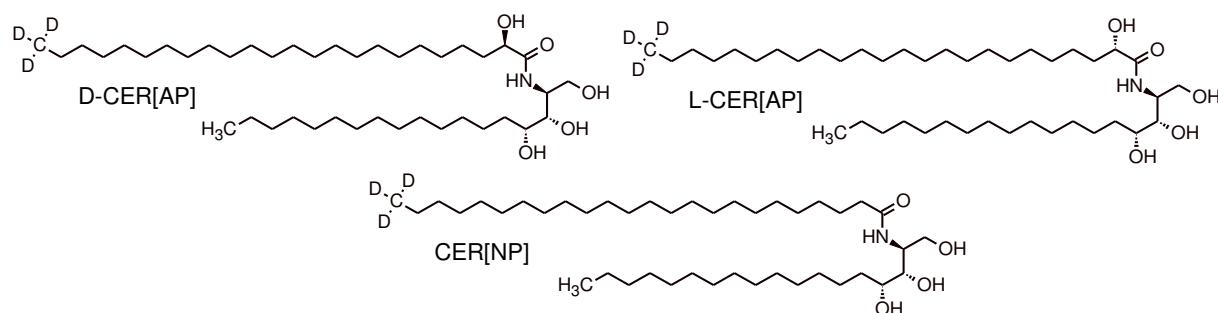


Figure 26: Structures of the deuterated lipids used for these experiments.

The SC model membranes were prepared on quartz glass slides. For sample application, the pure substances were dissolved in a 2:1 mixture of chloroform and methanol (analytical grade, Sigma Aldrich) with a concentration of 10 mg/ml. These solutions were then combined to generate the CER/CHOL/FFA mixtures, according to Table 10. For each system, a corresponding system with deuterated CER[AP] for use in neutron scattering experiments was prepared. For deposition, the mixtures were sprayed onto the surface, using an airbrush instrument (Harder & Steenbeck, Norderstedt, Germany).

Table 10: Used mixtures of CER[NP]/CER[AP]/CHOL/LA

Mixture	Molar ratio (n/n)
CER[NP] / D-CER[AP] / CHOL / LA	0.66/0.34/0.7/1
CER[NP] / D-CER[AP]-D ₃ / CHOL / LA	0.66/0.34/0.7/1
CER[NP] / L-CER[AP] / CHOL / LA	0.66/0.34/0.7/1
CER[NP] / L-CER[AP]-D ₃ / CHOL / LA	0.66/0.34/0.7/1
D-CER[AP] / CHOL / LA	1/0.7/1
D-CER[AP]-D ₃ / CHOL / LA	1/0.7/1
L-CER[AP] / CHOL / LA	1/0.7/1
L-CER[AP]-D ₃ / CHOL / LA	1/0.7/1

The samples were sprayed at a temperature of 70.5 °C which is below the melting point of the mixture. Afterwards the samples were annealed, to form the multilamellar structure by heating under high humidity for 2 h, cooling at room temperature for 1 h and again heating under high humidity for 1 h.

4.2.1.3 Neutron Diffraction Experiments

For the neutron diffraction experiments the SC model membranes were prepared as described above. Diffraction data were collected at the small-angle diffraction instrument D16 located at the Institute-Laue-Langevin (ILL) in Grenoble, France. A highly oriented pyrolytic graphite monochromator was used to reflect neutrons with a wavelength of $\lambda=4.55$ Å to the sample. The sample angle ω was rotated in ω -scans and the intensity of the scattered neutrons was recorded as a function of the scattering angle 2Θ

on a 2D ^3He detector placed at a distance of 950 cm from the sample. The detector is made of arrays of 320 anodes x 320 cathodes spaced by a distance of 1 mm providing a detector resolution of 1 mm x 1 mm. For contrasting against the water scattering length density, three different $\text{H}_2\text{O}/\text{D}_2\text{O}$ ratios of 0:100, 50:50 and 92:8 (w/w) were applied. A higher D_2O content also generates a higher signal-to-background ratio, which allows for the detection of peaks of higher diffraction orders with high precision. These higher order peaks are very important for calculation of a detailed neutron scattering length density profile (NSLD). For the scans, the temperature for contrast variation was kept at 32 °C. The relative humidity was kept at either 98 % or 57 % using the D16 humidity chambers developed at ILL to see the influence of humidity. Since it could be observed that no change in the diffraction signal occurred after about 6 h of equilibration, samples were given a period of at least 7 h after any change of either temperature, humidity or $\text{H}_2\text{O}/\text{D}_2\text{O}$ ratio. The membrane spacing was determined according to Bragg's law $n\lambda = 2d \sin(\theta)$. The NSLD $\rho(x)$ was calculated by Fourier synthesis of the structure factors F_n according to:

$$\rho(x) = a + b \frac{2}{d} \sum_{n=1}^{n_{max}} F_n \cos\left(\frac{2\pi nx}{d}\right)$$

The coefficients a and b are for relative normalisation of $\rho(x)$, d is the lamellar periodicity and n the order of diffraction. The absolute values of the structure factors could be calculated as $|F_n| = \sqrt{h_n A_n I_n}$, with h_n as the Lorentz correction, A_n as absorption correction^[146] and I_n as Intensity of the nth peak. The integration of the Bragg's peak intensities were performed using the IGOR Pro 6.1 software (WaveMetrics Inc., Portland, OR, USA). For the Fourier transform, both the absolute value as well as the phase sign of each structure factor F_n is required. Assuming a Gaussian water distribution with a maximum position $x = \frac{d}{2}$ within the hydrophilic head group region, allows determination of the F_n by application of different $\text{H}_2\text{O}/\text{D}_2\text{O}$ contrasts, representing an *isomorphous* replacement^[146,149]. The centro-symmetric lipid arrangement which is to be expected of CER-membranes leads to a phase of either + or – for each F_n . A three point measurement with three different $\text{H}_2\text{O}/\text{D}_2\text{O}$ contrasts is thus sufficient for the calculation of the phase of each structure factor. A detailed description of this can be found elsewhere^[146–148].

4.2.1.4 Small angle X-Ray diffraction

For small angle X-ray diffraction (SAXD) measurements, a small amount of about 5 mg of sprayed material was scraped from the glass support. This material was brought onto a supporting membrane (Whatman nucleopore polycarbonate) together with a droplet of water to stick it to the support for the measurement. The membrane was mounted in a clamp and positioned parallel to the beam. The diffraction data were collected during 120 seconds at 25 °C on a 2D detector (Pilatus 1M). The diffraction rings were integrated over 40 degrees to obtain a one-dimensional intensity profile. The scattering vector q as indicated on the x-axis is calculated from the scattering angle Θ as follows: $q = \frac{4\pi \sin(\Theta)}{\lambda}$. The wavelength λ was 0.1033 nm and the sample to detector distance was 2.1 meter. The measurements were performed at station BM26B of the European Synchrotron Radiation Facility in Grenoble, France.

4.2.2 Results

From the measured diffraction patterns, NSLDs were calculated as described above. Due to the use of the specifically deuterated CERs, additionally to the lamellar arrangement, the molecular nanostructure of the systems could be assessed. All structure factors that could be determined by the $\text{D}_2\text{O}/\text{H}_2\text{O}$ -contrast variation were in phase with uneven factors with a negative and even factors with a positive

sign as shown in Table 11. For the solely L-CER[AP] based system no structure factors could be determined and will be explained in further detail later.

Table 11: Structure factors F_n for diffraction orders 1-5 at 100 % D₂O and 98 % R.H.

	CER [NP]/D-[AP] (2:1)	CER [NP]/D-[AP]-D3 (2:1)	CER [NP]/L-[AP] (2:1)	CER [NP]/ L-[AP]-D3 (2:1)
F ₁	-0.335 ± 0.001	-0.287 ± 0.001	-0.411 ± 0.003	-0.337 ± 0.002
F ₂	0.220 ± 0.002	0.244 ± 0.006	0.193 ± 0.008	0.232 ± 0.004
F ₃	-0.185 ± 0.003	-0.192 ± 0.006	-0.196 ± 0.014	-0.191 ± 0.009
F ₄	0.160 ± 0.005	0.151 ± 0.012	0.111 ± 0.018	0.130 ± 0.013
F ₅	-0.100 ± 0.006	-0.126 ± 0.013	-0.088 ± 0.022	-0.110 ± 0.020
	CER D-[AP]	CER D-[AP]-D3	CER L-[AP]	CER L-[AP]-D3
F ₁	-0.421 ± 0.003	-0.297 ± 0.005	n.a. ± n.a.	n.a. ± n.a.
F ₂	0.206 ± 0.008	0.347 ± 0.006	n.a. ± n.a.	n.a. ± n.a.
F ₃	-0.173 ± 0.016	-0.122 ± 0.020	n.a. ± n.a.	n.a. ± n.a.
F ₄	0.131 ± 0.022	0.155 ± 0.018	n.a. ± n.a.	n.a. ± n.a.
F ₅	-0.069 ± 0.022	-0.079 ± 0.036	n.a. ± n.a.	n.a. ± n.a.

The data for the CER[NP]/D-CER[AP]/CHOL/FFA (0.66/0.33/0.7/1) system are taken from a prior already published experiment at the V1 membrane diffractometer at the Helmholtz center Berlin^[159]. From the results of this study, it could be observed that the D- and the L-CER[AP] have a distinctly different influence on the lamellar structure, both CER together with CER[NP] and as only CER in the mixture. Despite the small difference between the two isomers, they promote a completely different nanostructural arrangement of the lipid lamellae. For the CER[NP]/D-[AP] system from an earlier experiment^[159], the overall scattering profile is flat, hinting to a mostly straight carbon chain arrangement. No distinct minimum in the lamellar middle was observed. This together with the two observed deuteration positions indicates the C24 chains overlapping in the lamellar mid-plane. The system shows a repeat distance of 5.48±0.09 nm, which is also conclusive with mostly straight, overlapping lipid chains (Figure 27 a).

For the CER[NP]/L-[AP] system the profile is instead V-shaped with a distinct scattering minimum in the lamellar mid-plane. This indicates a tilted arrangement, with both CH₃ located in the lamellar-centre, leading to the minimum. The single very strong deuteration position in the lamellar centre is also conclusive with this arrangement and results from both CD₃ being in direct proximity. The repeat distance of 5.49±0.04 nm is equal to the first system. This and the single deuteration position are conclusive with an arrangement with tilted chains. Otherwise without the overlapping long chains, the repeat distance would necessarily increase, compared to the overlapping system (Figure 27 b).

The D-CER[AP] as only CER also led to a V-shaped scattering profile, much like the CER[NP]/L-[AP] mixture. The profile again had a distinct minimum in the lamellar centre, indicating an arrangement of CER with tilted chains. The very strong single deuteration signal also supports such an arrangement as the most likely one. The very strong deuteration signal furthermore hints to a very rigid chain arrangement, not dispersing the deuterium atoms due to a limited movement of the tails and especially the terminal groups. This could be hinting to a more crystalline-like arrangement compared to other CER mixtures. The thickness of 5.28±0.03 nm is shorter than for the mixed systems. This together with the single deuteration position suggests a strong chain tilt (Figure 27 c).

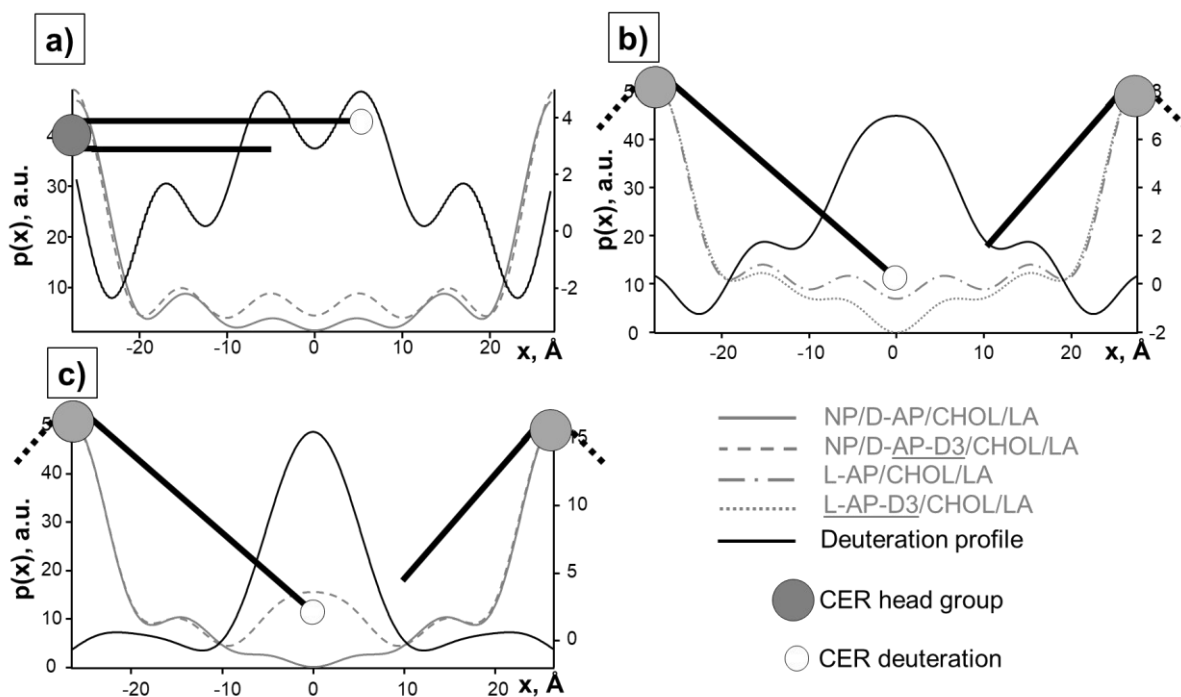


Figure 27: Resulting neutron scattering length density profiles for the investigated samples. Difference profiles between the deuterated and non-deuterated samples, shown in black, indicate the localization of the deuterium labels (right axis). Suggested most likely arrangements of the used deuterated CER are indicated by a stylized CER molecule. a): CER[NP]/D-CER[AP]/CHOL/LA (0.66/0.34/0,7/1). b): CER[NP]/L-CER[AP]/CHOL/LA (0.66/0.34/0,7/1). c): D-CER[AP]/CHOL/LA (1/0,7/1).

The D- and L-CER[AP] expressed a distinctly different behaviour. Considering the more crystalline characteristics of the L-CER[AP], it was assumed, that the system may yield a lamellar structure if annealed at a higher temperature. Re-annealing of the sample at a higher temperature was consequently tried. This was performed in three steps, first at 75 °C, later at 80 °C and 85 °C, checking the sample again after every temperature step. However, no changes were observed up to 85 °C which led to a complete loss of signal for the sample, indicating a complete disordering of the system.

Using SAXD, it could be shown that all three lamellar systems show only one main phase, that is very similar for all three. Additionally, a very small amount of phase separated crystalline CHOL at 3.42 nm was detected (Figure 28 a-c) which is in perfect conclusion with the observations made using the neutron diffraction. Furthermore, a small amount of CER[NP] also seemed to be phase separated, detectable at ~3.8 nm. This can be considered as an artefact from the preparation, since the CER[NP] is not well soluble and re-precipitates pre-emptively in a small amount. For the system with the L-CER[AP] as only CER, no distinct diffraction pattern and thus no lamellar structure could be observed from the neutron diffraction data. For the L-CER[AP] just like in the neutron diffraction experiments, with the SAXD, no clear phase was observable. The observed peaks were very broad, maybe indicating an inhomogeneous phase arrangement. The repeat distance for this phase with about 4.56 nm was also much shorter than for the other systems. Unfortunately, since the phase could not be observed clearly, neither using neutron diffraction nor using SAXD, its structure could not be validated any further. There was also a weak third phase observed for this sample with a repeat distance of about 2.11 nm which could correspond for example with a phase separated CER monolayer (Figure 28 d).

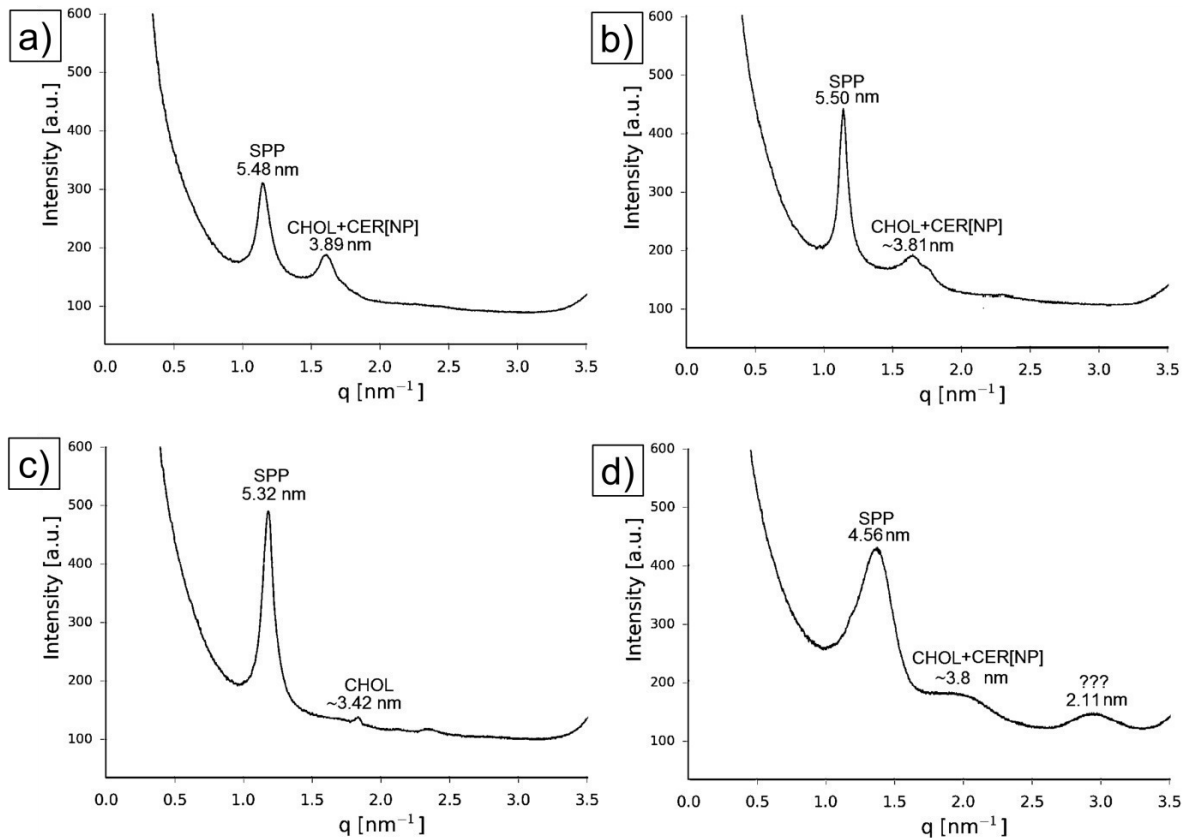


Figure 28: Resulting SAXD profiles for the investigated base mixtures. a): CER[NP]/D-CER[AP]/CHOL/LA (0.66/0.34/0,7/1). b): CER[NP]/L-CER[AP]/CHOL/LA (0.66/0.34/0,7/1). c): D-CER[AP]/CHOL/LA (1/0,7/1). d): L-CER[AP]/CHOL/LA (1/0,7/1).

For none of the systems, which formed a lamellar phase, swelling could be observed upon raising the humidity from 57 to 98 % (Figure 29 a, b and c). Due to the contrast variation it was possible, to locate the water within the system. Except for the HG region, no water could be located within the lamellar structure (Figure 29 d, e and f). To gain information on the relative water content within the different systems, the difference between the minimum and maximum point of the water profile (100 % D₂O-8 % D₂O) at 98 % R.H. was determined and normalized to the difference between the minimum and maximum point of the corresponding 100 % D₂O 98 % R.H. NSLD. It could be shown, that the water content is about 52 % for the CER[NP]/D-[AP] system (Figure 29 d), 20 % for the CER[NP]/L-[AP] system (Figure 29 e) and 30 % for the D-CER[AP] system (Figure 29 f).

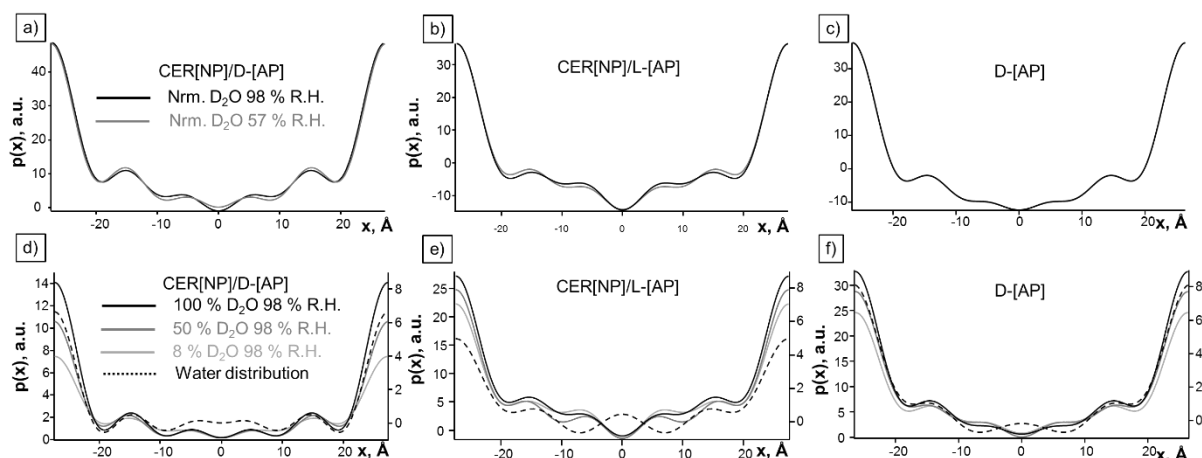


Figure 29: Resulting neutron scattering length density profiles for the investigated samples. The differences between the different applied humidities of 57 % and 98 % are shown above. (a-c) The differences between the three D₂O/H₂O contrasts and water profiles (right axis) are shown below (d-f). a+d): CER[NP]/D-CER[AP]/CHOL/LA (0.66/0.34/0,7/1). b+e): CER[NP]/L-CER[AP]/CHOL/LA (0.66/0.34/0,7/1). c+f): D-CER[AP]/CHOL/LA (1/0,7/1).

The much lower water content for the D-CER[AP] and especially the CER[NP]/L-[AP] systems could again be hinting to a more crystalline arrangement with the water content being mainly dependent on the CER[AP] content, the overall arrangement and the respective Isomer.

Reflection and transmission microscopy was performed on the sprayed mixtures as well as the pure crystalline CER spread on a microscopic glass slide to gain additional information on the phase behaviour (Supporting Material). The results confirmed a more liquid-like behaviour for CER[NP]/D-[AP] based mixtures and a crystalline-like character for D-CER[AP]. L-CER[AP] and its mixture with [NP] showed mixed features, depending on the scale. In a small scale, L-CER[AP] formed crystalline-like structures, however on a larger scale it was mainly disordered and wax-like (Figures S9-11).

4.2.3 Discussion

The findings of this study are in good conclusion with prior results and observations made during the synthesis and purification of the used CER. The CER[AP] expressed crystalline-like characteristics, the L- even more, than the D-isomer. Crystalline CER show some distinct features compared to lipid mixtures. Crystalline CER[NP] C18 and C24 for example were shown to be polymorphic, yielding multiple different crystal modifications, depending on the crystallization conditions. Either a V-shaped or extended conformation were concluded for most modifications. For the C24 variant partial interdigitation of the long chains could be observed only for some of the different modifications^[75,79,83,85]. The observed thickness of a single layer for crystalline CER is generally lower than for lipid mixtures. Simpler for example CHOL+CER or FFA+CER mixtures tend more towards crystalline-like behaviour than complex mixtures. This is a result of the often V-shaped or somehow tilted arrangements as described above and furthermore, of the slightly disturbed and thus less dense chain packing in more complex mixtures^[111,160–162]. Furthermore were crystalline CER phases shown to hardly be influenced by water penetration due to a very low water content^[163]. On the other hand, for many of the modifications, also a hydration dependent increase in repeat distance was reported. This effect was attributed to the V-shaped conformation, assuming that the chain opening angle increases with increasing hydration^[75,79,83,85].

For the mixture of CER[NP] and L-[AP] and the one with only D-CER[AP], the observed results hint to such a crystalline-like arrangement. First of all many features of the NSLDs that were calculated hint towards slightly angled V-shaped arrangement of the CER, which is very atypical for lipid mixtures but very well in consensus with a crystalline arrangement as described above. Especially the single and very strong deuteration position for both systems hints towards such an arrangement, without the long chains overlapping, due to the small tilt angle. Furthermore the much lower water content compared to the CER[NP]/L-[AP] system also fits a crystalline-like behaviour. However no phase separation was observed, meaning the CHOL and FFA partake in the formation of this phase. An increased repeat distance upon hydration assumingly caused by the V-shaped CER was not observed. This however has most likely just to be contributed to the annealing process, since it was shown, that crystalline CER can only be hydrated above the chain melting temperature, as long as the head group interactions stay intact^[164]. Since the head group interactions including the bound water molecules are very strong they should stay intact, if the sample is not excessively heated or dried. The described crystalline-like behaviour was also confirmed by the observations made in reflection and transmission microscopy.

The phase arrangement for the L-CER[AP] as a single CER cannot be discussed in detail, since no clearly distinguishable phase arrangement could be observed, neither using neutron diffraction nor SAXD. It is possible, that the structure of the L-CER[AP] does not allow correct mixing with CHOL and LA, if not moderated by the CER[NP]. The L-CER[AP]'s irregular phase behaviour which was observed in the SAXD and neutron diffraction experiments could be partially be explained by its crystallisation characteristics. In the performed microscopic experiments L-CER[AP] was observed to be able to form

crystalline-like arrangements but only on a nanoscopic scale. Mixed with CER[NP] this seems to be the favoured characteristic. On a macroscopic scale however it had a rather disordered and wax-like appearance, which could explain the lack of a lamellar phase in the neutron diffraction experiments and the broad peaks observed in the SAXD-experiments. This could be for example a result of the L-CER[AP]s HG featuring strongly with intramolecular interactions, leading to a full extended conformation with the tails partially disordered, due to a unfavourable geometrical arrangement. If mixed with the CER[NP] the HG interactions could be shifted to intermolecular instead if intramolecular, possibly reducing or preventing a chain disordering.

The mixture of CER[NP] and D-[AP] on the other hand seemed to be arranged with mostly straight chains and overlapping long chains in the lamellar mid-plane. This is in good conclusion with observations made for the native SC as well as native-like model mixtures^[69,70]. The Lamellar thickness for all three systems is near the native SC short periodicity phase with 5 - 6 nm^[104]. This system is discussed in more detail elsewhere^[159]. For the SPP of a native-like model a value of 5.45 nm was observed. The two CER[NP]/[AP] mixtures fit this thickness while the D-CER[AP] mixture is slightly shorter. The compared to the other investigated systems overall more gel-like character of this mixture was also confirmed by the microscopic investigations. Overall, the CER[NP]/D-[AP] mixture closely resembles the native lipid matrix, while the other two show a rather different arrangement. The distinct differences between the two mixed CER[NP]/[AP] systems clearly demonstrates the very strong influence of the CER[AP] HG on the chain and overall lamellar arrangement.

However, most intriguing about this were the drastic differences, between the two isomers of the CER[AP]. This should be enough to showcase the strong influence of even minor differences within the CER HG. This demonstrates that even though differences between most CER species are rather minute, no high redundancy in their function is to be expected. This is in good accordance to some earlier results also comparing different isomers of α -hydroxy CER. In a monolayer study for example, the D-CER[AS] C18 could be shown, to assume a tighter chain packing than the L-enantiomer, hinting to a disturbance of the chain packing for the D-enantiomer, most likely making it less crystalline^[88]. Crystalline D-CER[AP] C18 showed two and the L-enantiomer three crystalline modifications. A fully extended conformation was suggested for the D- and a V-shaped one for the L-enantiomer^[93]. These results further confirm the differences that were observed in this study. A further interesting detail that was first observed here is the difference in relative hydration between the different systems. This further demonstrates very distinct characteristics between the two isomers and also of the CER[AP] in general. It seems, that at least in the simple two component system with CER[NP] and [AP], the [AP] is the main contributor for the incorporation of water molecules into the HbN. This is especially clear comparing the CER[NP]/L-CER[AP] and D-CER[AP] with the CER[NP]/D-CER[AP] system. The relative water content of the D-CER[AP] with about 30 % is already much lower than for the system in which the [AP] is mixed with the [NP] with 52 %. This is most likely to be contributed to the more crystalline-like behaviour and thus tighter interactions. The relative water content within the CER[NP]/L-[AP] system with only 20 % however is even lower than for the crystalline-like D-CER[AP], despite the presence of the CER[NP]. This hints towards a very high influence of the CER[AP] on lamellar hydration. In this case, the L-CER[AP] if applied for example in a mixture of both isomers would pose the risk of lowering the SC hydration and thus possibly lead to dry skin and a disturbed barrier function. It has to be considered however, that these differences may also solely be a result of the overall different lamellar arrangements and resulting different HG interactions strongly influenced by small changes within these simple model membranes. Within the complex native SC, the impact of this different hydration behaviour could be much smaller or even higher. To further verify this hypothesis, a more complex system with its overall arrangement being less influenced by a change in CER[AP] content, would need to be investigated towards differences in hydration properties.

The differing characteristics of the D- and L-CER[AP] is of much importance for future investigations. For a SC model system or substitute, the CER[AP] content would have to be very precisely right. Only this way, it would be possible to simulate the SC properties correctly, since it has such a strong influence on the nanostructure of both the head group and tail region and also on the overall lamellar arrangement. On the other hand can CER[AP] very well be used to fine tune the nanostructure of simple model systems, to better mimic the complex SC behaviour more closely without the need of a highly complex composition. This together with the possible strong influence on lamellar hydration is most likely also the biological function of the CER[AP] within the lipid matrix. In this case, the CER[AP] could be one of the CER with the most variable relative and possibly also absolute content. This would serve, to counteract small changes in the composition of the other CER, with its strong influence on the lamellar arrangement. This is especially true, since the CER[AP] is one of the two most abundant CER^[26]. This however was not investigated thoroughly so far. Due to these results, it is definitely clear, that no mixture of isomers should be used for scientific research, trying to emulate the properties of the native SC. The unnatural L-isomer has a highly different influence on the lamellar nanostructure of both head group and tail region and on the head group hydration, than the D-isomer. This is even more important for possible pharmaceutical applications of this CER. The L-CER[AP] is an unnatural substance and not contained in the native SC. Since it shows a different behaviour than the natural D-enantiomer, it cannot yet be considered safe. It is possible, that the more crystalline character would lead to a disturbance within the lamellar structure rather than supporting or repairing it, which could lead to negative side effects. On the other hand, if this tendency to form a more crystalline like arrangement has a positive influence on the lipid matrix, the L-CER[AP] could possibly be an attractive substance for pharmaceutical applications. Further investigations, concerning this matter are already in progress.

4.2.4 Conclusion

Overall this study was able to demonstrate the very strong influence of the CER[AP] on the lamellar and nanostructure of multilamellar lipid systems. Of special interest is the strong difference between the D- and L-isomer of CER[AP]. The D-CER[AP] alone shows a crystalline-like behaviour, but together with other CER, in this case CER[NP], it adopts a more native-like arrangement. The L-CER[AP] on the other hand promoted a very crystalline-like behaviour even if mixed with the CER[NP]. For the L-CER[AP] alone no lamellar phase could be observed. This difference is of much importance for future investigations as well as applications of the CER[AP]. No isomeric mixtures can be used, if a native like lipid matrix is supposed to be simulated or if the repair of the native SC is the target. It is possible however, that the L-CER[AP] becomes an interesting target for research and pharmaceutical applications itself, if its more crystalline like characteristics show some kind of fortunate effect on the SC. At this point however the unnatural L-isomer cannot be considered safe, since its exact influence on the SC is yet unknown. It has furthermore to be considered, that it could have a negative influence on skin hydration and could possibly lead to dry skin and a disturbed barrier function, as discussed above. The observed differences clearly showcase the enormous differences, that can result from even small variations in the CER architecture. This demonstrates, that the different CER species, even though variations in their head groups in some cases may be very minor, are not to be expected to show a high functional redundancy. As suggested above, the influence of the CER[AP] on the SC hydration as well as the amount of CER[AP] variability could be interesting targets for future research, to clarify the importance and influence of this CER within the native SC.

4.3 The structure organisation of CER[NS] and CER[AP] in SC modelling membrane systems is surprisingly similar yet noticeably different: A Neutron diffraction study

4.3.1 Abstract

For this study mixtures based on the ceramides [NS] (NS=non-hydroxy-sphingosine) and [AP] (AP= α -hydroxy-phytosphingosine) in a 2:1 and 1:2 ratio, together with cholesterol and lignoceric acid, were investigated. These mixtures are modelling the uppermost skin layer, the *stratum corneum*. Neutron diffraction, utilizing specifically deuterated ceramide molecules, was used to obtain a maximum amount of experimental detail. Highly detailed molecular dynamics simulations were used to generate even more information from the experimental data.

It was possible to observe a single lamellar phase for both systems. They had a lamellar repeat distance of 5.43 ± 0.05 nm for the [NS]/[AP] 2:1 and a slightly shorter one of 5.34 ± 0.05 nm for the 1:2 system. The structure and water content was uninfluenced by excess humidity. Both the experimental and simulation data indicated slightly tilted ceramides, with their C24 chains overlapping in the lamellar mid-plane. This arrangement is well comparable to systems investigated before. The structure of both systems, except for the differing repeat distance, looks similar at first. However, on a smaller scale there were various distinct differences, demonstrating only low redundancy between the different ceramide species, despite only minor chemical differences. The mainly ceramide [AP] determined 1:2 system has a slightly smaller repeat distance. This is a result of a tighter arrangement of the lipids chain along the bilayer normal and increased overlapping of the long chains in the lamellar middle. For the CER[NS] some novel features could be shown, despite it being the overall most investigated ceramide. These include the low adaptability to changed lateral interactions, leading to an increased chain opening. This effect could explain its low miscibility with other lipids.

The investigated model systems allows it to directly compare results from the literature which have used ceramide [NS] to the most recent studies using the phytosphingosine ceramides such as ceramide [AP].

<https://doi.org/10.1016/j.chemphyslip.2018.05.006>

4.3.2 Introduction

The *stratum corneum* (SC) is the outermost layer of the epidermis and provides main barrier against exogenous biological (e.g. pathogens), physical (e.g. UV radiation) or chemical (e.g. toxins) noxae. This layer furthermore limits the trans-epidermal water loss, preventing dehydration. The SC is an almost impenetrable barrier for many relevant pharmaceuticals, preventing a needle-free trans-epidermal application. The SC is made up of corneocytes and lipid lamellar domain which are arranged in a brick and mortar assembly. The structure and packing of lipid lamellae determines the barrier function of the SC. Hence, there is a need to study the nanostructure arrangement of the SC lipids. There are also a variety of skin conditions, which are a direct result of an impaired SC such as psoriasis^[12–14], atopic dermatitis^[15–17] or lamellar ichthyosis^[18,19]. Due to a severe lack of knowledge their pathophysiology is just partly understood.

The SC is a rigid about 9-13 μm thick tissue, constructed from 15-30 layers of terminally differentiated, heavily keratinized corneocytes^[31,39–41]. A complex multilamellar lipid matrix (LM) is located in between the corneocytes, surrounding the cells and filling the extracellular space. This structure also leads to a low water content within the SC of 18-58 wt%^[38]. The composition of the LM is unique in comparison to

other biological membranes. It mainly consists of ceramides (CERs) (40 wt%), cholesterol (CHOL) (25 wt%), free fatty acids (FFA) (25 wt%) and a small amount of cholesterol sulphate (ChS) (1.5-6 wt%). Phospholipids which are a main constituent of most other biological membranes are only found in traces^[52,53,165,166]. The CERs have a highly variable head group region, determining their properties^[25,26,58,59]. They were shown to be a main contributing factor for a proper function of the skin barrier^[167], the overall phase behaviour and the nanostructure^[24,64]. The detailed nanostructure and many of the biophysical properties of the SC, have yet to be studied in detail.

Previous studies by our group were mainly focused on the most common skin CERs the phytosphingosine based CER[NP] (NP=non-hydroxy-phytosphingosine) and [AP] (AP=α-hydroxy-phytosphingosine)^[25,50,51] because they are two of the most abundant skin CERs. However, most previous studies including most of the studies based on theoretical simulations, focused on the sphingosine based CER[NS]. The CER[NS] is the overall most investigated CER, particularly its short chain C16 and C18 variants. However, many of these studies did show an unphysiological behaviour, for example a rather strong phase separation, especially for the short variants^[150–152,168]. In recent years some data on the long chain C24 CER[NS] were presented. This variant is more relevant within the native SC, since the shorter variants are almost not present. For this long CER[NS] in a complex CER, FFA and CHOL mixture, no phase separation was observed. A symmetric hairpin folded configuration with the long C24 tails overlapping in the lamellar mid-plane was concluded^[69]. This arrangement is supported by a simulation based study which was recently published^[70]. Short CER are unable to produce such an overlapping middle layer. It is necessary to investigate the interaction between the long C24 CER[NS] and the phytosphingosine based CERs to obtain (1) more detailed information regarding the influence on the nanostructure of the SC LM, induced by the sphingosine based CER[NS] and (2) to determine potential differences to the phytosphingosine based system investigated previously.

Therefore, the CER[NP]/[AP] based system used in previous experiments was changed to an CER[NS]/[AP] system. This change can directly highlight the interaction between the sphingosine based CER[NS] and the phytosphingosine based CER[AP] as well as the differences between the closely related CER[NP] and [NS]. The difference between these two CER is an exchange of a 4-OH-group (CER[NP]) for a 4,5-double bond ([NS]) within the head group of the sphingoid base. In a number of studies, using modifications of the CER[NP]/[AP] system, it was possible to investigate the nanostructure of the system in much detail, due to the use of specifically deuterated CER in combination with neutron diffraction experiments. These results show much promise to obtain more detailed information on the properties of the CER[NS] as well. This kind of approach, which can generate details on the location and arrangement of a single CER species within the model membrane, was not utilized for the CER[NS] yet (particularly not for the C24 derivative). In this study, we have also performed detailed molecular dynamics simulations (MDS) to generate even more information from the experimental observations.

4.3.3 Materials and Methods

4.3.3.1 Ceramide Mixtures

For the performed experiments, mixtures of CER, CHOL and the C24 FFA, Lignoceric acid (LA) were prepared. The used CER[NS] (N-(tetracosanoyl)-sphingosine) and CER[AP] (N-(2R-hydroxytetracosanoyl)-phytosphingosine), as well as their deuterated derivatives (Figure 1) were processed to obtain a purity of ≥ 95 %. CHOL and LA (purity ≥99.9 %) were purchased from Sigma Aldrich GmbH (Taufkirchen, Germany).

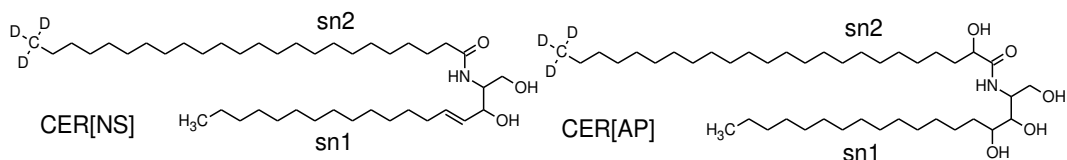


Figure 30: Structures of the deuterated lipids used for these experiments.

4.3.3.2 Sample Preparation

The SC model membranes were prepared on quartz glass slides. For sample application the pure substances were dissolved in a 2:1 mixture of chloroform and methanol (analytical grade, by sigma Aldrich) with a concentration of 10 mg/ml. These solutions were then combined, to generate CER/CHOL/EFA mixtures with molar ratios of 1/0.7/1. The CER[NS] and [AP] were mixed in a molar ratio of 0.67 /0.33 or 0.33/0.67 to study bilayer structures determined predominantly by only one of the CER. This approach was taken in a prior study, using a CER[NP]/[AP] mixture^[159]. For each CER species, an additional system containing the corresponding deuterated CER was prepared for use in the neutron diffraction experiments. For deposition the mixtures were sprayed onto the surface, using an airbrush instrument (Harder & Steenbeck, Norderstedt, Germany). The samples were sprayed at a temperature of 70 °C which is just below the melting point of the mixture. Afterwards the sample was annealed to form the multilamellar structure by heating to 66 °C under high humidity for 2 h, cooling at room temperature for 1 h and again heating under high humidity for 1 h.

4.3.3.3 Neutron Diffraction Experiments

For the neutron diffraction experiments the SC model membranes prepared on quartz glass slides were used. Diffraction data were collected at the membrane diffractometer V1 located at the Lise-Meitner campus of the Helmholtz-Zentrum Berlin für Materialien und Energie. Neutrons generated by the research reactor BER II were cooled using a H₂ cold source to increase the flux of neutrons around 4 Å wavelength. A pyrolytic graphite monochromator was utilized to diffract neutrons with a wavelength of $\lambda=4.567$ Å. A beryllium filter suppressed higher harmonic wavelengths. The distance between sample and detector was 101.8 cm. While rotating the sample angle ω and the detector angle 2θ in an ω - 2θ -scan, the intensity of the scattered neutrons was recorded as a function of the scattering angle 2θ . For contrasting against the water background the three different H₂O/D₂O ratios of 0:100, 50:50 and 92:8 (w/w) were applied. A higher D₂O content also generates a higher signal-to-background ratio, which allows for detection of peaks of higher diffraction orders with high precision. These higher order peaks are very important for calculation of a detailed neutron scattering length density profile (NSLD). The temperature was kept at 32 °C, and the relative humidity at either 57 % or 98 %. Since it could be observed that no more changes in the diffraction signal occurred after about 6 h of equilibration, samples were given a period of at least 7 h after any change of either temperature, humidity, or H₂O/D₂O ratio before data collection. The membrane spacing was determined according to Bragg's law $n\lambda = 2d \sin(\theta)$. The resolution of the calculated spacing can be estimated using the number of lamellar orders n and the lattice constant d as $a = \frac{2n}{d}$. A more precise estimation around ± 0.05 nm can be given by determining the maximum of the nearly Gaussian diffraction peaks. Using repeated measurements, can furthermore increasing the statistical weight of the data, improving the error estimation. The NSLD $\rho(x)$ was calculated by Fourier synthesis of the structure factors F_h according to:

$$\rho(x) = a + b \frac{2}{d} \sum_{n=1}^{n_{max}} F_n \cos\left(\frac{2\pi nx}{d}\right)$$

The coefficients a and b are estimating a linear background of $\rho(x)$, d is the lamellar periodicity and n the order of diffraction. The absolute values of the structure factors could be calculated as $|F_n| = \sqrt{h_n A_n I_n}$, with h_n as the Lorentz correction, A_n as absorption correction^[146] and I_n as Intensity of the n^{th} peak. To obtain profiles comparable for different measurements with different quality and thus different absolute scattering intensity, the NSLDs are normalized to the absolute scattering values. The integration of the Bragg's peak intensities and further calculations were performed using the IGOR Pro 6.1 software (WaveMetrics Inc., Portland, OR, USA). For the Fourier transform, both the absolute value as well as the phase sign of each structure factor F_n is required. Assuming a Gaussian water distribution with a maximum position $x = \frac{d}{2}$ within the hydrophilic head group region, allows determination of the F_n by application of different H₂O/D₂O contrasts, representing an *isomorphous* replacement^[146,149]. The centro-symmetric lipid arrangement which is to be expected for CER-membranes leads to a phase of either + or – for each F_n . A three point measurement with three different H₂O/D₂O contrasts is thus sufficient for the calculation of the phase of each structure factor. A detailed description of this can be found elsewhere^[146–148].

At 8 % D₂O the sum of the coherent scattering lengths of H₂O and D₂O becomes 0. Consequently, the water layer does not contribute to the Bragg peak intensities. Subtracting the 8 % profile from the 100 %, profile which shows a maximum water signal, a profile of the water distribution can be obtained. The relative contribution of water to the scattering length density in the head group of a NSLD can be estimated by determining the difference between the minimum and maximum scattering length density of the water profile at 98 % R.H.. It can be made comparable by normalizing it to the difference of the minimum and maximum scattering length density of the corresponding 100 % D₂O 98 % R.H. profile. From this calculation the contribution of water relative to the maximum scattering density can be obtained as a value comparable for different systems^[169].

4.3.3.4 Molecular Dynamics Simulations

The SC lipids are arranged in multiple lamellar domains. Two kinds of bilayer systems namely, a) simple bilayer and b) triple bilayer were simulated. The first one consist of a single bilayer, hydrated with water at both ends, while the latter one consists of three bilayers hydrated only at the outermost borders. The middle layer of the second system, with two bilayer-bilayer instead of bilayer-water interfaces, resembles the native multilamellar lipid structure much more closely. The bilayer as well as the triple layer simulations were performed for both ratios of CER[NS]/[AP] 2:1 and 1:2. The structure of each individual CER was reconstructed using an earlier model of CER[NS]^[71]. The combination of GROMOS87^[170] and Berger force fields^[171] was used for dynamic modelling of each CER. The parameters for CHOL and LA were taken from previous simulation studies^[172,173]. In the simple bilayer setup, lipid molecules were distributed in the two leaflets and solvated with water molecules. Each bilayer consists of 270 lipids (CER[NS], CER[AP], CHOL and LA) and 10800 water molecules. The molar ratios of CHOL and LA were 0.7 and 1 respectively. This was done, to be consistent with the experimental approach, where the lower CHOL ratio was employed to avoid a separate crystalline CHOL phase, typical for simple model systems. For the triple layer model, in total 810 lipids and 10800 water molecules were used. At first, each lipid molecule was energetically minimized in vacuum using a steepest decent algorithm. These optimized molecules were subsequently used to assemble the bilayer and triple layer model. The packing of the bilayer was carried out using the software PACKMOL^[174]. The generated bilayers were further hydrated with the simple extended point charge (SPC)^[175] water model. For the triple layer

system, the packed lipids were replicated in Z direction and then solvated. To remove energetically unfavourable contacts in between molecules, which occurred during the packing, another energy minimization was carried out, using the steepest descent method for each bilayer/triple layer system. For the proper solvation of the bilayer/triple layer, each system was subjected to a 3 ns NVT (N =number of atoms, V =volume of the simulation box and T =temperature) run with a constraint set on the lipids. Furthermore, constraints on each lipid chain were released in XY direction (3 ns) followed by a release in Z direction (3 ns). The properly solvated systems were then subjected to a 10 ns NPT (N = number of atoms, P = Pressure and T = temperature) run at a temperature of 305 K and a pressure of 1 bar. The lipid layers were further subjected to a simulated annealing procedure, where the bilayers/triple layers were heated to 380 K and cooled down to 305 K in 50 ns total. The simulated annealing procedure ensures a lipid assembly, independent of the initial packed structure. These structures were further equilibrated in NPT ensemble for 100-200 ns. The structures obtained through these approaches were finally ran for 300 ns (triple layer) and 500 ns (bilayer) in NPT ensemble. All simulations were performed using GROMACS software^[176]. In the equilibration run, the temperature and pressure were controlled using the Berendsen thermostat and barostat with a time constant of 1 ps and 5 ps, respectively. In the final production run, temperature and pressure were controlled by Nose-Hoover thermostat and Parrinello-Rahman barostat with a time constant of 2 ps and 5 ps, respectively. The pressure was coupled separately in normal and lateral direction with the isothermal compressibility of $4.5 \times 10^{-5} \text{ bar}^{-1}$. The electrostatic and van-der-Waals cut-off was set to 1.2 nm. The particle mesh Ewald sum method was used for treatment of the long range electrostatic interactions. The trajectory was saved after every 20 ps. All the bilayers and triple layers studied here have their normal in z direction, unless it is stated otherwise.

4.3.4 Results

4.3.4.1 Phase behaviour

In total, 5 diffraction orders could be observed for both ratios (2:1 and 1:2). For the 2:1 ratio the position of the 6th order could be estimated. However, the peak was too small to calculate its integral intensity with adequate accuracy.

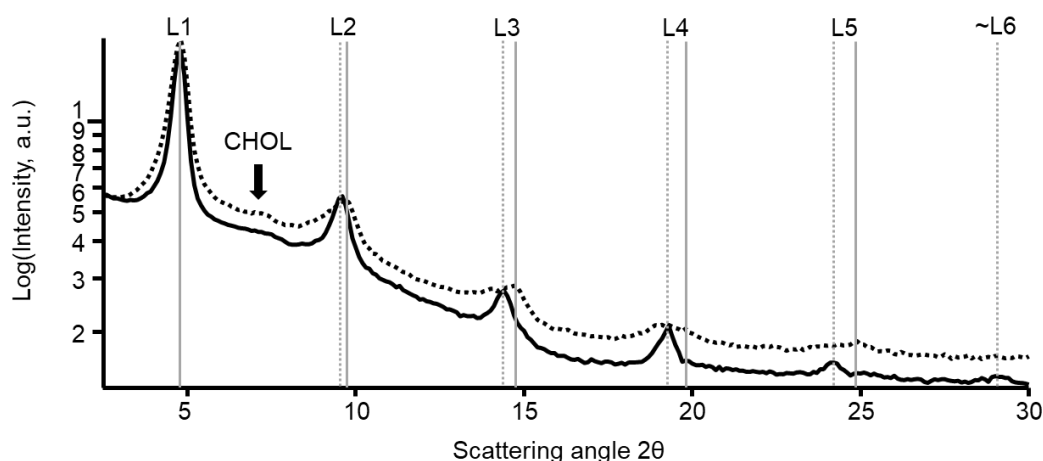


Figure 31: Representative diffraction data for the investigated systems at 100 % D_2O and 98 % R.H.. Continuous line: CER[NS]/[AP]/CHOL/LA 0.67/0.33/0.7/1. Broken line CER[NS]/[AP]/CHOL/LA 0.67/0.33/0.7/1. 5 lamellar diffraction orders are observed for both systems indicated by L1-L5 and a 6th can be estimated for the [NS]/[AP] 1:2 system indicated by ~L6. A weak peak for crystalline CHOL is indicated with an arrow.

The diffraction patterns show that the peaks for the ratio of 1:2 are getting broader with each lamellar order. The peaks for the ratio of 2:1 on the other hand are all relatively sharp with a narrow base (figure 2, 3).

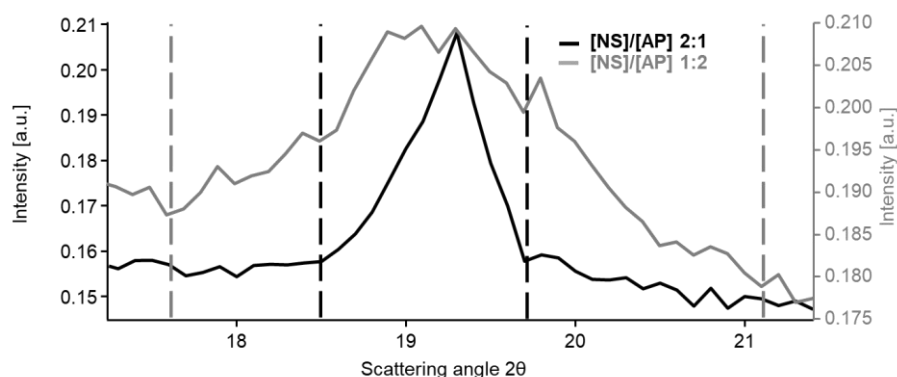


Figure 32: Comparison of the 4th order peak of the two different molecular ratios 2:1 and 1:2 of the CER[NS]/[AP] based SC model system. Diffraction signals as measured at 98 % R.H. and 100 % D₂O.

This indicates that the 1:2 ratio, containing more CER[AP], most likely does not yield a completely uniform phase. However, even for orders as high as the 5th order, no actual separation into two peaks and thus no clear phase separation became apparent. This indicates, that the domains, even though differently composed, have almost the same lattice constant. This indicates, that they coexist as nano-sized clusters or domains, within a single phase.

The presence of nano-sized lateral domains, without a complete phase separation, could also be observed for the simulated bilayers as well as the triple layers of the CER[NS]/[AP] 1:2 model system. This effect is particularly pronounced for the fatty acids shown in purple (Figure 4 and S1 supporting material).

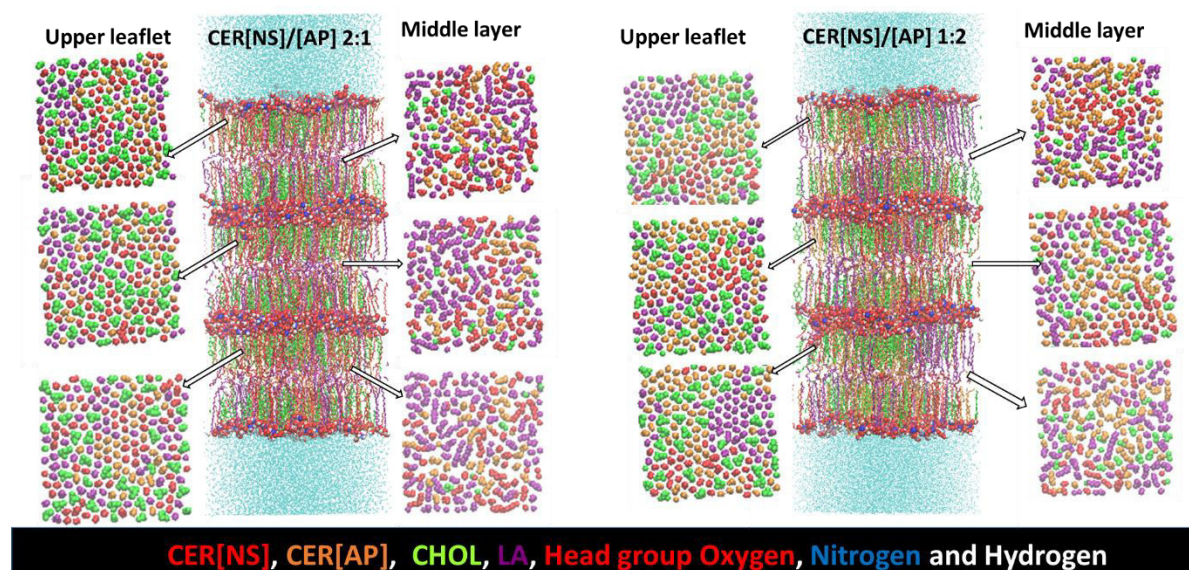


Figure 33: The structure of each triple layer structure in the end of 300 ns simulation. The lateral packing of mid of upper leaflet and middle of each bilayer with in triple layer has also been shown. The images were created using visual molecular dynamics (VMD) software.^[177] The bilayer and lateral packing are shown in dynamic bond and VDW mode of VMD respectively.

4.3.4.2 Lamellar repeat distance

The lamellar repeat distance for the two different systems was observed to differ slightly. The CER[NS]/[AP] 2:1 system had a repeat distance of 5.43 ± 0.05 nm and the 1:2 system a slightly shorter one with 5.34 ± 0.05 nm ($\Delta = 0.09$ nm). This difference between the two systems could also be confirmed with the MDS simulations showing a 5.14 nm and 5.05 nm repeat distance for the 2:1 and 1:2 system respectively. The difference between the two systems indicates a difference in chain arrangement between the CER[NS] and [AP], with the CER contained in a higher proportion determining the repeat distance.

4.3.4.3 Head group region

All structure factors determined by the D₂O/H₂O-contrast variation were in phase with uneven factors with a negative and even factors with a positive sign for all systems of both ratios (Table 1).

Table 12: Structure factors F_n for diffraction orders 1-5 at 100 % D₂O and 98 % R.H.

	CER [NS]/[AP] (2:1)	CER [NS]-D ₃ /[AP] (2:1)	CER [NS]/[AP]-D ₃ (2:1)
F₁	-0.373 ± 0.003	-0.307 ± 0.002	-0.333 ± 0.002
F₂	0.241 ± 0.006	0.263 ± 0.007	0.244 ± 0.004
F₃	-0.157 ± 0.022	-0.144 ± 0.014	-0.161 ± 0.008
F₄	0.147 ± 0.015	0.155 ± 0.013	0.154 ± 0.008
F₅	-0.083 ± 0.034	-0.131 ± 0.017	-0.108 ± 0.009
	CER [NS]/[AP] (1:2)	CER [NS]-D ₃ /[AP] (1:2)	CER [NS]/[AP]-D ₃ (1:2)
F₁	-0.392 ± 0.003	-0.350 ± 0.003	-0.347 ± 0.004
F₂	0.221 ± 0.006	0.239 ± 0.005	0.264 ± 0.009
F₃	-0.145 ± 0.022	-0.135 ± 0.030	-0.144 ± 0.025
F₄	0.141 ± 0.015	0.137 ± 0.019	0.118 ± 0.014
F₅	-0.102 ± 0.034	-0.139 ± 0.028	-0.127 ± 0.021

Within the NSLDs, the head group regions located at the outer borders are easily identified by their higher scattering length density, caused by the contained positively scattering oxygen, nitrogen and carbon, as well as the bound D₂O. Other than these regions of stronger scattering, the NSLDs for both systems are overall mostly flat, indicating the chain region with the low scattering density of CH₂. They show no pronounced scattering minimum in the lamellar mid-plane demonstrating, that the CH₃-groups are not located at one single position. Except for the repeat distance, the profiles for both ratios show no distinct differences (see Figure 5).

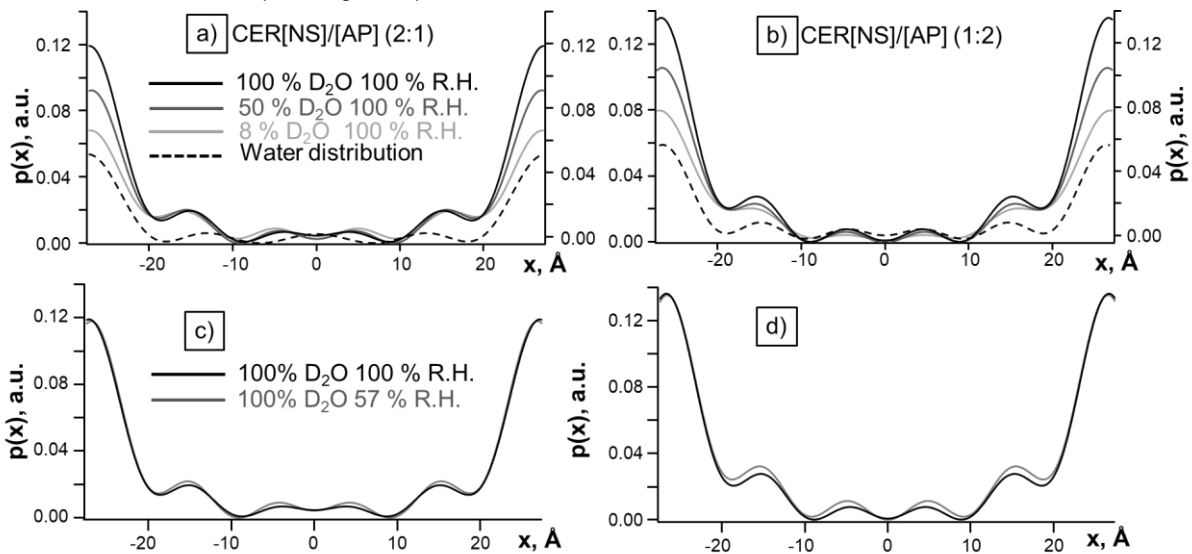


Figure 34: Calculated (non-normalized) neutron scattering length density profiles for the investigated samples. The differences between the three D₂O/H₂O contrasts (left axis) and water profiles (right axis) a) and b) are shown above. The differences between the applied humidities of 57 % and 98 % c) and d) are shown below. a)/c): CER[NS]/[AP]/CHOL/LA (0.67/0.33/0,7/1). b)/d): CER[NS]/[AP]/CHOL/LA (0.67/0.33/0,7/ 1).

For the simulated triple layer models, it could be shown, that the head group density is increased, for the two head group regions of the middle layer. The slightly higher density for the CER[NS]/[AP] 1:2 system in general is mostly a result of the higher CER[AP] content, which is the heavier of the two CER. It could be slightly amplified by the shorter repeat distance, leading to more mass per z position (Figure 6).

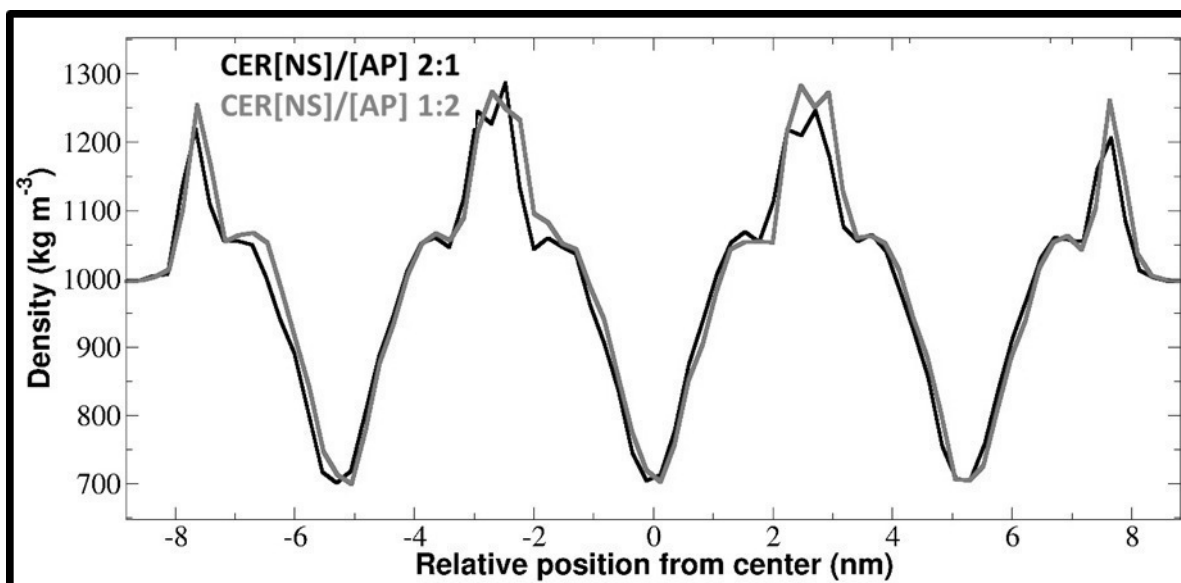


Figure 35: Overall system density along the bilayer normal z in both triple layer CER[NS]/[AP] 2:1 and 1:2. Here, $z = 0$ corresponds to the centre of the triple layer.

4.3.4.4 Water distribution

The water within the system was located using the NSLD profiles shown in figure 5. No water was present within the inner lamellar structure but only at the outer borders in the head group region (Figure 5a, b)). To gain information on the relative water content within the different systems, the percentage values were determined as described above. It could be shown, that the relative water content is about 47 NSLD-% for the CER[NS]/[AP] 2:1 system and about 44 NSLD-% for the [NS]/[AP] 1:2 system. There is thus no relevant difference in relative water content between the two systems (Figure 5 a, b)). For none of the two systems, swelling or any other distinct change could be observed upon raising the humidity from 57 to 98 % (Figure 5 c) and d)). The system has thus a constant water content which is uninfluenced by the humidity of the surrounding air, if ≥ 57 %.

For the simulations, water was correspondingly only located at the outer borders, within the head group region (for the triple layer only the outermost borders). The increased density of the bilayer-bilayer interface of the central lamellae shows that it has significantly different properties compared to the water-bilayer interface. Since only bilayer-bilayer interfaces with minimal bound water content are present in the natural LM, this arrangement resembles the natural situation much closer than simple bilayer models.

4.3.4.5 CHOL distribution

The small local maximum in the NSLDs, slightly inward from the head group region, is caused by the CHOL with an increased scattering length density because of its higher C/H ratio. This is consistent with the position, which was determined for the CHOL, employing MDS (See Figures S3, S4, S5 supporting material). The CHOLs OH is thus located slightly inward from the head group region of the CER and FFA. For the simulation studies, a small number of CHOL molecules, with their head group located in the opposing bilayer, were observed (Figure S5).

Both the CER[NS] as well as the [AP] did show a better miscibility with CHOL than the CER[NP]. For the [NS]/[AP] system no pronounced CHOL peak is detectable, independent of the ratio between both CERs. For the [NP]/[AP] system investigated in an earlier study, the 1:2 ratio with more [AP] did show only a very small CHOL peak^[159]. The CHOL peak for the 2:1 ratio, containing more [NP] was still weak compared to the lamellar peaks but very pronounced compared to the other systems (Figure 7)^[159].

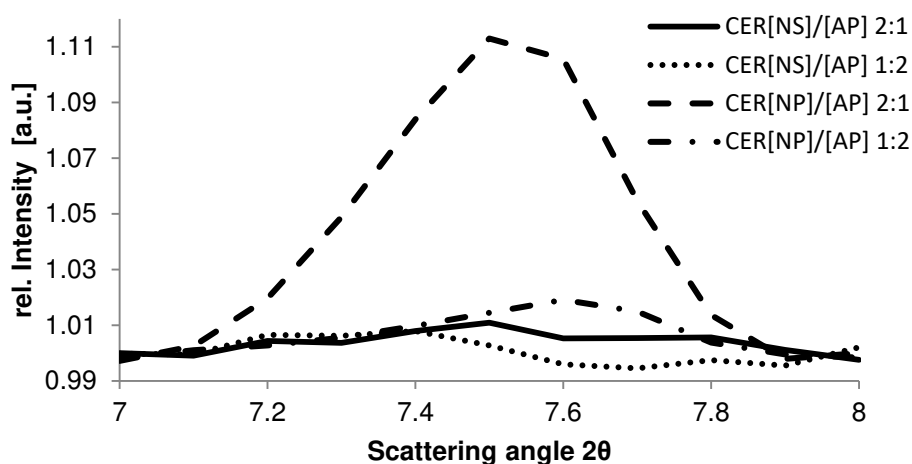


Figure 36: Comparison of the CHOL peaks between the two ratios 2:1 and 1:2 of the CER[NS]/[AP] system (investigated here) and the [NP]/[AP] system (investigated in a prior study)^[159]. A 4-point baseline normalisation as well as an intensity normalisation (based on the difference between the maximum of the first lamellar peak and the baseline) was used to directly compare the different measurements to each other.

4.3.4.6 Molecular nanostructure: Overlapping long chains

The highly detailed information on the lamellar and molecular nanostructure of the CER was obtained using the specifically deuterated variants of CER[NS] and [AP]. Assuming a length of about 3.25 nm for one C24 CER^[85], the repeat distance of both systems is shorter than two directly opposing long chains. For both CER[NS] and [AP] in both ratios, the deuterated terminal carbons could be observed at two different positions within the unit cell (See figure 8). The location of the two corresponding NSLD-peaks is slightly outward from the lamellar mid-plane. Each of the deuteration positions indicates the terminal end of the CER from one half of the lamellae. The two positions are a result of an overlapping of the long chains in the lamellar mid-plane, with each of the two peaks correlating to the head group further away from it (See figure 8).

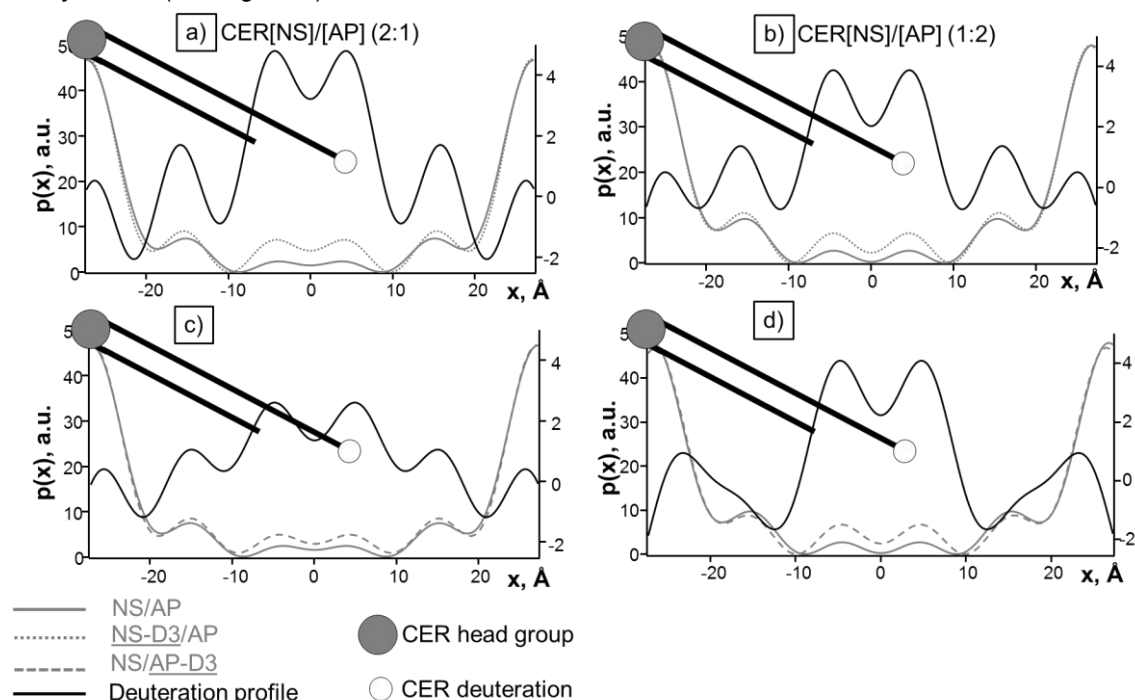
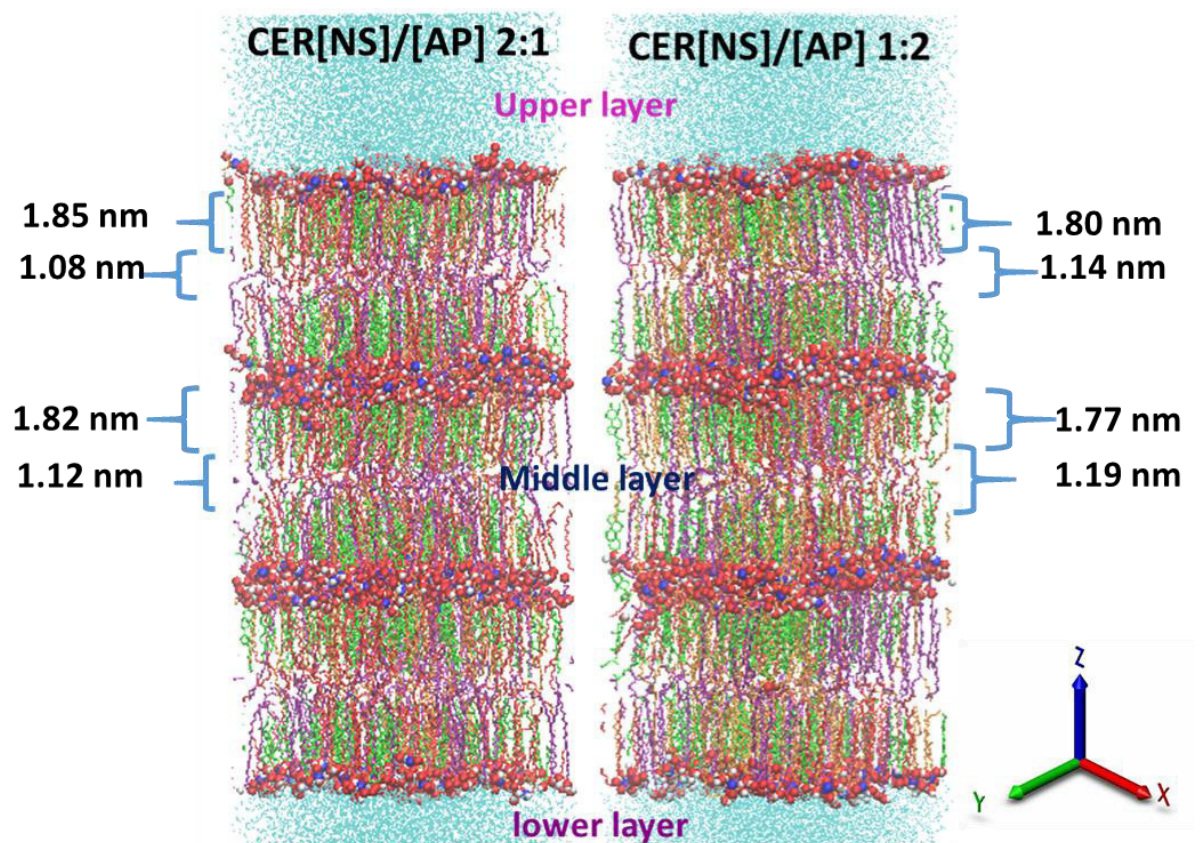


Figure 37: Calculated normalized neutron scattering length density profiles for the investigated samples (left axis). Deuterated samples are compared to the base systems. Difference profiles between the deuterated and non-deuterated samples, shown in

black, indicate the localization of the deuterium labels (right axis). Suggested most likely arrangements of the used CER are indicated by a stylized CER molecule. a): CER[NS]-D₃/[AP]/CHOL/LA (0.67/0.33/0,7/1). b): CER[NS]-D₃/[AP]/CHOL/LA (0.67/0.33/0,7/1). c): CER[NS]/[AP]-D₃/CHOL/LA (0.67/0.33/0,7/1). d): CER[NS]/[AP]-D₃/CHOL/LA (0.67/0.33/0,7/1).

The thickness of the head group and water layer was estimated from the NSLDs, by measuring the length of the region of high scattering density corresponding to the head group region. According to this estimation, the head group region takes up about 0.71 nm (Figure 8). The length of the chain region was estimated using the region of low scattering density. Considering the two deuteration positions it could be determined, that in the 2:1 system the C24 and C18 chains of the CER[NS] (minus the head group) take up a length of 2.43 nm and 1.60 nm, respectively, accounting for a total length of the CER[NS] of 3.14 nm, with an overlap of the long chains of 0.83 nm. For the CER[AP] the chains are 2.42 and 1.57 nm respectively, accounting for total length of the CER[AP] of 3.11 nm with an overlap of the long chains of 0.85 nm. Within the 1:2 system, the CER[NS] C24 and C18 chains take up a length of 2.41 nm and 1.49 nm, leading to a total CER[NS] length of 3.11 nm, with the long chains overlapping 0.92 nm. For the CER[AP] it is 2.40 nm and 1.47 nm, leading to a total CER[AP] length of 3.09 nm with an overlap of 0.92 nm. The increased overlap of +0.09 nm for the CER[NS] and +0.08 nm for the CER[AP] observed for the 1:2 system accounts for the decrease in lamellar repeat distance of -0.09 nm. This is consistent with the lipid arrangements of the bilayer as well as the triple layer obtained from the MDS (see Figure S1 and Figure 9 respectively).



CER [NS], CER [AP], CHOL, LA, Head group Oxygen, Nitrogen and Hydrogen

Figure 38: The schematic of the triple layer divided in different region (upper, middle and lower layer) for analysis. The region of headgroup, rigid layer and overlapping area are shown in each of the triple layer system. The headgroup atom "H22" has been used for the calculation of overall repeating distance of each layer. The rigid layer is the distance between the N23 and the C1 atoms of each CER. The overlapping area is calculated by subtracting rigid and headgroup layer thickness from the repeating distance. The images were created using VMD software.⁴² The triple layer has normal in z direction. The atom names of CER are shown in the Figure S8 (please see supporting information).

In the triple layer model, the long (Sn2) and short CER (Sn1) chains in the 2:1 system were about 2.39 and 1.85 nm for the outer layer and 2.38 nm and 1.82 nm for the middle layer, which fits the experimental

data quite well. For the 1:2 system, the length of both chains was 2.37 nm and 1.8 nm for the outer and 2.37 nm and 1.77 nm for the middle layer, again showing the same tendency in as the experimental data. The overlapping distance for upper and middle bilayer is slightly different for the 1:2 and 2:1 systems (Figure 9). The overlapping distances obtained through MDS are 1.08 nm and 1.14 nm for the outer layer of the 2:1 and 1:2 respectively. Following the same trend of being shorter for the middle layer, with 1.12 nm and 1.19 nm for 2:1 and 1:2 system respectively. The obtained distances are slightly longer than the experimentally obtained values. However, the general trends are the same for MDS and experimental data, with an increased overlapping distance of +0.07 nm for the 1:2 system, confirming the described stronger overlapping arrangement for this system.

It can be observed that the middle layer of each lamellae shows an absolute chain density minimum (Figure 6). It can furthermore be noted, that in both the bilayer and the triple layer model, a minimum chain order was observed for the lamellar middle layer (see figure S2 and S7). Both these effects are visualized in the lipid arrangement in Figure 4. The upper chain regions of the triple layer all show a dense orthorhombic to hexagonal chain packing, while the packing in the middle layer is much less dense and ordered, indicating oil-like properties.

4.3.4.7 Molecular nanostructure: Chain tilt and chain opening angles:

The tilts of the chains were calculated using both NSLD and MD simulations. The lengths of the long chains determined from the NSLDs were still about 0.1 nm below their estimated length of about 3.25 nm^[85]. This shows, that the CER are arranged with slight overall lateral tilt, which can be estimated as $\overline{\beta_{Z,CER,ND}} \sim 15\text{-}16^\circ$. This chain tilt was confirmed by the MDS results with the chain tilt angle $\overline{\beta_{Z,CER[NS],Sn1}} = 12.90^\circ$, $\overline{\beta_{Z,CER[NS],Sn2}} = 16.56^\circ$, $\overline{\beta_{Z,CER[AP],Sn1}} = 13.57^\circ$ and $\overline{\beta_{Z,CER[AP],Sn2}} = 16.38^\circ$ in the CER[NS]/[AP] 2:1 system. In the 1:2 systems the tilt angles for CER[NS] were about the same with $\overline{\beta_{Z,CER[NS],Sn1}} = 12.20^\circ$ and $\overline{\beta_{Z,CER[NS],Sn2}} = 16.87^\circ$. For the CER[AP] it was slightly lower with $\overline{\beta_{Z,CER[AP],Sn1}} = 10.98$ and $\overline{\beta_{Z,CER[AP],Sn2}} = 13.62^\circ$ (see Table S1 supporting material). Overall, the lipid chain tilt keeps within a range of about $\overline{\beta_{Z,CER,MDS}} \sim 10\text{-}20^\circ$.

The decreased difference in tilt, for both CER[AP] chains in the CER[NS]/[AP] 1:2 ratio, shows an overall more straight arrangement for this CER. This is consistent with the observed larger overlapping distance. For the CER[NS], the tilt angles change much less but in different directions for both chains. This increases the average chain opening angle $\bar{\alpha}$ by about 1° . This indicates an increased ratio of CER[NS] with a slightly more open conformation in the 1:2 system.

To fit this arrangement, the longer LA molecules show a slight increase in tilt angle from $\overline{\beta_{Z,LA}} = 14.68^\circ$ in the 2:1 system to $\overline{\beta_{Z,LA}} = 15.16^\circ$ in the 1:2 system ($\Delta\overline{\beta_{Z,LA}} = 0.48^\circ$). For CHOL this effect is less pronounced with a difference of ($\Delta\overline{\beta_{Z,CHOL}} = 0.11^\circ$).

In the CER[NS]/[AP] 1:2 system, the chain order parameters of the base chain (Sn1) for CER[NS] are lower than for the CER[AP]. This can be considered another effect of the decreased extended conformation of the CER[NS], reducing the space in between its chains and increasing the attractive interactions and thus the order parameter. For the CER[NS], the base chain is more ordered for the higher carbon atoms, compared to the CER[AP]. For the fatty acid chain (Sn2), the order parameters are almost equal along the z axis for both CER (Figures S2 and S7).

4.3.5 Discussion

The CER[NS] used in this study can be considered the most basic CER with a sphingosine as a base and an unmodified C24 acyl chain. Furthermore, considering the high amount of about 40 - 70 mol% of sphingosine CER, especially the CER[NS], found in many previous studies, they seem to be the easiest

to extract from skin, using a variety of solvents. In these studies, the CER[NS] and [NdS] were not yet separated, also leading to an overestimation of the CER[NS] ratio^[100,110,127,129]. Furthermore, they seem to be more abundant in pig skin -use for most previous investigations- compared to human skin^[110,130,178]. Because of these factors, the CER[NS] is the most widely investigated CER so far. However, in human skin CER[NS] has a proportion of only about 7 %^[25,50,51]. Introducing CER[NS] into the simple model mixture together with CER[AP] made it possible to directly compare the result for the phytosphingosine CER to many of these previous studies using CER[NS] or mixtures mainly based on it.

4.3.5.1 Repeat distance

The results obtained in this study are in good agreement with previous results and with what is known from literature. The repeat distances of 5.43 ± 0.05 nm for the [NS]/[AP] 2:1 ratio and 5.34 ± 0.05 nm for the 1:2 ratio are consistent with the estimated lamellar thickness of 5 - 6 nm for the native SC LM^[104]. The spacing for the 2:1 ratio is also consistent with the previously investigated CER[NP]/[AP] systems which had a repeat distance of 5.45 ± 0.10 nm for both ratios 2:1 and 1:2^[159]. The modified CER[NP]/[AP] system, additionally containing a native like ratio of 10 mol% of a CER[EOS] analogue (EOS=esterified- ω -hydroxyacyl-sphingosine), also had a comparable repeat distance of 5.47 ± 0.02 nm [Soon to be published]. For a more complex 13 component system with a high content of CER[NS] C24 of 60 mol% -comparable to the [NS]/[AP] 2:1 ratio- a repeat distance of 5.36 nm was described^[69]. The slightly shorter repeat distance -which is more similar to the 1:2 ratio- in this case is to be attributed to a change in chain arrangement, e.g. possibly also increased overlapping due to decreased lateral chain order caused by the complex composition. The repeat distance for the simulated models was determined to be slightly shorter than experimentally observed. This is most likely to be considered a result of overestimated molecular attractions or underestimation of the influence of water compared to the natural system. However, the same trend of a slightly shorter repeat distance for the 1:2 ratio is observed. It even exhibited the exact same difference of ~ 0.1 nm. For the [NS]/[AP] mixture, the repeat distance was determined by the CER with the higher ratio. For the CER[NP]/[AP] system this was not the case, even though both of the CER were shown to slightly differ in length arrangement^[159,169].

4.3.5.2 Phase behaviour of lipids

The broader width of the diffraction peaks for the CER[NS]/[AP] 1:2 system, indicates an incomplete mixing of the lipids. However, up to the 5th order no actual peak splitting or shift of the peak centre is observed. Since the diffraction peaks show the average diffraction of all observed layers, nano-domains with a comparable lattice constant are the most likely cause for this. These would increase the variation of the lamellar thickness, broadening the diffraction peaks, without being different enough to show a complete peak splitting or shift in peak centre.

The molecular simulations for this system confirmed this, showing the formation of especially FFA but also CER enriched nano-sized domains. A smaller amount of CER[AP] was thus well miscible with a high amount of [NS], a small amount of [NS] however was not well miscible with a high amount of [AP]. The CER[NS] is already known to not mix well with other lipid^[150-152,168].

A high CER[NS] content could thus lead to domain formation or phase separation, which have to be considered unwanted features for an effective barrier structure. Such a phase separation was not observed for the -previously investigated- CER[NP]/[AP] system with the same two ratios 1:2 and 2:1. This is most likely the result of a better miscibility of the two phytosphingosine CER^[159,169]. To investigate the absolute phase proportions and properties, further small angle X-ray and other experiments, directly focusing on these Features could be performed.

4.3.5.3 Water distribution

For the CER[NS]/[AP] based systems, a relative water content of 47 NSLD% for the 2:1 ratio and 44 NSLD% for the 1:2 ratio were determined. This is in good agreement with the relative water content determined for the related CER[NP]/[AP] 2:1 system with 51 NSLD%^[159] as well as the [NP]/[AP]+10 % [EOS] system with 47 NSLD% [soon to be published]. The lack of any distinct change in structure, upon an increase of the relative humidity from 57 %, to 98 % shows that the water within the system is very tightly bound. A maximum hydration is thus reached at 57 % humidity or less. This result is in good agreement with the above mentioned previous results, where under the same conditions no change in hydration could be observed^[169]. Furthermore, it is consistent with another study that investigated the influence of humidity on the lamellar phase and did not find any water uptake or structural change^[155].

4.3.5.4 CHOL distribution and its influence

Both the experimental and the MDS data did show a uniform distribution of CHOL within the lamellae, near the head group region. This is in agreement with the experimental observations. It is also consistent with both prior simulations^[71] and detailed experimental data^[115].

It is known however, that in simple model systems, it can easily be partially excluded, forming a small amount of separated crystalline CHOL, showing as a peak between the first and second lamellar order. This effect is also the reason for the slight reduction of CHOL ratio to 0.7 instead of an equimolar amount as found in the natural system. A very distinct difference between the CER[NS]/[AP] system and the [NP]/[AP] system -investigated previously- is the better miscibility with the CHOL. Even in the CER[NS]/[AP] 1:2 system, clustering was observed for the CER and even stronger for the LA molecules, no noticeable CHOL nano-domains could be observed. For the [NP]/[AP] 2:1 system, a pronounced separate CHOL peak was present, while the 1:2 ratio containing more [AP] only showed a very small indication of a CHOL peak^[159]. The exclusion of CHOL from the lamellar phase has thus to be contributed to the CER[NP] and is most likely caused by the tight organisation of its head group. The CER[NP] with its additionally laterally organized OH-group features strong in-plane H-bonds^[92]. This way, the CER[NP] is laterally fixed in position, providing enough space for the CHOL, to fit in between. The other ceramides seem to be able, to slightly bend around the CHOL, possibly causing the increased lateral chain tilt within these systems. The CER[AP] and [NS] have a less tightly arranged head group. For the CER[AP], this was suggested to be an effect caused by its α -OH group, disturbing the head group H-bonding network^[74]. For the CER[NS] this feature was attributed to the fewer OH-groups and double bonds, changing the head group organization^[74,84,163,179]. For the CER[NS] a better miscibility with CHOL can additionally be assumed as an effect caused by its double bond.

The CHOL serves as an important mediator for the miscibility of CER and FFA and has a strong influence on the thermotropic phase behaviour of the mixture^[150]. In the MDS, the localisation of their OH group in the head group region of the opposing lamellar leaflet could be observed for a few CHOL molecules. This indicates the possibility of CHOL performing a flip-flop, switching between different leaflets as was reported before^[180]. This exchange could be of much importance for the adaptability to curvature and other geometrical changes.

4.3.5.5 Nanostructure overlapping in middle-layer

The overall flat NSLD profiles together with the lack of a distinct minimum in the bilayer centre, as well as the two distinguishable deuteration positions and the repeat distance all strongly suggest an arrangement of CERs with the long overhanging tail ends of the CER C24 acyl-chains and the long C24 LA overlapping in the lamellar middle. They are opposed by the shorter C18 chains of the sphingoid base (Sn1) and CHOL, allowing the opposing longer chains to fill these gaps. This arrangement was

confirmed by the MDS data and is also in good agreement with previous results including the above mentioned CER[NP]/[AP]-based systems and its modifications^[159,169], the more complex 13 component mixture^[69] as well as other MDS of C24 CER[NS]/CHOL/LA mixtures^[70,71].

In the natural LM, this overlapping middle layer is discussed, to possibly hold an important function for the mechanical stability of the LM. The more liquid middle layer would allow the outer rigid regions, to slide against each other, providing a buffer for lateral shear stress^[70]. With the increased compressibility of this less dense region, an increased resistance against perpendicular pressure is also possible. The connection of both leaflets by this overlap could also enhance the molecular attraction between the two leaflets, compared to sharp end to end connections as observed in C18 CER based model systems, stabilizing the overall structure. A third possibility is a trapping effect for penetrating molecules. This less dense region would have the highest space availability and thus best miscibility compared to the tightly packed outer regions. The reduced order and less strong intramolecular interactions would further increase the solubility of most molecules, compared to the rigid almost crystalline outer regions. These effects would favour lateral diffusion along this more fluid layer, instead of diffusion through the outer more rigid regions.

For the 2:1 system, the overlap was determined, to be increased. This is induced by the increased proportion CER[AP], which's short sn1 chain is slightly less ordered than for the CER[NS]. This increases its' lateral but decreases its normal space occupation, providing more space for the long chains of the opposing leaflet.

4.3.5.6 Nanostructure conformation

The increased ratio of slightly more open CER[NS] is most likely also contributing to the larger overlapping region, since it is leaving more gaps for chains of the opposing layer as well. However, since the difference in chain opening is small, this effect is most likely negligible. Since the CER chains are still measured shorter than they are estimated, it can be concluded, that they show a chain tilt of about 15 - 16° in both systems. The MDS did confirm the slight chain tilt of about 10-20°. The slightly longer LA chains are force fitted into this shorter arrangement, slightly increasing their tilt angle. This force fitting of longer FFA chains was observed for the racemic D/L-CER[AP] C18 earlier as well^[64,94]. This mechanism can also explain, how longer lipids can fit into the 5 - 6 nm long short periodicity phase (SPP) arrangement within the native LM, without disturbing the ordering of the opposing leaflet, as was observed for the D/L-CER[AP] based model system^[64].

Since the CER[NS] is discussed to have a generally more ordered structure than the phytosphingosine CER^[72-74,84], its lower order parameter in the CER[AP] determined 1:2 ratio, was unexpected at first. The domain formation is the most likely cause for this effect, disordering the chains in the border region. A disordering of the chains could be caused by the C4,5-double bond, inducing this less ordered more open conformation, if too little lateral interaction forces work against it. These less ordered boarder region would most likely increase the rate of passive transport trough the lamellar structure, reducing the barrier function.

As mentioned above, an overlap of the long C24 chains in the lamellar mid-plane was also observed for the much more complex 13 component system. In this case, a perdeuteration of its C24 chain served to locate the CER[NS] within the lamellae. The use of a perdeuterated chain allows to see the full length chain in the NSLD^[69]. However it is nearly impossible to exactly pinpoint the beginning and end of the overlapping region because the perdeuteration does not allow for an exact localisation of the terminal CH₃/CD₃ groups. With the specifically deuterated CER[NS]-D₃ and [AP]-D₃ on the other hand, it was possible to exactly locate the two terminal groups in two different positions. This allowed us to determine the nanostructure of the lipid lamellae with a great amount of detail, especially combined with the detailed MDS yielding highly detailed models which confirmed certain features and were suitable to

predict additional features. Effects of chain tilt, chain opening, chain order, individual chain lengths, chain interdigitation and more could be determined, even showing novel results for the CER[NS], as previously most investigated CER. Obtaining this much details was impossible before, especially using only a single measurement method.

4.3.6 Conclusion

As a result of the obtained data it became apparent, that the CER[NS] and [AP], show a surprisingly similar influence on the lamellar structure. However, both CER show a noticeably different impact on the systems nanostructure.

The observed CER[NS]/[AP] system has many features which are defining for the native lipid matrix. The repeat distance of for both ratios 2:1 and 1:2 was natural-like. However, the 1:2 system showed slightly reduced lipid miscibility, with LA and CER enriched nano-domains but without complete phase separation. This is an effect resulting from the low adaptability of the CER[NS] to changed lateral interaction forces. In both systems the lipid chains were slightly tilted and both formed an arrangement with the long C24 chains overlapping in the bilayer centre. The overlapping is discussed, to possibly be an important feature for the native SC. Both of the CERs seem to have an enhanced miscibility with CHOL compared to the CER[NP].

These effects are solely dependent on the small chemical differences in their head groups. So far, CER[NS] is the only ceramide reported to exhibit not only intralamellar but also interlamellar H-bonding^[90,91]. It is possible, that either this or other special features of the CER[NS] could probably be of much importance for the formation of the 12 - 13 nm long periodicity phase. For most of the other observed differences between these two and other CER, we do not even know yet, which important function they may have for the overall LM.

The used combination of neutron diffraction and molecular dynamics simulations proved extremely useful for the analysis of the lamellar nanostructure and will be used for more studies in the future. The investigated model systems allow to directly compare results from literature, which have used CER[NS], to the most recent studies, using the phytosphingosine CERs such as CER[AP].

4.4 The long periodicity phase (LPP) controversy Part I: The influence of a natural-like ratio of the CER[EOS] analogue [EOS]-br in a CER[NP]/[AP] based stratum corneum modelling system: A Neutron diffraction study

4.4.1 Abstract

This study used neutron diffraction to investigate a ceramide-[NP] C24/[AP] C24 /[EOS]-br C30/cholesterol/lignoceric acid (0.6 : 0.3 : 0.1 : 0.7 : 1) based stratum corneum modelling system. By adding specifically deuterated ceramides-[NP]-D3, [AP]-D3, and [EOS]-br-D3, detailed information on the lamellar and the nanostructure of the system was obtained. For the short periodicity phase a native-like lamellar repeat distance of 5.47 ± 0.02 nm was observed, similar to the [NP]/[AP] base system without the [EOS]-br. Unlike in this system the ceramides here were slightly tilted, hinting towards a slightly less natural arrangement. Due to the deuteration it was possible to observe that the long ceramide chains were overlapping in the lamellar mid-plane. This is considered to be an important feature for the native stratum corneum. Despite the presence of a ceramide [EOS] analogue – able to form a long phase arrangement – no distinct long periodicity phase was formed, despite a slightly higher than natural ω -acyl ceramide ratio of 10 mol%. The deuterated variant of this ceramide determined that the very long ceramide was integrated into the short periodicity phase, spanning multiple layers instead. The – compared to the base system – unchanged repeat distance highlights the stability of this structure. Furthermore, the localisation of the very long ceramide in the short periodicity phase indicates the possibility of a crosslinking effect and thus a multilayer stabilizing role for the ceramide [EOS]. It can be concluded, that additionally to the mere presence of ceramide-[EOS] more complex conditions have to be met in order to form this long phase. This has to be further investigated in the future.

DOI: n.d.

4.4.2 Introduction

The epidermis is the main barrier of the body to most environmental factors like UV-radiation, pathogens and chemical penetrants. Particularly its outermost layer, the *stratum corneum* (SC), is of much importance for this barrier. Detailed investigations of its nanostructure and properties are necessary. A number of pathological conditions like psoriasis^[12–14], are the direct result of an altered SC structure and still only partly understood. Furthermore, the SC is an almost impenetrable barrier for most pharmaceuticals. Detailed knowledge of the SC architecture and function could help to solve these long-standing problems.

The SC is a 9-13 μm thick rigid network of 15-30 layers of terminally differentiated highly keratinized corneocytes^[31,39–41]. It has a low water content of 18 - 58 %^[38]. The cells are embedded within a multilamellar ordered lipid matrix. Two distinct phase arrangements are observed within this matrix: The short periodicity phase (SPP), with 5 - 6 nm and the long periodicity phase (LPP), with 12 - 14 nm lamellar repeat distance^[104,119,120]. The exact natural nanostructure of the SPP and particularly the LPP are still mostly unknown. Various studies that used diverse model systems often generated contradictory data or did not detect a LPP at all (see also Table 1S Supporting Material).

The lipid matrix (LM) has a very unique lipid composition of mainly ceramides (CERs) (40 wt%), cholesterol (CHOL) (25 wt%), free fatty acids (FFA) (25 wt%) and cholesterol sulphate (ChS) (6

wt%)[52,53,165,166]. The CERs are a highly variable family of lipids with a complex head group molecular structure[25,26,58,59]. They are not only a main contributing factor for a proper function of the skin barrier[167], but also for the overall phase behaviour and lamellar nanostructure[24,64]. Especially CER[EOS] is presumed to be a prerequisite for the formation of the LPP. Furthermore it is presumed, that CER[EOS] has a very special function within the SPP and is able to span over and thus crosslink both lamellar leaflets and even multiple lamellae. This could be an important factor for the stabilization of the lamellar structure[95,101].

CER[EOS] is a member of the ω -hydroxy-CERs, which typically have very long ω -hydroxy-fatty acids bound to their amide group. Most commonly, unsaturated C16 -C20 fatty acids like linoleic acid are ester bound to the ω -hydroxy-group[96]. So far, the most accepted and well-known theoretical model describing the LPP structure is the sandwich model. According to this model, the unsaturated ω -hydroxy-fatty acids are presumed to be located in a middle layer within the LPP together with CHOL and unsaturated FFAs forming a very fluid middle layer[134–136]. For CER[EOP], which differs from [EOS] only in its head group structure, the formation of the LPP was reported to be reduced and the phase was less defined[97]. The native ratio of CER[EOS] to total CER is 2.9 - 4.6 mol% and for overall ω -hydroxy-CERs to total CER the ratio is 4.6 – 9.6 mol% (see Table 1S Supporting Material). However, almost all studies detecting a LPP in the past used a much higher CER[EOS] and/or total ω -hydroxy-CERs ratio than the one found within the native LM (see Table 1S Supporting Material). Therefore, it is even more important to study the influence of a native ratio of CER[EOS]/ ω -hydroxy-CER as well as to start from simple systems to identify each individual influencing factor. Ultimately only this approach can explain observations in the complex near-native model systems and the native skin.

Simple synthetic CER, CHOL and FFA mixtures have been used before to generate SC simulating models. These models were shown to be powerful tools in order to assess the influence of individual factors on the lamellar structure and the interaction between different lipid species. Neutron scattering combined with specifically deuterated lipids allows their exact localisation within the lamellar structure. The aim of this study, consequently, was to investigate the influence of a native-like ratio of the CER[EOS] on the nanostructure and possible formation of a LPP within the CER[NP]/[AP] C24 based system[159]. This model – even though its composition was very simple, containing only CER[NP], CER[AP], CHOL and lignoceric acid (LA) – showed a good overall conformity with far more complex model mixtures and the native SC. Its repeat distance was similar to the complex situation. No apparent lateral domain formation or phase separation was observed. A middle layer, where the long C24 chains were overlapping, was observed. These features are often described as important for the biological and biophysical properties of the SC LM[159]. Since the CER[EOS] is presumed to be such an important influencing factor and prerequisite for the formation of a LPP, this study could help to further understand its special role and the structure and properties of the LPP within a simple system. In this study 10 mol% of a CER[EOS] equivalent – CER[EOS]-br – was applied. This molecule has a C10-methyl-palmitic- ω -hydroxy-fatty acid. 10 mol% are about the maximum of the total ω -hydroxy-CER content reported for the native SC (see Table 1S in Supporting Material). For the neutron diffraction experiments, a deuterated variant the CER[EOS]-br-D₃, deuterated at the terminal carbon of the ω -OH-fatty acid was used for contrast measurements as described above. Since no deuterated natural [EOS] was available, CER[EOS]-br was chosen as a substitute. The CER[EOS]-br, however, also has some particular advantages, which led to the selection of this analogue. For this analogue, three different deuterated variants were available. Considering various descriptions of the LPP structure, most other deuteration positions would have been hard to detect, since they would have been located extremely close to the head or ω -acyl group. With this deuteration, the double hairpin conformation with the ω -fatty acid folded back towards the base chain as described by Eichner et al.[181] and the commonly decried single hairpin conformation could be distinguished. Furthermore, the saturated branched variant is much more stable against ω -deacetylation and oxidation. Considering the low applied ratio these effects could otherwise

have a relevant impact. Especially oxidation by reactive oxygen activated by the ionizing radiation could give a false indication of additional scattering intensity due to oxidized double bonds or distort the overall signal. Since the CER[EOS]-br was shown to yield a detectable LPP structure, it was deemed a suitable [EOS] substitute for the experiments^[181].

4.4.3 Materials and Methods

4.4.3.1 Ceramide Mixtures

Mixtures of CER, CHOL and LA were prepared for the experiments. CER[NP] (N-(tetracosanoyl)-phytosphingosine), CER[AP] (N-(2R-hydroxy-tetracosanoyl)-phytosphingosine), CER[EOS]-br (N-(30-(10-methyl-hexadecanoxyl)-tricontanoyl)-sphingosine), as well as their terminally deuterated analogues were synthesised and purified to $\geq 95\%$ published elsewhere^[157–159]. CHOL and LA were purchased from Sigma Aldrich GmbH (Taufkirchen, Germany). The chemical structures of the deuterated molecules are displayed in Figure 1.

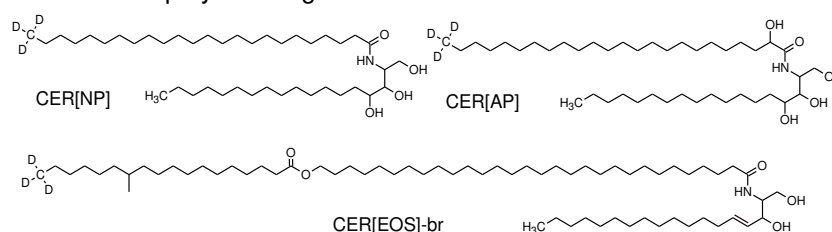


Figure 39: Structures of the deuterated lipids used for these experiments.

4.4.3.2 Sample preparation

The SC model membranes were prepared on quartz glass slides. For sample application, the pure substances were dissolved in a 2:1 mixture of chloroform and methanol (analytical grade, by Sigma Aldrich) with a concentration of 10 mg/ml. Following this, the solutions were combined to generate CER/CHOL/FFA mixtures with molar ratios of 1 / 0.7 / 1. The CER[NP]/[AP]/[EOS]-br were mixed in a molar ratio of 0.6 / 0.3 / 0.1 which is a native-like [NP]/[AP] and [EOS]/total CER ratio. For each CER species, a corresponding system with the respective deuterated CER was prepared for use in the neutron scattering experiments. The mixtures were sprayed onto quartz glass slides, using an airbrush instrument (Harder & Steenbeck, Norderstedt, Germany). The samples were sprayed at a temperature of 70.5 °C which is just below the melting point of the mixture. Afterwards, the samples were annealed to form the multilamellar structure by heating under high humidity for 2 h, cooling at room temperature for 1 h and a further heating under high humidity for 1 h.

4.4.3.3 Neutron Diffraction Experiments

Diffraction data were collected at the small angle diffraction instrument d16 located at the Institute-Laue-Langevin (ILL) in Grenoble, France. A highly oriented pyrolytic graphite (HOPG) monochromator was used to reflect neutrons with a wavelength of $\lambda=4.55 \text{ \AA}$ to the sample. With a fixed detector Θ -position, the sample angle ω was rotated in an ω -scan. The intensity of the scattered neutrons was recorded as a function of the scattering angle 2Θ on a 2D ^3He detector placed at distance of 950 mm from the sample. The detector is made of arrays of 320 anodes x 320 cathodes spaced by a distance of 1mm providing a detector resolution of 1 mm x 1 mm. For contrasting against the water scattering length density, three different $\text{H}_2\text{O}/\text{D}_2\text{O}$ ratios of 0:100, 50:50 and 92:8 (w/w) were applied. A higher D_2O content also generates a higher signal-to-background ratio, which allows for detection of peaks of higher

diffraction orders with high precision. These higher order peaks are very important for calculation of a detailed neutron scattering length density profile (NSLD). For the scans, the temperature for contrast variation was kept at 32 °C. The relative humidity was kept at either 98 % or 57 % using the D16 humidity chambers developed at ILL to see the influence of humidity. Since it could be observed that no change in the diffraction signal occurred after about 6 h of equilibration, samples were given a period of at least 7 h after any change of either temperature, humidity or H₂O/D₂O ratio. The membrane spacing was determined according to Bragg's law $n\lambda = 2d \sin(\Theta)$. The NSLD $\rho(x)$ was calculated by Fourier synthesis of the structure factors F_n according to:

$$\rho(x) = a + b \frac{2}{d} \sum_{n=1}^{n_{max}} F_n \left(\frac{2\pi nx}{d} \right)$$

The coefficients a and b are for relative normalisation of $\rho(x)$, d is the lamellar periodicity and n the order of diffraction. The absolute values of the structure factors could be calculated as $|F_n| = \sqrt{h_n A_n I_n}$, with h_n as the Lorentz correction, A_n as absorption correction^[146] and I_n as Intensity of the nth peak. The integration of the Bragg's peak intensities was performed using the IGOR Pro 6.1 software (WaveMetrics Inc., Portland, OR, USA). For the Fourier transform, both the absolute value as well as the phase sign of each structure factor F_n is required. Assuming a Gaussian water distribution with a maximum position $x = \frac{d}{2}$ within the hydrophilic head group region, allows determination of the F_n by application of different H₂O/D₂O contrasts, representing an *isomorphous replacement*^[146,149]. The centro-symmetric lipid arrangement which is to be expected of CER-membranes leads to a phase of either + or – for each F_n . A three-point measurement with three different H₂O/D₂O contrasts is thus sufficient for the calculation of the phase of each structure factor. A detailed description can be found elsewhere^[146–148].

4.4.4 Results

From the measured diffraction patterns^[182] NSLDs were calculated as described above. Due to the use of the specifically deuterated CER, additionally to the lamellar arrangement, the molecular nanostructure of the systems could be assessed. All structure factors that could be determined by the D₂O/H₂O-contrast variation were in phase with uneven factors with a negative sign and even factors with a positive sign as shown in Table 1.

Table 13: Structure factors F_n for diffraction orders 1-5 at 100 % D₂O and 98 % R.H..

	CER[NP]/[AP]/[EOS]	CER[NP]-D ₃ /[AP]/[EOS]	CER[NP]/[AP]-D ₃ /[EOS]	CER[NP]/[AP]/[EOS]-D ₃
F ₁	-0.394 ± 0.003	-0.368 ± 0.003	-0.368 ± 0.003	-0.411 ± 0.004
F ₂	0.218 ± 0.007	0.247 ± 0.006	0.265 ± 0.008	0.198 ± 0.008
F ₃	-0.176 ± 0.012	-0.152 ± 0.013	-0.154 ± 0.011	-0.154 ± 0.017
F ₄	0.142 ± 0.012	0.117 ± 0.013	0.130 ± 0.009	0.151 ± 0.018
F ₅	-0.069 ± 0.009	-0.116 ± 0.019	-0.083 ± 0.018	-0.086 ± 0.012

Peaks for phase separated crystalline CHOL as often observed in simple model systems were present but only very faintly. The asymmetric long chain CER within this system formed an SPP with a lamellar repeat distance of 5.47±0.02 nm. This repeat distance is slightly shorter, than two opposing C24 chains. It would however perfectly fit an arrangement with each long chain opposing a short chain or CHOL and the long C24 chains thus overlapping in the lamellar mid-plane. Since the CER head groups have a very strong diffraction signal, they can easily be located at the borders of the NSLD. Otherwise the NSLD is very flat without other distinct minima or maxima. The head group region also was the only part of the NSLD that showed an influence of the contrast variation. At a D₂O/H₂O ratio of 8/92 water is invisible for the neutron beam. This occurs because the positive D and negative H coherent scattering length' silence each other. This makes it possible to isolate the signal of the lipids themselves. Compared to the 100 %

D₂O profile, where a maximum water signal is obtained, the location of the water can be identified. The 100 % - 8 % D₂O profile only shows a change in intensity within the outer head group regions. The inner ω -acyl-groups could not be located, despite the two oxygen atoms contained, which is most likely a result of the small amount contained at all. They also don't seem to be hydrated since no water was detected anywhere aside from the head group region. The otherwise flat profile and the lack of a distinct minimum also support an arrangement with overlapping long chains (Figure 2a). No change in the profile could be observed as a result of the change from about native humidity of 57 % (R.H.) to 98 %. This shows that the model membrane does not take up any more water at increased humidity. Also no swelling, which would have been indicated by a change in repeat distance or any other distinct changes, could be detected over hydration (Figure 2 b).

The bound water can be considered basically static, because it is so strongly bound within the H-bonding network of the head groups. Only very little exchange with the surrounding medium takes place and no further water is taken up into the head group region, not even under extremely high humidity conditions. The relative water content was thus constant at about 47 %.

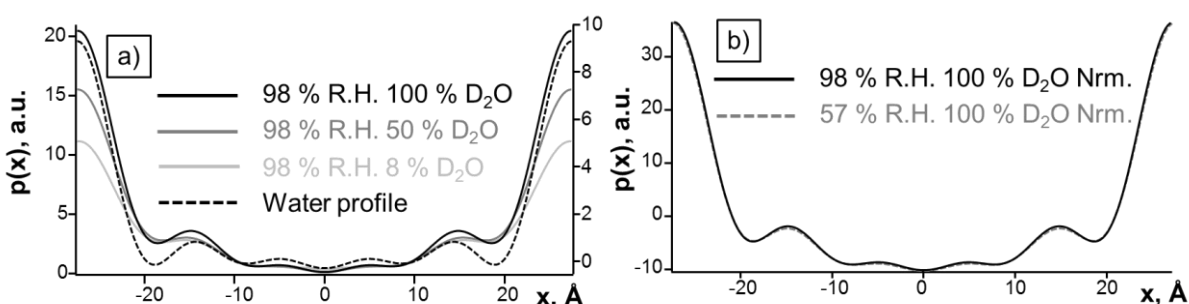


Figure 40: NSLD for the three H₂O/D₂O contrasts. a) For the non-deuterated CER[NP]/[AP]/[EOS]-br system and the water profile (difference profile between 100 % and 8 % D₂O on the right axis). b) The NSLD of the non-deuterated CER[NP]/[AP]/[EOS]-br at the two different humidities 98 % and 57 %.

For CER[NP]-D₃ the difference profile shows two well resolved maxima, slightly outwards from the lamellar center. This shows that the deuterium labels at the terminal end of the C24 chains are located at these two distinct positions. This is coherent with the presumed arrangement with the ends of the long C24 acyl-chains overlapping in the lamellar middle. Considering the estimated length of a single CER molecule of about 2.2 nm for the C18 chain and 3.2 nm for the C24 chain, the deuteration positions suggest a slightly tilted arrangement of the two CER. Otherwise the repeat distance would have to be increased as well, because of the reduced overlapping of the long chains (Figure 3a). For CER[AP]-D₃ also two deuteration positions were observed. They were however closer to the lamellar center as for CER[NP]-D₃ and therefore they were also closer to each other and much less dissolved, making them almost indistinguishable. This leads to a merging of the two peaks, they appear as one broad peak. However, the shape of the peak shows clearly that there are actually two deuteration positions being very close to each other. Considering that the chains are most likely already arranged with a slight lateral tilt angle as described above, CER[AP] appears to be arranged in a way that makes it somehow shorter than CER[NP] (Figure 3b). For CER[EOS]-br also two deuteration positions were detected, slightly inward from the head group region. The only possible arrangement for CER[EOS]-br that would lead to such an appearance is the very long CER spanning both lamellar leaflets, with its terminal end located near the head group region of the opposing leaflet, and its ω -acyl-group near the lamellar center (Figure 3c).

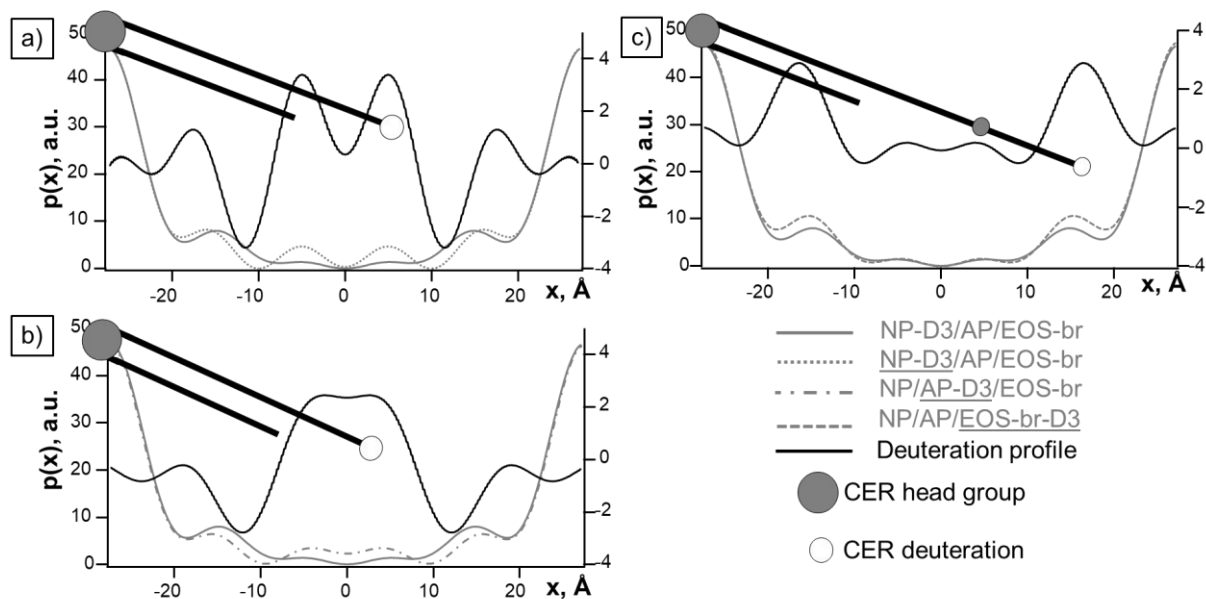


Figure 41: NSLD for the investigated CER[NP]/[AP]/[EOS]-br based model system. a) compared to the sample with deuterated CER[NP]. b) compared to the sample with deuterated CER[AP]. c) compared to the sample with deuterated CER[EOS]-br. A difference = deuteration profile is added to each NSLD (right axis). A most likely arrangement of the contained CER is indicated by a stylized CER molecule.

CER[EOS]-br thus almost completely spans both lamellar leaflets with the end of its ω -acyl-chain located slightly inward from the head group region of the opposing lamellar leaflet. The shorter C24 CER, on the other hand, are arranged with overlapping ends of the C24 chains, with CER[AP] being slightly shorter than CER[NP]. The peaks observed in the difference profiles in Figures 3 a and b, slightly inward from the head group region, are experimental artifacts. These are errors from the Fourier synthesis and are a result of the changed overall shape of the diffraction profile. Since the number of observed diffraction peaks is finite (5 orders in this case), a change of one structure factor and thus one altered wave function can lead to these error peaks at certain positions. However, the intensity of the real peaks is about twice as high as the intensity of the error peaks, so they can still be distinguished from each other.

Except for the described SPP no pronounced additional phases, including the LPP were detected in a measurable amount, despite the use of a nearly native ratio of CER[EOS]-br together with two of the most common SC CER. In the sample containing the deuterated CER[EOS]-br where the signal for [EOS]-br should be the strongest, small traces of a second phase with an estimated repeat distance of 11.1 nm were detected (Figure 4).

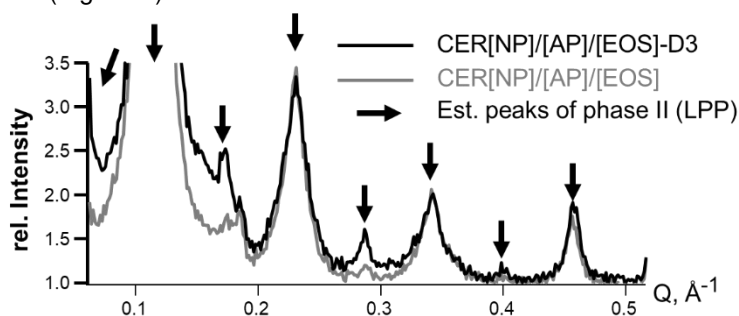


Figure 42: Relative neutron diffraction profiles of the CER[NP]/[AP]/[EOS]-br system and its counterpart with the deuterated CER[EOS]-br (normalized on intensity of the first order lamellar peak). For the latter one, the observed and estimated positions of the diffraction peaks of a weak second phase are indicated.

In the other samples, peaks indicating a second phase were irrelevantly small or not present at all. Using this particular method, at least several hundred layers contribute to the final diffraction signal. Even though an absolute quantification is not possible when evaluating the difference in absolute signal intensity for the main phase and the second phase, it is certain, that the signal of the second phase can only be the result of a single digit number of layers. This is not enough to indicate a physiologically relevant phase. In order to compare the two diffraction patterns of the different profiles directly, they were normalized using the intensity of the first order peak. This peak has the highest intensity and should also be independent of the deuteration. However, the intensities for the peaks of the additional phase were too low to evaluate the corresponding profile. Additionally, the spacing of the second phase was approximately double that of the primary phase, so every second position peak was overlaid by one of the peaks of the first phase. Therefore, these peak positions could only be estimated (Table 2).

Table 14: Observed and estimated peak positions for the second phase.

Lam. Ord.	Q position [\AA^{-1}]	$\Delta Q_{L_n-L_{n+1}}$ [\AA^{-1}]	
L1	0.058	---	
L2 (est.)	0.116	Δ_{L1}	0.058
L3	0.173	Δ_{L2}	0.058
L4 (est.)	0.229	Δ_{L3}	0.057
L5	0.285	Δ_{L4}	0.057
L6 (est.)	0.340	Δ_{L5}	0.056
L7	0.394	Δ_{L6}	0.056
L8 (est.)	0.449	Δ_{L7}	0.058
Standard deviation		\pm	0.001
$=\Delta_{\max}-\Delta_{\min}$		$=0.058-0.056$	Δ_{\max} 0.002

Since the second order peak of the first phase was overlaid with the fourth order of the second phase, the relative intensity of the peak was overestimated. To correct the intensity and obtain a correct neutron scattering length density profile, which is absolutely essential for the analysis of the systems' nanostructure, the intensity of the fourth order peak of the long phase was estimated and subtracted from the peak of the main phase. The estimation was based on two factors. Firstly, the intensity of the second order peak was reduced until the difference profile was conclusive with a possible lipid structure. Secondly, the measured and estimated relative peak intensities were then compared to the relative peak intensities of the long phase described by Eichner et al.^[181]. Eichner et al. used the same deuterated CER[EOS]-br and reported a very similar long phase. The relative peak intensities were found to be extremely similar between the two, and the estimation was slightly adjusted accordingly. The long phase as detected by Eichner et al. is most likely solely or mainly based on this long CER, FFA and CHOL, since none of the used deuterated D/L-CER[AP] C18 could be detected within this phase^[181]. Since no second phase was detected using the deuterated CER[NP] and D-CER[AP] either, the same conclusion can be made here. Since the two phases are likely to be very similar if not identical in their structure, this method should be able to give a very good estimation of the relative peak intensity. Using this method, it was also possible to conclude, that no corrections were necessary for the other orders that were overlaid by a second phase peak, since the peaks would be undetectable or irrelevantly small. Comparing the corrected and uncorrected NSLD, the final correction was minimal and did not change the main finding for the two deuteration positions, but substantially reduced the overestimated error in the lamellar middle region (see Figure 5). No reasonable CER arrangement could be found, to fit such a deuteration position.

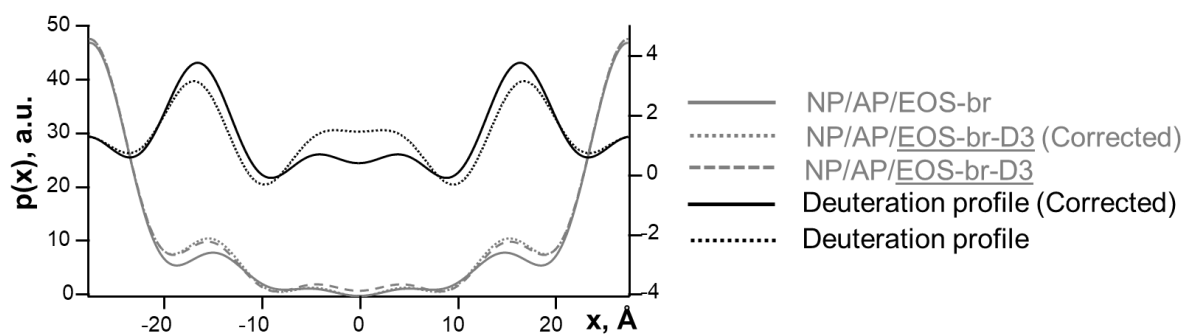


Figure 43: Comparison of the corrected and uncorrected NSLD and deuteration profiles for the CER[NP]/[AP]/[EOS]-br-D₃ mixture (correction was only necessary for the 2nd diffraction order).

4.4.5 Discussion

The results provide important information on both the properties of two CER abounding in the native SC in general as well as the influence of the CER[EOS]-br in particular. The observed lamellar repeat distance of 5.47 ± 0.02 nm is conclusive with the thickness of the native SPP with 5 - 6 nm^[104]. For the SPP of a more native-like model system consisting of 13 different lipid components, a very similar value of 5.4 nm was observed^[69]. A study investigating a wide variety of mixtures including CER[EOS], [EOP] and [EODS] found a repeat distance of about 5.4 nm the SPP^[183]. The overall flat NSLD lacking a distinct minimum, the lamellar repeat distance, and the deuteration positions that were observed, all hint towards the same structure. This is an arrangement with the short C18 chains together with CHOL opposed by the longer C24 acyl-chains. The ends of the C24 chains are overlapping in the lamellar mid-plane. Upon increased humidity, neither a swelling nor any other structural changes were observed. This is conclusive with the observation that the SPP does not change under the influence of excess hydration^[155]. All these observed results, especially the overlapping SPP nanostructure, are similar to the base system without the addition of 10 mol% CER[EOS]-br. They are also comparable to the more complex 13 component system^[69]. A molecular dynamics simulation study, reconstructing a C24 CER[NS]/CHOL/LA system, delivered very comparable results^[70]. The calculated relative hydration of 47 % is about the same as for the system without the CER[EOS]-br, which had a relative hydration of 51 %^[159]. These data demonstrate, that the SPP forming base system consisting of CER[NP] and [AP] is already simulating native SPP quite closely, despite the simplicity of the system.

The lamellar repeat distance of the SPP was completely uninfluenced by CER[EOS]-br. The CER was just incorporated into the SPP, which is conclusive with a study using CER[NS] C18 together with [EOS]-br^[157]. The low variability upon hydration and even the addition of the very long CER[EOS]-br also show the high stability of the base systems SPP, which is a very common property of short CER based multilamellar systems. However, one small change was observed, indicating an increase in lateral chain tilt for CER. This can be concluded from the deuteration positions with a shortening of the overlapping region while the repeat distance was unchanged, compared to the base system. This change is a result of CER[EOS]-br being incorporated into the SPP. From the observed deuteration positions it was possible to conclude, that CER[EOS]-br adopts the commonly described single hairpin conformation, with its ω -acyl fatty acid extended. Considering its calculated length as well as the length observed by Eichner et al. ^[181], the only possible way, the CER can fit the observed features, is by almost completely spanning both lamellar leaflets. The terminal ω -CH₃/CD₃-group is located slightly inward from the opposing head group region. This slightly shorter than calculated length also hints towards a chain tilt, partially decreasing the actual spanned length. This tilt observed for CER[EOS]-br is most likely the main factor inducing the observed increased tilt for the C24 CER. This might be a result of an otherwise energetically unfavourable arrangement due to the length of the CER[EOS]-br. Without the tilt it would

span the whole SPP and its terminal chain would be located within the opposing head group region. The chain could instead get laterally tilted locating it slightly inward from this polar region. Another important factor causing this increase in chain tilt within the system could be the methyl branch of CER[EOS]-br. This feature increases the lateral space requirement for the chain. Since it is located within the opposing chain region, near the head group, it could induce a tilt of the neighbouring chains. Unexpectedly, no change in the NSLD indicating the ω -acyl-group could be observed while the deuteration was well locatable. This is most likely a result of the low concentration and the lower signal compared to the still detectable deuteration. Calculating a cumulated scattering for the atoms found in each group, not considering bond length and other factors, the values are as follows: acyl group (R-CO₂-R) = $18 \cdot 10^{-12}$ cm; Deuteration (R-CD₃) = $27 \cdot 10^{-12}$ cm. The localisation within the chain region might make the acyl group harder to detect, because it is partially silenced by the strong negative scattering of the hydrogens in this region, especially the terminal CH₃-groups in exactly this region giving an overall very low signal that has too little contrast to be detectable. This effect is further favoured by the limited amount of diffraction orders, allowing only a certain degree of detail in the NSLD. Due to the oscillating error caused by the addition of a limited number of wave functions, it is even harder to identify such a very small difference. The incorporation of the very long ω -hydroxy CER into the SPP could have a crosslinking effect between both lamellar leaflets. This effect could be important for the stabilization of the perpendicular structure of the SPP and therefore increase the resistance against physical stress and reduce separation between the leaflets upon chemical disturbances e.g. contact with nonpolar liquids like organic solvents and perpendicular physical pulling forces.

With the particular mixture used in this study no distinct separate LPP could be observed, despite the presence of a nearly native ratio of a CER[EOS] analogue which was shown to be able to form a long phase^[181]. However, at least traces of an 11.1 nm phase were observed in this study. The diffraction peaks of this phase were only visible in the sample containing the deuterated CER[EOS]-br, where the signal for this molecule should be the strongest. In the other samples the peaks were undetectable or vaguely visible at best. The presence of multiple consecutive diffraction peaks clearly indicates the presence of a defined lamellar phase. However, the obtained data, especially the extremely low signal intensity compared to the SPP, suggest only a negligibly small proportion of this phase. Even though it is not quantifiable from the neutron data, the proportion on overall lamellae can be estimated to be less than the main phase at least by the factor of $\geq 2 \cdot 10^2$. This indicates, that the long phase is not yielded in a physiologically relevant proportion in this specific model system, using the applied spraying and annealing protocol.

The observed repeat distance, which could be estimated as 11.1 nm, is also noticeably shorter than what would be expected for a native LPP with 12 - 14 nm^[104,119,120]. This could be a result of the slightly shorter C16 instead of C18 ω -hydroxy fatty acid, of course. The unsaturated chain of the natural CER[EOS] however, should be much more fluid, which would most likely yield a comparably shorter repeat distance. This estimation was already considered for the design of this analogue. Another possible reason for the reduced repeat distance is some change in molecular interaction for this CER due to the increased lateral size caused by its methyl branch. Assuming a lipid arrangement according to the sandwich model^[134-136,184], the increased freedom of movement for the less dense chain in the middle layer would suggest less difference in repeat distance for the laterally slightly larger breached fatty acid. However, considering the most recently introduced, more rigid model according to Mojumdar et al. ^[138,139], an increase in repeat distance would be more likely to occur. The observed repeat distance is in coherence with at least one other study which investigated an equimolar mixture of CER/CHOL and FFA, with the CER being a mixture of 90 mol% CER[NP] C24 and 10 % CER[EOS]. A long phase with a repeat distance of 11.6 nm (about the same as for the mixture investigated here) was observed^[185]. Compared to the SPP, this second phase was also very weak and the diffraction peaks were less defined. Eichner et al., who used the same CER analogue CER[EOS]-br but deuterated at a different

position – at the methyl branch CER[EOS]-D₃-br – together with the racemic D/L-CER[AP] and stearic acid, observed a similar repeat distance ranging from 11.4-11.8 nm depending on hydration^[181]. The long phase found by Eichner et al., which is based on the same CER that was used in our current study, was determined to be very similar to the long phase observed in our study. For this phase it was reported, that the used deuterated D/L-CER[AP] could not be located within the long phase, neither could the CER[EOS]-br be located within the two observed short phases. A different repeat distance and nanostructure is also reported for the two short phases, which are most likely solely or mainly based on one of the two stereoisomers of CER[AP]^[181]. This observation hints towards each of the CER species/isomers forming its own unique phase in this experiment. This is even more likely, considering the used preparation method. Instead of spraying, the lipids were applied to the substrate as a droplet of 10 mg/ml lipid solution. The solvent quickly dried at the generated substrate surface temperature of 80 °C^[181]. This preparation procedure is much stronger influenced by the crystallization process than the spraying of the lipid mixture with a basically instant evaporation of the solvent. The CER are almost crystalline substances, which have a low solubility even in the chloroform methanol mixture used. Since this solubility is different for each CER species, the formation of each phase was thus determined by the crystallization conditions of each CER and the very limited co-crystallization in such a process, mainly involving the shorter and more mobile CHOL and stearic acid. The sample was annealed, using the same procedure as in our study. The strong phase separation still present shows, that the effect the annealing had on mixing of the lipids was minimal to negligible. This is not unexpected, considering the almost crystalline properties of the CER and the low mobility of the lipids in such mixtures, especially of the very long CER[EOS]-br. The observed repeat distance is also very close to what was observed for phase separated crystalline CER[EOS] or simple, solely CER[EOS] based systems. The single CER is commonly detected with a repeat distance of 9.3-10.4 nm^[98,186]. A CER[EOS]/CHOL mixture was detected with a repeat distance of 9.3-9.8 nm^[186]. A CER[EOS]/CHOL/PA mixture showed a repeat distance of 9.5 nm^[127]. This indicates, that the phase observed in both the recent experiments as well as the experiments performed by Eichner et al. are much closer to separated CER[EOS] or at least are solely or mainly CER[EOS]-br based systems. This composition is very far from what is commonly observed for LPP models like the sandwich model^[134–136,184] and other models^[138,139]. This indicates, that this phase could rather be a product of phase separation than of a native-like LPP arrangement. At this point, it could be argued of course, that the opposite effect which was described for the preparation of Eichner et al. is true for the current experiments. In this case instead of favoring a separated CER[EOS]-br phase by performing a more crystallization based preparation, the spraying could favor the artificial incorporation of the CER[EOS]-br into the SPP. Both states could possibly be only semi-stable. However, for the described SPP, a high stability over a long period of time could be observed, while Eichner et al. reported sensitivity of the observed long phase to moisture and especially time, with a reduction of the proportion of the long phase over time ^[181].

The lack of a defined LPP or the very reduced and structurally most likely altered LPP respectively, could have possibly contributed to the structure of the CER[EOS]-br. For other CER[EOS] containing a saturated instead of a unsaturated ω -hydroxy fatty acid, a similar lack of a distinct LPP was reported^[111,187]. Furthermore it is unclear, how the branched ω -fatty acid influences the phase behavior and structure. The partial separation into a separate long phase by using not only a crystallization based preparation and an overblown CER[EOS] ratio of 58 %^[181] but also a more native-like lipid mixture and ratio, demonstrates at least the tendency for this CER to form a long phase. The described finding for the difference between saturated and unsaturated ω -hydroxy fatty acids could also be of much importance, indicating different purposes for the two variants. The saturated variants could serve to stabilize the SPP, while the unsaturated form the LPP.

However, it is still unclear, whether the structure of the LPP as it is described by the sandwich model or any other model so far comes even close to the situation as observed within the natural LM. The

extremely increased CER[EOS] ratios used here could easily induce the formation of a long phase, as the results of Eichner et al. show^[181]. But as mentioned earlier, almost all prior studies used a highly increased CER[EOS] ratio. This increase could easily be solely responsible for the artificial formation of a LPP in these model systems, despite the fact that additional necessary conditions might not have been met^[110,132,184,188]. This would most likely alter the structure of this artificial LPP compared to the natural LM. Furthermore, the content of other very long chain ω -hydroxy-CER could be of significant importance. Several studies found the formation of a LPP even without the presence of the CER[EOS], but [EOP] instead ^[97,99,100] (See also Table 1S supporting material). Opálka et al. was even able to show the lack of LPP in a complex system containing almost all natural CER species as C24 variant, if only CER[EOS], [EOP] or [EODS] were present. The LPP did form however, when all three were present. This could indicate a problem related to the chain packing or the head group interactions. The complex mixture would make the presence of multiple very long ω -acyl-CER species necessary, to moderate each other and optimize the mixing behaviour for the formation of the LPP^[183].

So far only two studies used an nearly native CER[EOS] ratio, and both found only minimal LPP formation with this CER ratio^[183,185]. Opálka et al. was able to show a concentration dependent increase in LPP proportion with solely the LPP being present at 30 mol% of CER[EOS] to total CER^[183]. One study even detected a LPP without the presence of any very long chain ω -acyl-CER^[127]. Since CER[NS] isolated from pig skin was used in this study, it is likely that this effect is simply based on the fact that the CER[NS] contain only a small amount of CER[EOS]. The CER[EOS] and [NS], when chromatographically separated using the common methods at the time, are the first and second fraction and could thus be contaminated with the other fraction respectively, if separation was not performed well enough^[189]. Only one other study was able to find the formation of a LPP with a very low estimated amount of ω -hydroxy-CER of only 0.3 mol% of total CER mass^[100]. Since CERs isolated from pig skin were used in this study and CER[AP] and [EOP] were not separated, the 0.3 mol% are only an estimated amount and consider only CER[EOP]. However, using isolated CERs most likely other fractions are also containing small amounts of other ω -acyl-CER like [EOH], which were discovered later. This makes it nearly impossible to determine the effective amount of ω -acyl-CER in these mixtures. Other studies, which did not use any very long ω -acyl-CER, only found SPP structures. This shows, that by applying a native-like CER[EOS] ratio, every study based on model mixtures failed to find a strong distinct LPP so far, not to mention the analysis of its nanostructure.

The study that most closely simulated the native CER ratios and composition was performed by Opálka et al. but still failed to observe the formation of a LPP with only 10 mol% CER[EOS]. The most convincing indication of the LPP, which could possibly represent the native LPP quite well, was given in the same study using a mixture of CER[EOS], [EOH] and [EODS]. The CER were applied in nearly native ratios and the repeat distance for the LPP with 12.71 nm was comparable to the thickness reported for the native skin.

Looking at the results found by studies using a highly increased CER[EOS] ratio, some of the studies still fail to find a LPP, others describe at least two different possible structures as mentioned above. Furthermore, there is a general trend for the model system based studies, which are observing a LPP. The repeat distance for the LPP in mixtures is always slightly shorter than described for the native LPP. For reconstructed mixtures most times the repeat distance is between 12.0 and 13 nm^[99,110,111,127–133], while for the native skin in most cases a slightly longer repeat distance of 13.2 - 13.8 nm is observed^[119–122,134,135,190,191] (See also table 1S supporting material). This hints towards a difference in the structure of the native and reconstructed LPP. The missing of the LPP in some mixtures, and the failing to observe a defined LPP in every mixture with only a native-like ω -acyl-CER ratio, clearly demonstrates that the context concerning the LPP is much more complicated. It cannot be concluded, that it is simply dependent on the presence or absence and concentration of CER[EOS] alone. The question at this point should thus concentrate less on the mere presence of a separate long phase and its dependence

on the CER[EOS] content. It should rather focus on the presence or absence of the LPP and the influence of other factors at a natural ω -acyl-CER ratio in the model system and the native skin. Especially important would it be to know, which factors determine a native-like structure. This is the only way to find out, whether or not any of the structural features observed for the LPP so far come even close to the native situation. Until we are able to show the formation of a strong and distinct native like LPP with only a native ratio of CER[EOS] or overall ω -hydroxy-CER, it is still questionable, if the observations made in the native LM may indicate a completely different kind of phase arrangement. This could for example be concluded for the structure described by Iwai et al., contributing the broad narrow arrangement solely to an asymmetric distribution of the long and short chains of fully extended asymmetric $>$ C20 CER. In this case, it could be the most native situation, that the CER[EOS] does not form its own phase but is incorporated into the SPP as described here. The results shown by Mojumdar et al., even though being classified as a LPP, also show that the CER[EOS]'s terminal linoleic acid can be incorporated in a more rigid SPP-like layer without a distinct broad narrow, but a uniform layer arrangement^[138,139].

Both CHOL and FFA have to be present, but seem to have very little influence on the presence of the LPP. The minimum ratio of CHOL, where a LPP was still observed, was 2.4 mol% of total lipids ^[132]; the minimum ratio of FFA was 18.5 mol%^[188]. The chain length of the used FFA also seems to have very little influence on the formation of a separate long phase. Of course, since not all these studies could determine a detailed structure nor do we know how the native LPP is constructed, it remains unclear, whether any of these variations have a negative influence on the structure of the LPP. As it stands however, the CER appear to be by far the greatest influencing factor for the LPP. A complete missing of the LPP, despite the presence of high amounts of CER[EOS], was mainly observed for phytosphingosine CER based mixtures with CER[AP] C18^[95,185] and [NP] C18^[185]. This could be the result of several factors, for example the different, less tight chain packing that was observed for phytosphingosine type CER^[74,84,163,179]. Another possibility are the differing head group interactions. For the phytosphingosine CERs, a stronger in-plane H-bonding than for sphingosine CERs was described^[92]. These CER could thus possibly have a negative impact on the formation of the LPP. For CER[NS] especially, interlamellar H-bonding was described^[90,91]. This could be a necessary factor for the formation of the LPP.

For two systems containing only phytosphingosine CER except the [EOS] with an only slightly higher than native total ω -hydroxy-CER ratio of 15 % and [NS] in a high ratio of $>$ 50 mol%, the formation of a defined LPP was observed^[97]. For future experiments investigating the LPP, it is therefore important to test mixed CER[NP]/[AP]/[NS], [NP]/[NS] or [AP]/[NS] systems in combination with [EOS], to learn more about the special influence of the [NS] on the LPP formation. If the addition of CER[NS] can serve as a suitable agent for the formation of a LPP in such a mainly [NP]/[AP] based system, it should be able to simulate the native situation quite well. The resulting system could be a good compromise: A very simple system containing only 6 components with only 4 of them CER, but still simulating native SC properties well enough.

The presence of CER[NS] alone however, does not seem to be enough, since no LPP was observed for a CER[NS] C18/[EOS]-br based system. Overall, we actually still know very little about the LPP and its formation. Since we do not know which or even if any of the LPP structures described so far represent the native structure of the LPP, it is almost impossible to draw any further conclusions about the optimal conditions and to recreate it in a model system, except to reconstruct the native LM as close as possible.

4.4.6 Conclusion

It can be concluded that the investigated CER[NP]/[AP]/[EOS]-br based model system does simulate the native SPP quite well despite its simplicity. The observed repeat distance as well as many of the details, like the overlapping long chains and the integrated CER[EOS]-br, are already native-like. The results are also conclusive with the data obtained for the corresponding system without CER[EOS]-br, which was investigated before^[159] and other data from the literature. The CER[EOS]-br, even though leaving the SPP structure almost unchanged, introduced a slight chain tilt for the other CER.

No distinct LPP was detected in this experimental set up. This could be a feature of the CER[EOS]-br itself. Since at least traces of a second phase have been observed and the formation of a separate long phase using the CER[EOS]-br was shown by Eichner et al. ^[181], it can be concluded that much more complex conditions have to be met for the formation of the LPP. As observed in other studies, phytosphingosine CER based systems appear less suitable to form a LPP together with CER[EOS]. Specifically the CER[NS] could also be of importance for the formation of the LPP. This might be a result of its special properties like the described interlamellar H-bonds.

At this state however, it is still mostly unclear, which conditions exactly are necessary for the formation of the LPP. Data from the literature do not allow to determine, how close the observed models in systems using an extremely increase CER[EOS] ratio are to the native LPP, nor is it possible to draw a final conclusion about the natural structure of the LPP. The exact factors relevant for the formation and structure of the LPP can only be determined step by step using simplified model systems. The specific deuteration has at least the same importance here, since it allows to locate the CER[EOS] within the system and to determine its nanostructure. Other specifically deuterated CER[EOS] variants are already in preparation, to gain even more information on its position within the SPP and possibly LPP in the future.

4.5 Co-authored publications

In this section publications are presented* which were co-authored by the author of this thesis, as a result of the thesis work. These publications are not necessarily directly relatable to the main focus of this thesis (Asymmetric long chain CER[NP] and [AP] C24). They are however part of the same general field of SC research and give interesting new insights in their own rights.

*Only the relevant part, contributed by the author will be presented here.

4.5.1 Synthesis of specific deuterated derivatives of the long chained stratum corneum lipids [EOS] and [EOP] and characterization using neutron scattering


Received: 28 February 2017 | Accepted: 27 March 2017

DOI: 10.1002/jlcr.3504

RESEARCH ARTICLE

WILEY Journal of
Labelled Compounds and
Radiopharmaceuticals

Synthesis of specific deuterated derivatives of the long chained stratum corneum lipids [EOS] and [EOP] and characterization using neutron scattering

Stefan Sonnenberger¹ | Adina Eichner¹ | Thomas Schmitt^{1,3} | Thomas Hauß⁴ | Stefan Lange^{1,2} | Andreas Langner¹ | Reinhard H.H. Neubert³ | Bodo Dobner¹ 

¹Institute of Pharmacy, Martin Luther University Halle-Wittenberg (MLU), Halle (Saale), Germany

²Institute for Medical Physics and Biophysics, University Leipzig, Leipzig, Germany

³Institute of Applied Dermatopharmacy, Martin Luther University Halle-Wittenberg, Halle (Saale), Germany

⁴Institute of Soft Matter and Functional Materials, Helmholtz-Zentrum Berlin für Materialien und Energie, Berlin, Germany

Correspondence

Bodo Dobner, Institute of Pharmacy, Martin Luther University Halle-Wittenberg (MLU), Wolfgang-Langenbeck-Str. 4, 06120 Halle (Saale), Germany.
Email: bodo.dobner@pharmazie.uni-halle.de

Funding information

Deutsche Forschungsgemeinschaft, Grant/Award Number: DO463/6-1

[10.1002/jlcr.3504](https://doi.org/10.1002/jlcr.3504)

The synthesis of specific deuterated derivatives of the long chained ceramides [EOS] and [EOP] is described. The structural differences with respect to the natural compounds are founded in the substitution of the 2 double bonds containing linoleic acid by a palmitic acid branched with a methyl group in 10-position. The specific deuteration is introduced both in the branched and in the terminal methyl group, which was realized by common methods of successive deuteration of carboxylic groups in 3 steps. These modified fatty acids resp. the corresponding ceramides [EOS] and [EOP] were prepared for neutron scattering investigations. First results of these investigations were presented in this manuscript showing that the deuterated compounds could be detected in the stratum corneum lipid model membranes. The deuterated ceramides [EOS] and [EOP] are valuable tools to investigate the influence of these long chained ceramide species on the nanostructure of stratum corneum lipid model membranes.

KEYWORDS

branched fatty acid, CER[EOP], CER[EOS], neutron scattering investigations, specific deuteration

4.5.1.1 Materials and Methods

The SC model membranes were prepared on quartz glass slides. For the sample application, the pure substances were solved in a 2:1 mixture of chloroform and Methanol (analytical grade, by sigma Aldrich) with a concentration of 10 mg/ml. These solutions were then combined, to generate CER[NS]/CER[EOS]-br/CHOL/FFA mixtures with a molar ratio of 0.8/0.2/0.7/1 table 1. For deposition, the mixtures were sprayed onto the surface, using an airbrush instrument (Harder & Steenbeck, Norderstedt, Germany).

Table 15: Measurement conditions for the neutron scattering measurements

Mischung	X [mol/mol]	ϑ [°C]	R.H. [%]	D ₂ O [%]
NS(18)/EOS-br/CHOLL/SA	0.8/0.2/0,7/1	32	98	98/50/8
NS(18)-D ₃ /EOS-BA _{br} /CHOL/SA	0.8/0.2/0,7/1	32	98	98/50/8
NS(18)/EOS-br-D ₃ /CHOL/SA	0.8/0.2/0,7/1	32	98	98/50/8
NS(18)/EOS-D ₃ -br/CHOL/SA	0.8/0.2/0,7/1	32	98	98/50/8

*Diffraction data were collected at the membrane diffractometer V1 located at the Hahn-Meitner campus of the Helmholtz-Zentrum Berlin and treated as described above.

4.5.1.2 Neutron Diffraction Experiments

Diffraction data were collected at the membrane diffractometer V1 located at the Hahn-Meitner campus of the Helmholtz-Zentrum Berlin. Neutrons generated by the research reactor BER II were cooled to a thermal level, using a H2 cold source. A gallium monochromator was utilized, to filter neutrons with a Wavelength of $\lambda = 4.567 \text{ \AA}$. The distance between sample and detector for this device was 101.8 cm. The intensity of the scattered neutrons was recorded as a function of the detector angle 2θ . For contrasting against the water background the three different H₂O/D₂O ratios of 0:100, 50:50 and 92:8 (w/w) were applied. A higher D₂O content also generates a higher signal-to-background ratio, which allows for detection of peaks of higher diffraction orders with high precision. These higher order peaks are very important for calculation of a details scattering length density profile.

Conditions according to Table 1 were applied for the measurements. For the base system and the sample containing the CER[EOS]-d3-br an additional measurement at a hydration of 57 %, which is about the natural moisture content of the skin, and 100 % D₂O, which gives the best signal was performed to investigate possible swelling under excess hydration. Temperature was kept at 32 °C which is about the average temperature of the human skin. Since it could be observed, that no more changes in the diffraction signal occurred after about 6 h of equilibration, samples were given a time of at least 7 h after any change of either temperature, humidity or H₂O/D₂O ratio. To determine the membrane spacing the scattering vector Q was calculated. Q is dependent of the scattering angle by $Q = \frac{4\pi \sin(\theta)}{\lambda}$, it is a result of the incoming wave vector \vec{k}_i and the scattering vector \vec{k}_s , with λ being the neutron wavelength. The repeat distance d of a series of equidistant peaks Q_n is then calculated as $d = \frac{2n\pi}{Q_n}$, with n being the diffraction order. The neutron scattering length density (NSLD) profile as function $p_s(x)$ was calculated by Fourier synthesis of the structure factors F_n according to:

$$p_s(x) = a + b \frac{2}{d} \sum_{n=1}^{n_{max}} F_n \left(\frac{2\pi nx}{d} \right)$$

The coefficients a and b are for relative normalisation of $p_s(x)$, d is the lamellar periodicity and n the order of diffraction. The absolute values of the structure factors could be calculated as $|F_n| = \sqrt{hA_nI_n}$, with h as the Lorentz correction, A_n as absorption correction ^{36[146]} and I_n as Intensity of the n th peak. For calculation of $p_s(x)$, at least three diffraction orders have to be determined. Contrasting with D₂O as mentioned above can be utilised, to determine diffractions of a higher order. Necessary Bragg's peak

determination and integration were performed using the IGOR Pro 6.1 software (WaveMetrics Inc., Portland, OR, USA). For the Fourier transform, both the absolute value as well as the phase of each structure factor F_n is required. Assuming a Gaussian water distribution with a maximum position $x = \frac{d}{2}$ within the hydrophilic head group region, allows determination of the F_n by application of different H₂O/D₂O contrast, representing an isomorphous replacement 36,37. The centro symmetric lipid arrangement which is to be expected of CER-Membranes leads to a phase of either + or – for each F_n . A three point measurement with three different H₂O/D₂O contrasts is thus sufficient for the calculation of the phase of each structure factor. A detailed description of this procedure (contrast variation) and of the neutron diffraction data evaluation can be assessed elsewhere 36,38,39.

4.5.1.3 Results and discussion

Neutron scattering can be used as a very efficient tool to determine the nanostructure of multilamellar CER based mixtures. These models as are used to model the properties of the SC the uppermost layer of the skin. To be able to access specific properties of single CER species only distinguished by a slightly different head group or chain length, pure synthetic CER as synthesized here are necessary. Only using very basic mixtures with these pure single CER or very basic mixtures of only a few CER, the complexity of the model system is low enough to contribute sometimes very minor differences to a specific component. Specifically deuterated CER as synthesized here, furthermore allow determination of the position of this label within the lamellar arrangement, due to the difference in the neutron scattering cross-section of H and D. This allows, to determine the position and chain arrangement of the CER within the system. At the moment, this is the most efficient way to get an insight into the details of the nanostructure of a specific model system.

For the CER[NS]/CER[EOS]-br based system investigated in this study, only a single phase was observed for all four investigated mixtures. This phase had a spacing of 3.94 ± 0.1 nm, thus no LPP with a spacing of 12-13 nm was observed^[104]. The observed spacing however is also shorter than what would be expected for an SPP with two opposing CER[NS] C18/18, which would be estimated as 4.42 nm^[85]. The difference of 0.48 nm cannot be explained by interdigitating chains, temperature or other minor influences. This difference is thus to be assumed, to be the result of a slightly tilted CER-chain arrangement. A chain tilt that would result in a corresponding distance difference would have a tilt-angle α of about 26° (solely considering geometrical factors). The position of the specific deuteration could be determined for all three deuterated CER. A distinct difference between the CER[EOS]-br-D₃ with its terminal end deuterated and the CER[EOS]-d3-br with its branching side chain deuterated could be shown. For the terminally deuterated CER[EOS]-br-d3, the difference is smaller than for the other CER but is observed over the whole range of measurements for the contrast variation and thus can be confirmed. The positions of the different deuterations also strongly support the assumption of a tilted chain arrangement. Furthermore, to fit the SPP arrangement, the CER[EOS] not including its ω -acyl-group was determined to most likely span two whole lamellar leaflets. Its ω -acyl-head-group would then be located in the head group region of the next neighbouring lamellar leaflet and its ω -hydroxy chain arranged parallel to the CER[NS] in a third leaflet. A possible arrangement is shown in Figure 2 for both the short CER[NS] and the very long CER[EOS]-br which is split into two parts to fit a single profile.

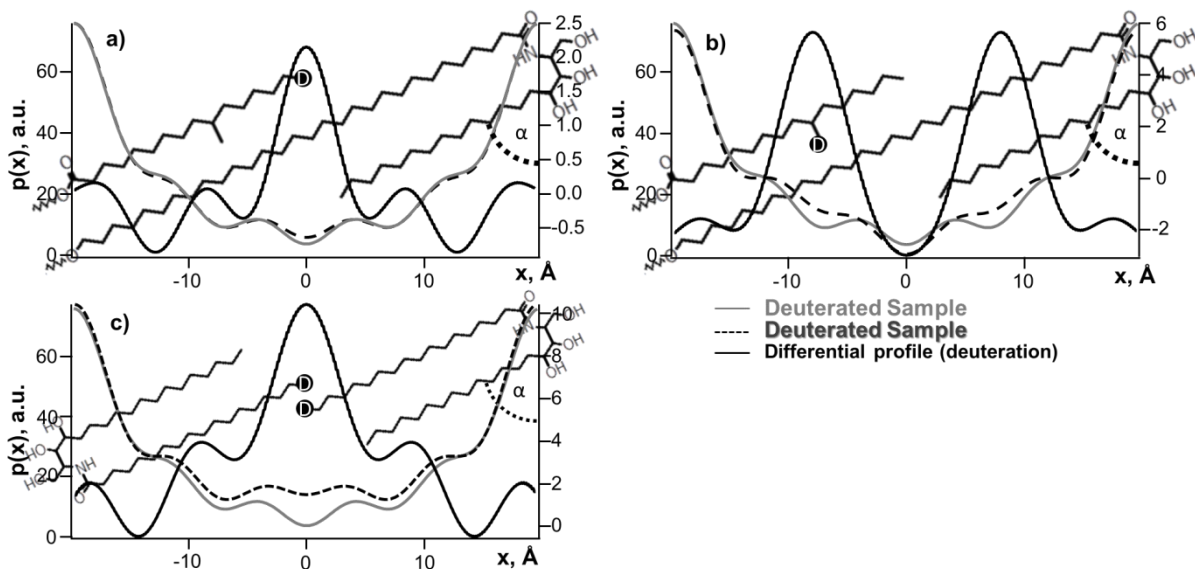


Figure 44: Neutron scattering length density profiles for the CER([NS]/[EOS])/SA/CHOL system with a molar ratio of (0.8:0.2)/1/0.7 in comparison to mixtures with deuterated CER. a) CER[EOS]-br-d3. b) CER[EOS]-d3-br and c) CER[NS]-d3. The very long CER[EOS]-d3-br spanning two lamellae is shown in two parts to fit a single profile.

4.5.1.4 Conclusion

Long chained ceramides EOS and EOP containing a methyl branched fatty acid instead of linoleic acid were synthesized. Besides the full protonated ceramides a specifically deuteration in the branched methyl group and / or at the end of the fatty acid were introduced. Two methods for the preparation of the methyl branched fatty acid were presented, a classic method by dialkylation of diethyl malonate and a shorter method by α alkylation of an acid dianion which needs some higher demands to the equipment and. For the ester formation of the branched fatty acid with a diol a modification of the “normal acylation” procedure was necessary because of the insolubility of the diol at low reaction temperatures. Regarding to the synthesis of natural CER [EOS] or [EOP] with linoleic acid the preparation of the derivatives is possible in a shorter way without a complex blocking group strategy. For the amid formation of the methyl branched ω -acyl ceramides PyBOP® was used as coupling reagent which ensures high yield and a simple work up. First results for the neutron scattering of a CER[NS] based System, containing the two variants of the synthesized deuterated CER[EOS]-br were already obtained. These results clearly show, that the CER[EOS]-br is incorporated into the SPP of CER based model membranes. It can be used to obtain further information on the lamellar nanostructure. It was even possible to distinguish the two differently deuterated long chain ceramides.

4.5.2 The Influence of a Novel Dimeric Ceramide Molecule on the Nanostructure and the Thermotropic Phase Behavior of a Stratum Corneum Model Mixture

LANGMUIR

Article

pubs.acs.org/Langmuir

Influence of a Novel Dimeric Ceramide Molecule on the Nanostructure and Thermotropic Phase Behavior of a Stratum Corneum Model Mixture

Sören Stahlberg,^{†,∇} Adina Eichner,^{‡,∇} Stefan Sonnenberger,^{†,‡,∇} Andrej Kováčik,^{†,§} Stefan Lange,[‡] Thomas Schmitt,^{‡,⊥} Bruno Demé,^{||} Thomas Hauß,[⊥] Bodo Dobner,[‡] Reinhard H. H. Neubert,^{‡,##} and Daniel Huster^{*,†,Ⓢ}

[†]Institute for Medical Physics and Biophysics, Leipzig University, Leipzig, Germany

[‡]Institute of Pharmacy and [#]Institute of Applied Dermatopharmacy, Martin Luther University Halle-Wittenberg, Halle (Saale), Germany

[§]Skin Barrier Research Group, Faculty of Pharmacy in Hradec Králové, Charles University, Akademika Heyrovského 1203, 50005 Hradec Králové, Czech Republic

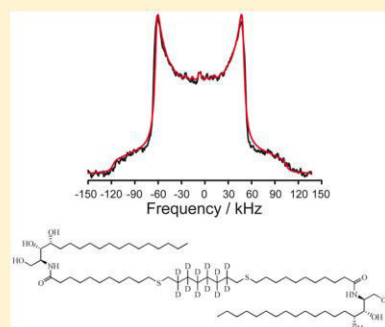
^{||}Institute Laue-Langevin (ILL), Grenoble, France

[⊥]Institute of Soft Matter and Functional Materials, Helmholtz-Zentrum Berlin für Materialien und Energie, Berlin, Germany

Supporting Information

ABSTRACT: The stratum corneum (SC) is the outermost layer of the skin and is composed of a multilayered assembly of mostly ceramids (Cer), free fatty acids, cholesterol (Chol), and cholesterol sulfate (Chol-S). Because of the tight packing of these lipids, the SC features unique barrier properties defending the skin from environmental influences. Under pathological conditions, where the skin barrier function is compromised, topical application of molecules that rigidify the SC may lead to a restored barrier function. To this end, molecules are required that incorporate into the SC and bring back the original rigidity of the skin barrier. Here, we investigated the influence of a novel dimeric ceramide (dim-Cer) molecule designed to feature a long, rigid hydrocarbon chain ideally suited to forming an orthorhombic lipid phase. The influence of this molecules on the thermotropic phase behavior of a SC mixture consisting of Cer[AP18] (55 wt %), cholesterol (Chol, 25 wt %), steric acid (SA, 15 wt %), and cholesterol sulfate (Chol-S, 5 wt %) was studied using a combination of neutron diffraction and ²H NMR spectroscopy.

These methods provide detailed insights into the packing properties of the lipids in the SC model mixture. Dim-Cer remains in an all-trans state of the membrane-spanning lipid chain at all investigated temperatures, but the influence on the phase behavior of the other lipids in the mixture is marginal. Biophysical experiments are complemented by permeability measurements in model membranes and human skin. The latter, however, indicates that dim-Cer only partially provides the desired effect on membrane permeability, necessitating further optimization of its structure for medical applications.



[10.1021/acs.langmuir.7b01227](https://doi.org/10.1021/acs.langmuir.7b01227)

*Since the aim of this investigation is partially different from the rest of the manuscripts, unlike for the other manuscripts, the specialized part of the introduction is given below.

4.5.2.1 Introduction

[...] Several conditions and diseases such as psoriasis^[192], atopic dermatitis,^[193–195] or irritant/allergic contact dermatitis^[193] are known to be associated with a depletion of the ceramide concentration within the SC, which lead to a disturbance of its structure and a compromised barrier function. On a molecular level, modifications of the thermotropic phase behavior, altered lipid packing, and compromised permeability of SC model systems have been revealed^[112,196,197]. In the literature, quite a lot of substances were described, which enhance skin penetration to relevant drugs and cosmetic actives, the so called penetration enhancer^[198,199]. In contrast, there is just limited knowledge about substances, which are able to reduce skin penetration by stabilizing the SC lipid structure^[200].

One approach stabilizing the integrity of the lipid layer of the SC is to incorporate molecules, which induce the orthorhombic lipid phase possibly at low concentrations. To this end, the synthesis of a novel dimeric ceramide molecule (dim-Cer) has been described recently^[201]. The structure of the dim-Cer is shown in Figure 1 and consists of two phytosphingosine moieties linked by a long artificial nonhydroxyl fatty acid, which renders this molecule a derivative of Cer[NP], which is one of the most abundant ceramides in the human SC^[110,202]. The long lipid chain was designed to promote the orthorhombic lipid phase in order to restore the barrier function of the outermost layer in the skin. Applying such putatively rigid molecules is promising as it has been shown that even small quantities of ceramides with altered structure have a profound impact on the microstructure and basic properties such as the permeability of skin lipid membranes^[183,203].

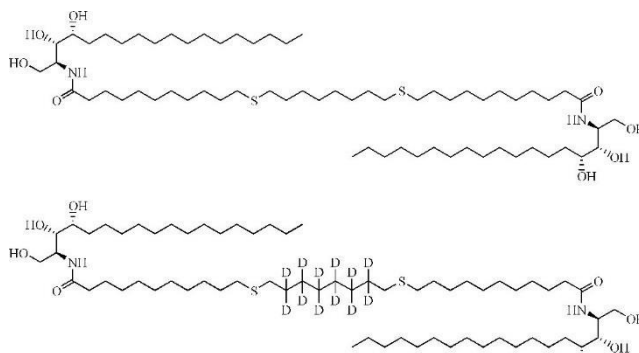


Figure 45: Structures of the dimeric ceramide (dim-Cer) and the deuterated variant dim-Cer-d₁₂.

Here, we have investigated the influence of the dim-Cer molecule on the thermotropic phase behavior of a SC mixture consisting of Cer[AP18] (55 wt%), cholesterol (Chol, 25 wt%), steric acid (SA, 15 wt%) and cholesterol sulphate (Chol-S*, 5 wt%). ²H-NMR spectroscopy was applied to investigate the phase state of the major components of the mixture as well as lipid chain order and packing properties. Neutron diffraction experiments were carried out to localize the deuterated central segment of dim-Cer in the SC multilamellar lipid layers exploiting the difference in the coherent scattering lengths b_{coh} of neutrons for hydrogen (0.374×10^{-12} cm) and deuterium (0.667×10^{-12} cm). Thus, the influence of this new ceramide analog on the crucial properties of the lipid organization in SC models could be evaluated.

*Chol-s: Cholesterol sulfate (equivalent to ChS in introductory part).

4.5.2.2 Materials and Methods

4.5.2.2.1 Sample Preparation for Neutron Diffraction Measurements

In order to determine the effect of dim-Cer, a well-characterized SC lipid model membrane was used as reference^[23,94]. Dim-Cer and dim-Cer-d₁₂ were added in ratios of 5, 10, and 20 wt% to observe an increasing impact of the dim-Cer to the lipid membranes. The fully protonated samples were required as a reference for the localization of the deuterated segments in the samples containing dim-Cer-d₁₂. The samples for the neutron diffraction measurements were prepared as described in the literature^[140].

All lipid components were dissolved separately in chloroform/methanol (2:1, v/v), reaching a concentration of 10 mg/mL and mixed according to the final sample composition listed in Table 1. The airbrush technique was used to deposit 1.2 mL of the final lipid solution onto heated (80°C) quartz wafers. The lipid membranes covered an area of 4.5 × 2.5 cm². Storage under vacuum for at least 12 hours guaranteed the total removal of residual solvent. Subsequently, annealing cycles were carried out, involving three heating periods (85°C for 90 min and 2 times 30 min) each followed by a cooldown to room temperature (30 min, 2 times 15 min). This procedure is known to result in a higher state of lamellar lipid order^[147,204]. A higher signal-to-noise ratio was gained by a subsequent carbonate buffer treatment^[23].

Table 16: Overview of the composition of the SC lipid model systems studied in neutron diffraction experiment

SC lipid model system	Ratio (wt%)	Designation
Cer[AP18]/Chol/SA/Chol-S +5% dim-Cer	55/25/15/5 +5% dim-Cer	AP_dim-Cer5
Cer[AP18]/Chol/SA/Chol-S +10% dim-Cer	55/25/15/5 +10% dim-Cer	AP_dim-Cer10
Cer[AP18]/Chol/SA/Chol-S +20% dim-Cer	55/25/15/5 +20% dim-Cer	AP_dim-Cer20
Cer[AP18]/Chol/SA/Chol-S +5% dim-Cer- <i>d</i> ₁₂	55/25/15/5 +5% dim-Cer- <i>d</i> ₁₂	AP_dim-Cer5- <i>d</i> ₁₂
Cer[AP18]/Chol/SA/Chol-S +10% dim-Cer- <i>d</i> ₁₂	55/25/15/5 +10% dim-Cer- <i>d</i> ₁₂	AP_dim-Cer10- <i>d</i> ₁₂
Cer[AP18]/Chol/SA/Chol-S +20% dim-Cer- <i>d</i> ₁₂	55/25/15/5 +20% dim-Cer- <i>d</i> ₁₂	AP_dim-Cer20- <i>d</i> ₁₂

4.5.2.2.2 Neutron Diffraction Experiments

For the collection of the neutron diffraction data, the D16 diffractometer at Institute Laue-Langevin (ILL, Grenoble, France) was used. The highly ordered pyrolytic graphite monochromator selected a neutron wavelength of $\lambda = 4.5 \text{ \AA}$. The distance between the samples and the position sensitive two-dimensional ³He detector (area = 320 × 320 mm², spatial resolution = 1 × 1 mm²) was 955 mm. The reflection mode was used for the measurements. Sample alignment was performed by goniometers. During the sample rocking scans (Ω scans), the samples were rotated in angular increments of 0.05° from $\Omega = 0$ (membrane stack parallel to the incoming beam) to 12° (detector position at $\gamma = 12.5^\circ$) for the first to the third diffraction order and from $\Omega = 8$ to 20° ($\gamma = 27^\circ$) for the fourth to the fifth diffraction order. To simulate in vivo conditions, a skin temperature of 32 °C was chosen for the experiments. A relative humidity (RH) of 98 % was achieved through the vapor phase of a saturated solution of K₂SO₄ (Sigma-Aldrich, Steinheim, Germany) in several D₂O/H₂O mixing ratios. Each sample was measured at 8/92, 50/50, and 100/0 % (mol/mol) D₂O/H₂O, referred to as contrast variation. The sample environment was constituted by lockable aluminum chambers, realizing constant measurement conditions. After each contrast change, the samples were equilibrated for at least 8 h in order to achieve the optimized level of hydration^[87].

The detector efficiency was corrected using a water calibration, and an empty aluminum chamber measurement was used as background. ILL software LAMP was used for the data reduction. Software package IGOR Pro, version 6.34A (WaveMetrics Inc., Portland, OR, USA) was used for determining the Bragg peak positions and Gaussian fitting of their intensities. From the position of equidistant Bragg peaks Q_n , the distance d between the scattering planes was calculated, which is identical to the repeat distance of the stacked bilayers:

$$d = (2 n \pi)/Q_n \quad (1)$$

Here, h is the Miller index of the $h00$ lamellar reflections or the Bragg peak order. Scattering vector Q correlates with scattering angle 2θ of the incoming neutrons by $Q = 4\pi \sin \theta/\lambda$. The absolute values of structure factor F_h were determined by

$$F_h = \sqrt{h \cdot A_h \cdot I_h} \quad (2)$$

with h as Lorentz factor, A_h as absorption correction, and I_h as integrated intensity of the h^{th} integrated intensity of the h^{th} -order Bragg peak. The thickness of the sample (7 μm) and a linear absorption coefficient of 6 cm⁻¹ were used for the absorption correction. The performed contrast variation enabled

the determination of the F_h phase signs. With a linear correlation between F_h and D_2O/H_2O ratio, the received phase signs were proven by the slope of the linear fit (Figure S1). The phase signs have a positive (+) or negative (-) slope, which is correct for centrosymmetric bilayers^[204].

The calculation of the neutron scattering length diffraction (NSLD) profiles $\rho_s(x)$ was done by Fourier transformation of F_h ^[148]:

$$\rho_s(x) = a + b \frac{2}{d} \sum_{n=1}^{h_{max}} F_h \cos\left(\frac{2\pi hx}{d}\right) \quad (3)$$

With a and b as constants for the relative normalization of $\rho_s(x)$. Using the structure factors of the deuterated samples F_{h_deut} and those from the protonated control sample F_{h_prot} the NSLD profiles $\rho_{deut}(x)$ and $\rho_{prot}(x)$ were calculated. The deuterium difference $\rho_{diff}(x)$ was calculated by:

$$\rho_{diff}(x) = \rho_{deut}(x) - \rho_{prot}(x) \quad (4)$$

The maxima in $\rho_{diff}(x)$ indicate the position of the deuterated segments in the lipid bilayer.

4.5.2.3 Results and Discussion

4.5.2.3.1 Lipid Organization in the SC Lipid Model System in the Presence of the Dimeric Ceramide

Neutron diffraction experiments are particularly well suited to characterize the atomistic details of the rigid lipid phase. Our measurements, showing five lamellar diffraction orders, revealed a single ordered phase in the system. Figure S2 displays the typical Bragg peak pattern of sample AP_dim-Cer5- d_{12} . Using eq 2, the d spacing for all samples was calculated from the diffraction data. Compared to a sample without dim-Cer^[23] membranes containing dim-Cer show a distinctly increased d spacing. In the absence of dim-Cer, a d spacing of 43.9 Å was reported^[23], which increases to 46.3, 46.8, and 47.7 Å in the presence of 5, 10, and 20 wt% dim-Cer, respectively, indicating that dim-Cer is part of the SC lipid model membranes and likely increases the membrane thickness of the rigid orthorhombic domains of the lipid membranes.

The phase signs of all samples were $- + - + -$ for the first to the fifth Bragg peak orders. They were determined by a linear fit of the correlation between F_h and the several D_2O/H_2O ratios (Figure S1). By Fourier transformation of the absolute F_h values according to eq 3, the neutron scattering length diffraction (NSLD) profiles $\rho_s(x)$ for all D_2O/H_2O ratios across the unit cell were obtained (reproduced in Figure S3). The profiles are nearly congruent in the middle of the unit cell, where the lipid alkyl chains are localized. Only at the edges, where the lipid headgroups are localized, are significant differences observed. Because of the water distribution function, we can conclude that there is no indication of the presence of water in the aliphatic alkyl chain regions; water is exclusively found in the polar headgroup regions. Boundary x_{HH} between the hydrophobic and hydrophilic unit cell areas is localized at $x = \pm 16.3$ Å (Figure S3). Thus, the hydrophobic thickness of the bilayer is about 32.5 Å, and each polar region covers a thickness of 6.9 Å in the presence of 5 wt % dim-Cer. In the SC lipid model system in the absence of dim-Cer, we determined a hydrophobic–hydrophilic boundary x_{HH} of 16.3 Å^[23], which is identical to the results described here. Furthermore, the hydrophobic part of the bilayer is comparable as well and has been determined to be 32.6 Å in the absence of dim-Cer. The higher d spacing detected for the dim-Cer-containing mixture translates to a larger polar region increased by about 1.2 Å on either side. This is quite interesting because the dimeric ceramide increases the unit cell scale only by stretching the polar membrane areas.

4.5.2.3.2 Localization of the Central Segments of the Dimeric Ceramide in the SC Lipid Model System

The specific deuteration of the dim-Cer- d_{12} variant enables the localization of the deuterated segments within the SC lipid model system. From the H/D contrast differences, the NSLD difference profiles $\rho_{diff}(x)$ was calculated for the dim-Cer containing SC mixtures and is displayed in Figure 6. Alterations in the values of $\rho_{deut}(x)$ and $\rho_{prot}(x)$ indicate the putative location of the six deuterated methylene segments of dim-Cer- d_{12} .

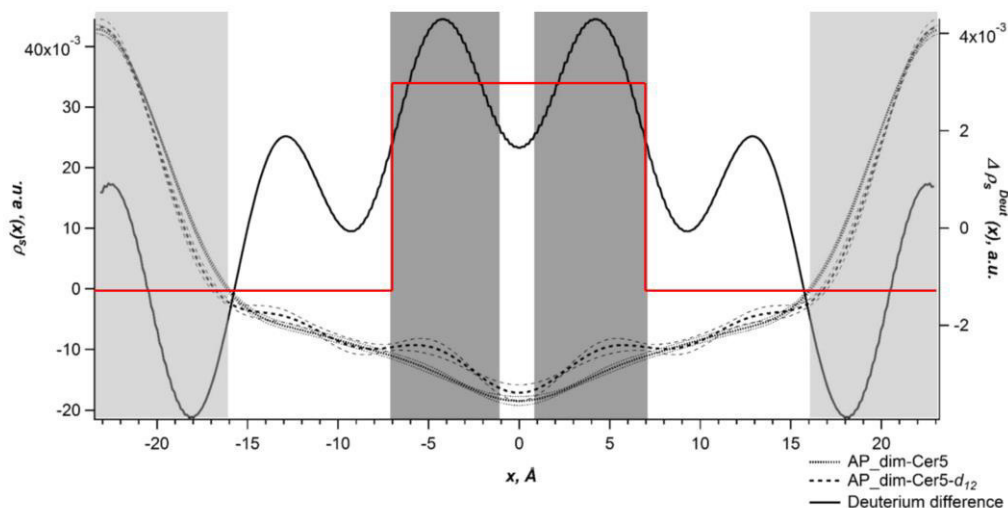


Figure 46: NSLD profiles $\rho_s(x)$ of sample AP_dim-Cer5 (thin dotted line) and sample AP_dim-Cer5- d_{12} (thin dashed line) at 50% D_2O , 98% RH and 32°C. The black solid line represents the deuterium difference $\rho_{diff}(x)$, indicating the position of deuterium labels.

The most prominent alterations in the two NSLD profiles are found in the center of the bilayer between ± 7.0 Å. Because of truncation artifacts caused by the relatively small number of Bragg peaks, an oscillation on the NSLD profiles is observed, and the interpretation of these local maxima/minima should be done with caution especially because the differences in the NSLD profiles are small. This particularly concerns the regions outside the centre (± 7.0 Å). To guide the eye, we have drawn a hypothetical distribution function for the deuterated segments.

Clearly, the data suggests that the long lipid alkyl chain is stretched over the complete unit cell. Assuming 1.27 Å per all-*trans* C-C bond^[205], a total length of 40.6 Å for the C32 chain can be estimated. The data suggests that the central region between ± 7.0 Å indicates the most probable localization of the deuterated segments, allowing us to conclude that one polar headgroup of the dim-Cer molecule may protrude into the polar region of the opposing bilayer. This could possibly explain the local minima in the NSLD difference profile at ± 18 Å, which could be caused by the depletion of the aliphatic region by the ceramide headgroups. Such a scenario would impose packing differences, which could be responsible for the segregation of cholesterol from the orthorhombic phase observed in the 2H -NMR data. Nevertheless, such an arrangement is surprising because it suggests that dim-Cer is not able to incorporate completely and symmetrically into a single bilayer. Although dim-Cer is increasing the unit cell dimension compared to a lipid model membrane in the absence of dim-Cer, the increase in bilayer thickness does not lead to a perfect length match of all molecules in the mixture. This could be caused by the presence of Cer[AP18], which seems to impose a stronger influence on the membrane-assembling process than does dim-Cer. The confidence levels of the NSLD profile of the deuterated sample are not overlapping with the NSLD profile of the protonated sample in the areas we have assigned to the positions of the deuterated methylene segments of dim-Cer. The impact of dim-Cer on the nanostructure of the SC lipid model system has been observed in penetration studies, which

revealed an enrichment of dim-Cer within the native SC^[206]. A model illustrating the arrangement of the lipids in the mixture is shown in Figure 7. The novel dim-Cer stretches over one unit cell and protrudes into the opposing bilayer. This position would explain the stabilizing effect of dim-Cer on the SC barrier function. Because of the comprehensive bilayer interlocking, the penetration of exogenous substances through the SC would be more difficult. Thus, the application of dim-Cer in cutaneous formulations would enable proper barrier properties of diseased skin.

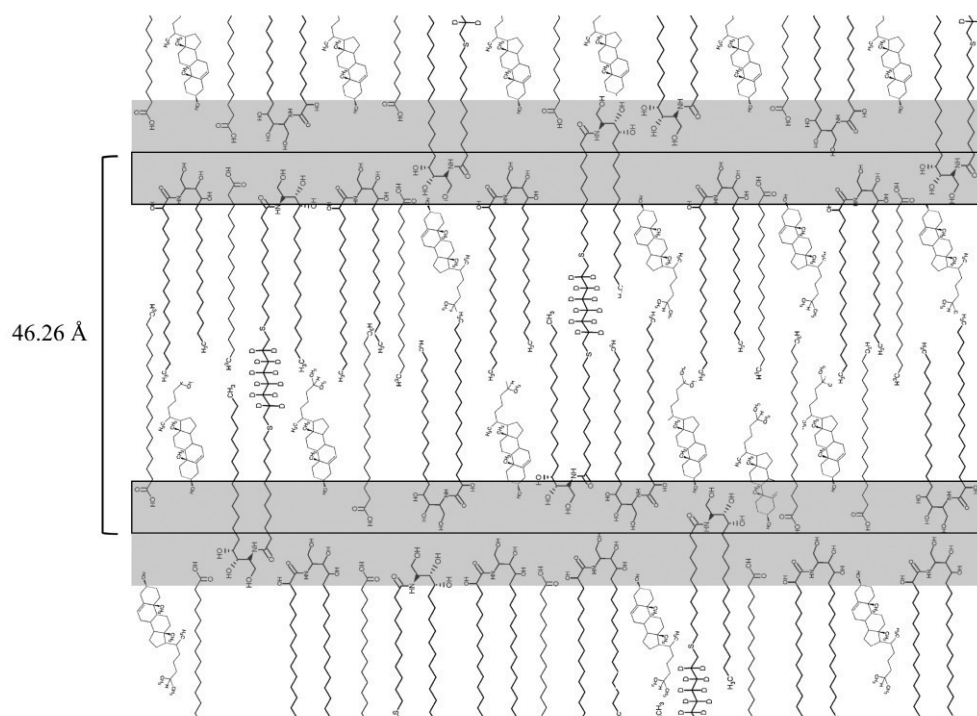


Figure 47: Structural model of the lipid mixture based on Cer[AP18], Chol, SA, Chol-S, and dim-Cer. The gray areas represent a rough interface region, where few water molecules are bound to the lipid headgroups only likely avoiding contact with the aliphatic chain

4.5.2.4 Conclusions

The intension for synthesizing new ceramide molecules potentially stabilizing SC lipid layers, particularly in skin diseases that are characterized by a loss in the ceramide concentration in the SC is the topical application of these molecules to the skin in order to strengthen and recover the barrier function of the diseased skin. The ceramides are very important constituents that reduce the permeability of the SC by inducing a very dense and rigid packing of all lipids. In clinical situations, where a loss in this lipid component of the SC is encountered, artificial ceramide-like molecules that are able to stabilize the skin barrier may represent interesting therapeutic approaches. We have investigated the influence of an artificial dimeric ceramide (dim-Cer) on the structure and thermotropic phase behavior of a typical SC lipid model system. Our results show indeed that the dim-Cer molecule can form a very rigid orthorhombic phase along with Cer[AP18] and SA as desired. Even at elevated temperature this rigid phase persists. Only the cholesterol does not seem to be compatible with this rigid orthorhombic phase state. The neutron diffraction studies reveal an incorporation of dim-Cer into the applied SC lipid model system. It increases the lamellar repeat distance due to its immense chain length. The stabilizing effect of the lipid variant to the SC barrier is visible by its interlocking arrangement beyond one unit cell, extending into the next one. This indeed suggests that the dim-Cer carries potential to stabilize the SC, whether it is also subject to treat skin diseases and the question of how to apply it in medical formulations remains subjects for further studies. Furthermore, it must be studied using specifically deuterated dim-CER derivative whether the dim-Cer is inside the SC bilayer present in the hairpin or in the fully extended conformation in the future.

5. Final Conclusions

With this thesis, it was possible to get a very detailed look on the two CER, [NP] and [AP]. It was shown, that CER[NP] as one of the most abundant skin CER promotes a very native-like LM structure, while the D-CER[AP] in higher concentration promotes a most likely unnatural chain tilt with less overlapping in the lamellar mid-plane. It is also arranged in a way, which makes its C24 chain shorter within the lamellae, possibly because it is pulled up into the HG-region by an additional H-bond of the α -OH. The unnatural L-CER[AP] promoted an even stronger chain tilt with a possibly V-shaped crystalline-like structure and was unable to form a lamellar phase without the addition of CER[NP]. Exchange of CER[NP] for CER[NS] showed, enhanced miscibility with CHOL and also seemed to lead to a more ordered structure, with a slightly shorter repeat distance. The addition of the very long ω -OH-CER[EOS]-br in an about natural ratio of 10 % did not promote the formation of the LPP. It was instead incorporated into the SPP, spanning multiple layers, only inducing a slight chain tilt. These results clearly indicate, that even though the chemical differences between CER species are small, the effects they have are by no means negligible. This is a result of the special structure of these lipids, with a small head group, which is interacting almost exclusively via H-bonds. Since H-bonds are both strong and directed interactions, additional OH-groups but also conformational changes, as they are induced for example by a double bond have a strong influence on the molecular interactions and thus on the structure.

The results especially for the CER[NP]/[AP] 2:1 system demonstrated, that it might be possible, to emulate the native LM quite well, with only very few CER components. Inclusion of the CER[NS] into the system could possibly enhance the miscibility with CHOL. Unfortunately the special role of most other CER is unknown so far, not allowing a final judgement about their necessity for a native-like behaving model. It is also still unclear, if the LPP is a natural structure and possibly of importance for a proper barrier function or other important aspects of the SC or if it is just a result of various artificial experimental conditions like the elevated ratio of very long ω -OH-CER in almost all diffraction experiments. It also became apparent, that the α -OH-CER may be an important contributor to the amount of water, bound within the lamellar HG-region. The CER[AP] generally seems to have a strong influence on the overall lamellar structure. The synthetic L-CER[AP] can be concluded, to be unsuitable, to emulate a natural LM structure, its strong crystalline-like characteristics could however still be interesting for modulating the skin barrier, if the effect can be utilised in a positive way.

6. References

- [1] A. Mayerhofer, L. C. U. Junqueira, J. Carneiro "Histologie: Mit 17 Tabellen, Springer, Berlin [u.a.]" 2005.
- [2] N. A. Campbell, A. Kratochwil, T. Lazar, J. B. Reece "Biologie, Pearson Studium, München [u.a.]" 2009.
- [3] G. Grubauer, P. M. Elias, K. R. Feingold: **Transepidermal water loss: the signal for recovery of barrier structure and function**, *Journal of Lipid Research*, 1989; Vol. 30 3, 323–333.
- [4] J. Reichrath, B. Lehmann, C. Carlberg, J. Varani, C. C. Zouboulis: **Vitamins as hormones**, *Hormone and Metabolic Research*, 2007; Vol. 39 2, 71–84.
- [5] R. J. Scheuplein: **Permeability Of The Skin-** A Review Of Major Concepts And Some New Developments, *The Journal of Investigative Dermatology*, 1976; Vol. 67 5, 672–676.
- [6] A. M. Weerheim, M. Ponc: **Determination of stratum corneum lipid profile by tape stripping in combination with high-performance thin-layer chromatography**, *Archives of Dermatological Research*, 2001; Vol. 293 4, 191–199.
- [7] W. M. Holleran, M.-Q. Man, W. N. Gao, G. K. Menon, P. M. Elias, K. R. Feingold: **Sphingolipids are required for mammalian epidermal barrier function. Inhibition of sphingolipid synthesis delays barrier recovery after acute perturbation**, *The Journal of Clinical Investigation*, 1991; Vol. 88 4, 1338–1345.
- [8] L. Coderch, O. López, A. de La Maza, J. L. Parra: **Ceramides and skin function**, *American journal of clinical dermatology*, 2003; Vol. 4 2, 107–129.
- [9] A. Z. Alkilani, M. T. C. McCrudden, R. F. Donnelly: **Transdermal Drug Delivery: Innovative Pharmaceutical Developments Based on Disruption of the Barrier Properties of the stratum corneum**, *Pharmaceutics*, 2015; Vol. 7 4, 438–470.
- [10] E. Abd, S. A. Yousef, M. N. Pastore, K. Telaprolu, Y. H. Mohammed, S. Namjoshi, J. E. Grice, M. S. Roberts: **Skin models for the testing of transdermal drugs**, *Clinical pharmacology advances and applications*, 2016; Vol. 8, 163–176.
- [11] A. S. Halim, T. L. Khoo, S. J. Mohd Yusoff: **Biologic and synthetic skin substitutes: An overview**, *Indian journal of plastic surgery official publication of the Association of Plastic Surgeons of India*, 2010; Vol. 43 Suppl, S23–8.
- [12] G. Bernard, M. Auger, J. Soucy, R. Pouliot: **Physical characterization of the stratum corneum of an in vitro psoriatic skin model by ATR-FTIR and Raman spectroscopies**, *Biochimica et Biophysica Acta*, 2007; Vol. 1770 9, 1317–1323.
- [13] H. Farwanah, K. Raith, R. H. H. Neubert, J. Wohlrab: **Ceramide profiles of the uninvolved skin in atopic dermatitis and psoriasis are comparable to those of healthy skin**, *Archives of Dermatological Research*, 2005; Vol. 296 11, 514–521.
- [14] S. Motta, M. Monti, S. Sesana, R. Caputo, S. Carelli, R. Ghidoni: **Ceramide composition of the psoriatic scale**, *Biochimica et Biophysica Acta*, 1993; Vol. 1182 2, 147–151.
- [15] K. M. Joo, J. H. Hwang, S. Bae, D. H. Nahm, H. S. Park, Y. M. Ye, K. M. Lim: **Relationship of ceramide-, and free fatty acid-cholesterol ratios in the stratum corneum with skin barrier function of normal, atopic dermatitis lesional and non-lesional skins**, *Journal of Dermatological Science*, 2015; Vol. 77 1, 71–74.
- [16] D. Paslin, P. W. Wertz: **A study to determine the effect of tacrolimus on ceramide levels in the stratum corneum of patients with atopic dermatitis**, *International Journal of Dermatology*, 2006; Vol. 45 4, 352–356.
- [17] P. G. Sator, J. B. Schmidt, H. Honigsmann: **Comparison of epidermal hydration and skin surface lipids in healthy individuals and in patients with atopic dermatitis**, *Journal of the American Academy of Dermatology*, 2003; Vol. 48 3, 352–358.
- [18] G. S. Pilgram, D. C. Visser, H. van der Meulen, S. Pavel, S. P. Lavrijsen, J. A. Bouwstra, H. K. Koerten: **Aberrant lipid organization in stratum corneum of patients with atopic dermatitis and lamellar ichthyosis**, *The Journal of Investigative Dermatology*, 2001; Vol. 117 3, 710–717.
- [19] A. P. Lavrijsen, J. A. Bouwstra, G. S. Gooris, A. M. Weerheim, H. E. Boddé, M. Ponc: **Reduced Skin Barrier Function Parallels Abnormal Stratum Corneum Lipid Organization in Patients with Lamellar Ichthyosis**, *The Journal of Investigative Dermatology*, 1995; Vol. 105 4, 619–624.
- [20] A. Eichner, S. Stahlberg, S. Sonnenberger, S. Lange, B. Dobner, A. Ostermann, T. E. Schrader, T. Hauß, A. Schroeter, D. Huster, R. H. H. Neubert: **Influence of the penetration enhancer isopropyl myristate on stratum corneum lipid model membranes revealed by neutron diffraction and ²H NMR experiments**, *Biochimica et biophysica acta*, 2017; Vol. 1859 5, 745–755.
- [21] A. Schroeter, S. Stahlberg, B. Školová, S. Sonnenberger, A. Eichner, D. Huster, K. Vávrová, T. Hauß, B. Dobner, R. H. H. Neubert, A. Vogel: **Phase separation in ceramideNP containing lipid model membranes: neutron diffraction and solid-state NMR**, *Soft matter*, 2017; Vol. 13 10, 2107–2119.
- [22] S. Stahlberg, A. Eichner, S. Sonnenberger, A. Kováčik, S. Lange, T. Schmitt, B. Demé, T. Hauß, B. Dobner, R. H. H. Neubert, D. Huster: **Influence of a Novel Dimeric Ceramide Molecule on the Nanostructure and Thermotropic Phase Behavior of a Stratum Corneum Model Mixture**, *Langmuir the ACS journal of surfaces and colloids*, 2017; Vol. 33 36, 9211–9221.
- [23] S. Sonnenberger, A. Eichner, T. Hauß, A. Schroeter, R. H. H. Neubert, B. Dobner: **Synthesis of specifically deuterated ceramide AP-C18 and its biophysical characterization using neutron diffraction**, *Chemistry and physics of lipids*, 2017; Vol. 204, 15–24.
- [24] D. Kessner, A. Ruettinger, M. A. Kiselev, S. Wartewig, R. H. H. Neubert: **Properties of ceramides and their impact on the stratum corneum structure. Part 2- stratum corneum lipid model systems**, *Skin Pharmacology and Physiology*, 2008; Vol. 21 2, 58–74.
- [25] Y. Masukawa, H. Narita, H. Sato, A. Naoe, N. Kondo, Y. Sugai, T. Oba, R. Homma, J. Ishikawa, Y. Takagi, T. Kitahara: **Comprehensive quantification of ceramide species in human stratum corneum**, *Journal of Lipid Research*, 2009; Vol. 50 8, 1708–1719.
- [26] Y. Masukawa, H. Narita, E. Shimizu, N. Kondo, Y. Sugai, T. Oba, R. Homma, J. Ishikawa, Y. Takagi, T. Kitahara, Y. Takema, K. Kita: **Characterization of overall ceramide species in human stratum corneum**, *Journal of Lipid Research*, 2008; Vol. 49 7, 1466–1476.
- [27] M. J. Lyons "Neutron scattering methods and studies, Nova Science Publishers, New York" 2011.
- [28] V. F. Sears: **Neutron scattering lengths and cross sections**, *Neutron News*, 2006; Vol. 3 3, 26–37.
- [29] G. Bergsson, J. Arnfinnsson, O. Steingrímsson, H. Thormar: **In vitro killing of Candida albicans by fatty acids and monoglycerides**, *Antimicrobial Agents and Chemotherapy*, 2001; Vol. 45 11, 3209–3212.

- [30] H. Lambers, S. Piessens, A. Bloem, H. Pronk, P. Finkel: **Natural skin surface pH is on average below 5, which is beneficial for its resident flora**, *International Journal of Cosmetic Science*, 2006; Vol. 28 5, 359–370.
- [31] P. W. Wertz, B. van den Bergh: **The physical, chemical and functional properties of lipids in the skin and other biological barriers**, *Chemistry and Physics of Lipids*, 1998; Vol. 91 2, 85–96.
- [32] S. M. Maricich, S. A. Wellnitz, A. M. Nelson, D. R. Lesniak, G. J. Gerling, E. A. Lumpkin, H. Y. Zoghbi: **Merkel cells are essential for light-touch responses**, *Science (New York, N.Y.)*, 2009; Vol. 324 5934, 1580–1582.
- [33] "philschatz" **"Layers of Skin"**: <https://creativecommons.org/licenses/by/4.0/> (CC BY 4.0 based licence) 04.07.2017.
- [34] G. F. Odland: **A Submicroscopic Granular Component in Human Epidermis**From the Department of Anatomy, University of Washington, Seattle, Washington**, *Journal of Investigative Dermatology*, 1960; Vol. 34 1, 11–15.
- [35] P. M. Elias: **Epidermal lipids, membranes, and keratinization**, *International journal of dermatology*, 1981; Vol. 20 1, 1–19.
- [36] L. Landmann: **Die Permeabilitätsbarriere der Haut**, *Pharmazie in Unserer Zeit*, 1991; Vol. 20 4, 155–163.
- [37] R. Abdayem, F. Formanek, A. M. Minondo, A. Potter, M. Haftek: **Cell surface glycans in the human stratum corneum: distribution and depth-related changes**, *Experimental dermatology*, 2016; Vol. 25 11, 865–871.
- [38] A. Alonso, N. C. Meirelles, V. E. Yushmanov, M. Tabak: **Water increases the fluidity of intercellular membranes of stratum corneum: correlation with water permeability, elastic, and electrical resistance properties**, *The Journal of Investigative Dermatology*, 1996; Vol. 106 5, 1058–1063.
- [39] K. A. Holbrook, G. F. Odland: **Regional differences in the thickness (cell layers) of the human stratum corneum: an ultrastructural analysis**, *The Journal of Investigative Dermatology*, 1974; Vol. 62 4, 415–422.
- [40] M. E. Loomans, D. P. Hannon: **An electron microscopic study of the effects of subtilisin and detergents on human stratum corneum**, *The Journal of Investigative Dermatology*, 1970; Vol. 55 2, 101–114.
- [41] R. J. Scheuplein, L. J. Morgan: **"Bound water" in keratin membranes measured by a microbalance technique**, *Nature*, 1967; Vol. 214 5087, 456–458.
- [42] Y. Kitajima: **Regulation and impairments of dynamic desmosome and corneodesmosome remodeling**, *European journal of dermatology EJD*, 2013.
- [43] M. Jarnik, M. N. Simon, A. C. Steven: **Cornified cell envelope assembly: a model based on electron microscopic determinations of thickness and projected density**, *Journal of Cell Science*, 1998; 111 (Pt 8), 1051–1060.
- [44] P. W. Wertz, D. C. Swartzendruber, D. J. Kitko, K. C. Madison, D. T. Downing: **The role of the corneocyte lipid envelopes in cohesion of the stratum corneum**, *The Journal of Investigative Dermatology*, 1989; Vol. 93 1, 169–172.
- [45] S. Meguro, Y. Arai, Y. Masukawa, K. Uie, I. Tokimitsu: **Relationship between covalently bound ceramides and transepidermal water loss (TEWL)**, *Archives of Dermatological Research*, 2000; Vol. 292 9, 463–468.
- [46] M. J. Behne, Y. Uchida, T. Seki, P. O. de Montellano, P. M. Elias, W. M. Holleran: **Omega-hydroxyceramides are required for corneocyte lipid envelope (CLE) formation and normal epidermal permeability barrier function**, *The Journal of Investigative Dermatology*, 2000; Vol. 114 1, 185–192.
- [47] P. M. Elias: **Structure and function of the stratum corneum permeability barrier**, *Drug Development Research*, 1988; Vol. 13 2-3, 97–105.
- [48] R. H. Guy, J. Hadgraft: **Physicochemical aspects of percutaneous penetration and its enhancement**, *Pharmaceutical research*, 1988; Vol. 5 12, 753–758.
- [49] B. W. Barry: **Mode of action of penetration enhancers in human skin**, *Journal of Controlled Release*, 1987; Vol. 6 1, 85–97.
- [50] J. van Smeden, W. A. Boiten, T. Hankemeier, R. Rissmann, J. A. Bouwstra, R. J. Vreeken: **Combined LC/MS-platform for analysis of all major stratum corneum lipids, and the profiling of skin substitutes**, *Biochimica et Biophysica Acta*, 2014; Vol. 1841 1, 70–79.
- [51] R. t'Kindt, L. Jorge, E. Dumont, P. Couturon, F. David, P. Sandra, K. Sandra: **Profiling and characterizing skin ceramides using reversed-phase liquid chromatography-quadrupole time-of-flight mass spectrometry**, *Analytical Chemistry*, 2012; Vol. 84 1, 403–411.
- [52] P. W. Wertz: **The nature of the epidermal barrier- Biochemical aspects**, *Advanced Drug Delivery Reviews*, 1996; Vol. 18 3, 283–294.
- [53] P. M. Elias: **The importance of Epidermal Lipids for the Stratum Corneum Barrier**, in *Topical drug delivery formulations* (Eds.: D. W. Osborne, A. H. Amann); Vol. 19894951, M. Dekker, p. 13" 1990.
- [54] T. Hornemann, A. Penno, M. F. Rutti, D. Ernst, F. Kivrak-Pfiffner, L. Rohrer, A. von Eckardstein: **The SPTLC3 subunit of serine palmitoyltransferase generates short chain sphingoid bases**, *The Journal of Biological Chemistry*, 2009; Vol. 284 39, 26322–26330.
- [55] S. T. Pruet, A. Bushnev, K. Hagedorn, M. Adiga, C. A. Haynes, M. C. Sullards, D. C. Liotta, A. H. Merrill, JR: **Biodiversity of sphingoid bases ("sphingosines") and related amino alcohols**, *Journal of lipid research*, 2008; Vol. 49 8, 1621–1639.
- [56] A. H. Merrill, JR, R. D. Williams: **Utilization of different fatty acyl-CoA thioesters by serine palmitoyltransferase from rat brain**, *Journal of lipid research*, 1984; Vol. 25 2, 185–188.
- [57] C. A. Haynes, J. C. Allegood, K. Sims, E. W. Wang, M. C. Sullards, A. H. Merrill, JR: **Quantitation of fatty acyl-coenzyme As in mammalian cells by liquid chromatography-electrospray ionization tandem mass spectrometry**, *Journal of lipid research*, 2008; Vol. 49 5, 1113–1125.
- [58] M. Rabionet, A. Bayerle, C. Marsching, R. Jennemann, H. J. Grone, Y. Yildiz, D. Wachten, W. Shaw, J. A. Shayman, R. Sandhoff: **1-O-acylceramides are natural components of human and mouse epidermis**, *Journal of Lipid Research*, 2013; Vol. 54 12, 3312–3321.
- [59] M. Rabionet, K. Gorgas, R. Sandhoff: **Ceramide synthesis in the epidermis**, *Biochimica et Biophysica Acta*, 2014; Vol. 1841 3, 422–434.
- [60] P. M. Elias, R. Ghadially: **The aged epidermal permeability barrier: basis for functional abnormalities**, *Clinics in Geriatric Medicine*, 2002; Vol. 18 1, 103.
- [61] A. Conti, J. Rogers, P. Verdejo, C. R. Harding, A. V. Rawlings: **Seasonal influences on stratum corneum ceramide 1 fatty acids and the influence of topical essential fatty acids**, *International Journal of Cosmetic Science*, 1996; Vol. 18 1, 1–12.

- [62] A. Di Nardo, P. W. Wertz, A. Giannetti, S. Seidenari: **Ceramide and cholesterol composition of the skin of patients with atopic dermatitis**, *Acta Dermato-Venerologica*, 1998; Vol. 78 1, 27–30.
- [63] A. Yamamoto, S. Serizawa, M. Ito, Y. Sato: **Stratum corneum lipid abnormalities in atopic dermatitis**, *Archives of Dermatological Research*, 1991; Vol. 283 4, 219–223.
- [64] A. Schroeter, M. A. Kiselev, T. Hauss, S. Dante, R. H. H. Neubert: **Evidence of free fatty acid interdigitation in stratum corneum model membranes based on ceramide [AP] by deuterium labelling**, *Biochimica et Biophysica Acta*, 2009; Vol. 1788 10, 2194–2203.
- [65] S. Wartewig, R. H. H. Neubert: **Properties of ceramides and their impact on the stratum corneum structure**- a review. Part 1: ceramides, *Skin Pharmacology and Physiology*, 2007; Vol. 20 5, 220–229.
- [66] I. Iwai, H. Han, L. den Hollander, S. Svensson, L.-G. Ofverstedt, J. Anwar, J. Brewer, M. Bloksgaard, A. Laloef, D. Nosek, S. Masich, L. A. Bagatolli, U. Skoglund, L. Norlén: **The human skin barrier is organized as stacked bilayers of fully extended ceramides with cholesterol molecules associated with the ceramide sphingoid moiety**, *The Journal of Investigative Dermatology*, 2012; Vol. 132 9, 2215–2225.
- [67] M. Boncheva, F. Damien, V. Normand: **Molecular organization of the lipid matrix in intact Stratum corneum using ATR-FTIR spectroscopy**, *Biochimica et Biophysica Acta*, 2008; Vol. 1778 5, 1344–1355.
- [68] E. ten Grotenhuis, R. A. Demel, M. Ponec, D. R. Boer, J. C. van Miltenburg, J. A. Bouwstra: **Phase behavior of stratum corneum lipids in mixed Langmuir-Blodgett monolayers**, *Biophysical Journal*, 1996; Vol. 71 3, 1389–1399.
- [69] D. Groen, G. S. Gooris, D. J. Barlow, M. J. Lawrence, J. B. van Mechelen, B. Demé, J. A. Bouwstra: **Disposition of ceramide in model lipid membranes determined by neutron diffraction**, *Biophysical Journal*, 2011; Vol. 100 6, 1481–1489.
- [70] C. Das, M. G. Noro, P. D. Olmsted: **Simulation studies of stratum corneum lipid mixtures**, *Biophysical Journal*, 2009; Vol. 97 7, 1941–1951.
- [71] R. Gupta, B. Rai: **Molecular Dynamics Simulation Study of Skin Lipids: Effects of the Molar Ratio of Individual Components over a Wide Temperature Range**, *The journal of physical chemistry. B*, 2015; Vol. 119 35, 11643–11655.
- [72] M. E. Rerek, H.-C. Chen, B. Markovic, D. van Wyck, P. Garidel, R. Mendelsohn, D. J. Moore: **Phytosphingosine and Sphingosine Ceramide Headgroup Hydrogen Bonding**- Structural Insights through Thermotropic Hydrogen/Deuterium Exchange, *The Journal of Physical Chemistry B*, 2001; Vol. 105 38, 9355–9362.
- [73] J. Shah, J. M. Atienza, R. I. Duclos, A. V. Rawlings, Z. Dong, G. G. Shipley: **Structural and thermotropic properties of synthetic C16:0 (palmitoyl) ceramide: effect of hydration**, *Journal of Lipid Research*, 1995; Vol. 36 9, 1936–1944.
- [74] E. Corbe, C. Laugel, N. Yagoubi, A. Baillet-Guffroy: **Role of ceramide structure and its microenvironment on the conformational order of model stratum corneum lipids mixtures**- an approach by FTIR spectroscopy, *Chemistry and Physics of Lipids*, 2007; Vol. 146 2, 67–75.
- [75] S. Raudenkolb, W. Hübner, W. Rettig, S. Wartewig, R. H. H. Neubert: **Polymorphism of ceramide 3. Part 1**- an investigation focused on the head group of N-octadecanoylphytosphingosine, *Chemistry and Physics of Lipids*, 2003; Vol. 123 1, 9–17.
- [76] P. Garidel: **Calorimetric and spectroscopic investigations of phytosphingosine ceramide membrane organisation**, *Physical Chemistry Chemical Physics*, 2002; Vol. 4 10, 1934–1942.
- [77] P. Garidel: **N-Stearoyl-Phytosphingosine Lipid Organisation as Observed by Synchrotron X-Ray and Atomic Force Microscopy**, *HASYLAB Ann. Rep.*
- [78] P. Garidel: **Aggregation Behaviour of Ceramide Class 3 Lipids**, *HASYLAB Ann. Rep.*
- [79] P. Garidel: **Molecular Association of Phytosphingosine Ceramides of Type III as Investigated by Synchrotron X-Ray: Part 1**, *HASYLAB Ann. Rep.*, 2005, 1053–1054.
- [80] P. Garidel: **Molecular Association of Phytosphingosine Ceramides of Type III as Investigated by Synchrotron X-Ray: Part 2**, *HASYLAB Ann. Rep.*
- [81] P. Garidel: **Structural organisation and phase behaviour of a stratum corneum lipid analogue**- ceramide 3A, *Physical Chemistry Chemical Physics*, 2006; Vol. 8 19, 2265–2275.
- [82] P. Garidel: **The Gel Phase Structure of Hydrated Ceramide 3b as Investigated by Synchrotron X-Ray and Atomic Force Microscopy**, *HASYLAB Ann. Rep.*
- [83] S. Raudenkolb, S. Wartewig, R. H. H. Neubert: **Polymorphism of ceramide 3. Part 2**- a vibrational spectroscopic and X-ray powder diffraction investigation of N-octadecanoyl phytosphingosine and the analogous specifically deuterated d35 derivative, *Chemistry and Physics of Lipids*, 2003; Vol. 124 2, 89–101.
- [84] H. Löfgren, I. Pascher: **Molecular arrangements of sphingolipids. The monolayer behaviour of ceramides**, *Chemistry and Physics of Lipids*, 1977; Vol. 20 4, 273–284.
- [85] B. Dahlén, I. Pascher: **Molecular arrangements in sphingolipids. Crystal structure of N-tetracosanoylphytosphingosine**, *Acta Crystallographica Section B-Structural Crystallography and Crystal Chemistry*, 1972; Vol. 28 8, 2396–2404.
- [86] B. Dahlén, I. Pascher: **Molecular arrangements in sphingolipids. Thermotropic phase behaviour of tetracosanoylphytosphingosine**, *Chemistry and Physics of Lipids*, 1979; Vol. 24 2, 119–133.
- [87] T. N. Engelbrecht, A. Schroeter, T. Hauss, B. Demé, H. A. Scheidt, D. Huster, R. H. H. Neubert: **The impact of ceramides NP and AP on the nanostructure of stratum corneum lipid bilayer. Part I**- neutron diffraction and ²H NMR studies on multilamellar models based on ceramides with symmetric alkyl chain length distribution, *Soft Matter*, 2012; Vol. 8 24, 6599.
- [88] M. E. Rerek, D. van Wyck, R. Mendelsohn, D. J. Moore: **FTIR spectroscopic studies of lipid dynamics in phytosphingosine ceramide models of the stratum corneum lipid matrix**, *Chemistry and Physics of Lipids*, 2005; Vol. 134 1, 51–58.
- [89] C. Laugel, N. Yagoubi, A. Baillet-Guffroy: **ATR-FTIR spectroscopy**- a chemometric approach for studying the lipid organisation of the stratum corneum, *Chemistry and Physics of Lipids*, 2005; Vol. 135 1, 55–68.
- [90] D. J. Moore, M. E. Rerek, R. Mendelsohn: **FTIR Spectroscopy Studies of the Conformational Order and Phase Behavior of Ceramides**, *The Journal of Physical Chemistry B*, 1997; Vol. 101 44, 8933–8940.
- [91] D. J. Moore, M. E. Rerek, R. Mendelsohn: **Role of ceramides 2 and 5 in the structure of the stratum corneum lipid barrier**, *International Journal of Cosmetic Science*, 1999; Vol. 21 5, 353–368.

- [92] S. Guo, T. C. Moore, C. R. Iacovella, L. A. Strickland, C. McCabe: **Simulation study of the structure and phase behavior of ceramide bilayers and the role of lipid head group chemistry**, *Journal of chemical theory and computation*, 2013; Vol. 9 11, 5116–5126.
- [93] S. Raudenkolb, S. Wartewig, R. H. H. Neubert: **Polymorphism of ceramide 6-** a vibrational spectroscopic and X-ray powder diffraction investigation of the diastereomers of N-(alpha-hydroxyoctadecanoyl)-phytosphingosine, *Chemistry and Physics of Lipids*, 2005; Vol. 133 1, 89–102.
- [94] A. Ruettinger, M. A. Kiselev, T. Hauss, S. Dante, A. M. Balagurov, R. H. H. Neubert: **Fatty acid interdigitation in stratum corneum model membranes-** a neutron diffraction study, *European Biophysics Journal*, 2008; Vol. 37 6, 759–771.
- [95] A. Schroeter, D. Kessner, M. A. Kiselev, T. Hauss, S. Dante, R. H. H. Neubert: **Basic nanostructure of stratum corneum lipid matrices based on ceramides [EOS] and [AP]-** a neutron diffraction study, *Biophysical Journal*, 2009; Vol. 97 4, 1104–1114.
- [96] A. Hinder, C. E. Schmelzer, A. V. Rawlings, R. H. H. Neubert: **Investigation of the molecular structure of the human stratum corneum ceramides [NP] and [EOS] by mass spectrometry**, *Skin Pharmacology and Physiology*, 2011; Vol. 24 3, 127–135.
- [97] M. de Jager, G. S. Gooris, M. Ponec, J. A. Bouwstra: **Lipid mixtures prepared with well-defined synthetic ceramides closely mimic the unique stratum corneum lipid phase behavior**, *Journal of Lipid Research*, 2005; Vol. 46 12, 2649–2656.
- [98] D. Kessner, G. Brezesinski, S. S. Funari, B. Dobner, R. H. H. Neubert: **Impact of the long chain omega-acylceramides on the stratum corneum lipid nanostructure. Part 1-** Thermotropic phase behaviour of CER[EOS] and CER[EOP] studied using X-ray powder diffraction and FT-Raman spectroscopy, *Chemistry and Physics of Lipids*, 2010; Vol. 163 1, 42–50.
- [99] M. de Jager, G. S. Gooris, M. Ponec, J. A. Bouwstra: **Acylceramide head group architecture affects lipid organization in synthetic ceramide mixtures**, *The Journal of Investigative Dermatology*, 2004; Vol. 123 5, 911–916.
- [100] J. A. Bouwstra, G. S. Gooris, F. E. R. Dubbelaar, A. M. Weerheim, A. P. Ijzerman, M. Ponec: **Role of ceramide 1 in the molecular organization of the stratum corneum lipids**, *Journal of Lipid Research*, 1998; Vol. 39 1, 186–196.
- [101] J. R. Hill, P. W. Wertz: **Molecular models of the intercellular lipid lamellae from epidermal stratum corneum**, *Biochimica et Biophysica Acta - Biomembranes*, 2003; Vol. 1616 2, 121–126.
- [102] A. S. Breathnach, T. Goodman, C. Stolinski, M. Gross: **Freeze-fracture replication of cells of stratum corneum of human epidermis**, *Journal of Anatomy*, 1973; Vol. 114 Pt 1, 65–81.
- [103] D. C. Swartzendruber, A. Manganaro, K. C. Madison, M. Kremer, P. W. Wertz, C. A. Squier: **Organization of the intercellular spaces of porcine epidermal and palatal stratum corneum: a quantitative study employing ruthenium tetroxide**, *Cell and tissue research*, 1995; Vol. 279 2, 271–276.
- [104] K. C. Madison, D. C. Swartzendruber, P. W. Wertz, D. T. Downing: **Presence of intact intercellular lipid lamellae in the upper layers of the stratum corneum**, *The Journal of Investigative Dermatology*, 1987; Vol. 88 6, 714–718.
- [105] S. Y. Hou, A. K. Mitra, S. H. White, G. K. Menon, R. Ghadially, P. M. Elias: **Membrane structures in normal and essential fatty acid-deficient stratum corneum: characterization by ruthenium tetroxide staining and x-ray diffraction**, *The Journal of Investigative Dermatology*, 1991; Vol. 96 2, 215–223.
- [106] D. T. Downing: **Lipid and protein structures in the permeability barrier of mammalian epidermis**, *Journal of lipid research*, 1992; Vol. 33 3, 301–313.
- [107] M. Fartasch, I. D. Bassukas, T. L. Diepgen: **Disturbed extruding mechanism of lamellar bodies in dry non-eczematous skin of atopics**, *The British Journal of Dermatology*, 1992; Vol. 127 3, 221–227.
- [108] D. C. Swartzendruber: **Studies of epidermal lipids using electron microscopy**, *Seminars in dermatology*, 1992; Vol. 11 2, 157–161.
- [109] G. S. Pilgram, A. M. Engelsma-van Pelt, J. A. Bouwstra, H. K. Koerten: **Electron diffraction provides new information on human stratum corneum lipid organization studied in relation to depth and temperature**, *The Journal of Investigative Dermatology*, 1999; Vol. 113 3, 403–409.
- [110] J. A. Bouwstra, G. S. Gooris, K. Cheng, A. M. Weerheim, W. Bras, M. Ponec: **Phase behavior of isolated skin lipids**, *Journal of Lipid Research*, 1996; Vol. 37 5, 999–1011.
- [111] J. A. Bouwstra, G. S. Gooris, F. E. R. Dubbelaar, M. Ponec: **Phase behavior of stratum corneum lipid mixtures based on human ceramides: the role of natural and synthetic ceramide 1**, *The Journal of Investigative Dermatology*, 2002; Vol. 118 4, 606–617.
- [112] B. Skolova, B. Janusova, J. Zbytovská, G. S. Gooris, J. A. Bouwstra, P. Slepicka, P. Berka, J. Roh, K. Palát, A. Hrabálek, K. Vávrová: **Ceramides in the skin lipid membranes-** length matters, *Langmuir*, 2013; Vol. 29 50, 15624–15633.
- [113] E. Sparr, L. Eriksson, J. A. Bouwstra, K. Ekelund: **AFM Study of Lipid Monolayers:-** III. Phase Behavior of Ceramides, Cholesterol and Fatty Acids, *Langmuir*, 2001; Vol. 17 1, 164–172.
- [114] E. H. Mojumdar, D. Groen, G. S. Gooris, D. J. Barlow, M. J. Lawrence, B. Demé, J. A. Bouwstra: **Localization of cholesterol and fatty acid in a model lipid membrane: a neutron diffraction approach**, *Biophysical Journal*, 2013; Vol. 105 4, 911–918.
- [115] D. Kessner, M. A. Kiselev, T. Hauss, S. Dante, S. Wartewig, R. H. H. Neubert: **Localisation of partially deuterated cholesterol in quaternary SC lipid model membranes-** a neutron diffraction study, *European Biophysics Journal*, 2008; Vol. 37 6, 1051–1057.
- [116] D. Kessner, M. A. Kiselev, S. Dante, T. Hauss, P. Lersch, S. Wartewig, R. H. H. Neubert: **Arrangement of ceramide [EOS] in a stratum corneum lipid model matrix-** new aspects revealed by neutron diffraction studies, *European Biophysics Journal*, 2008; Vol. 37 6, 989–999.
- [117] D. J. Moore, M. E. Rerek: **Insights into the molecular organization of lipids in the skin barrier from infrared spectroscopy studies of stratum corneum lipid models**, *Acta dermato-venereologica. Supplementum*, 2000; Vol. 208, 16–22.
- [118] M. Janssens, J. van Smeden, G. S. Gooris, W. Bras, G. Portale, P. J. Caspers, R. J. Vreeken, T. Hankemeier, S. Kezic, R. Wolterbeek, A. P. Lavrijsen, J. A. Bouwstra: **Increase in short-chain ceramides correlates with an altered lipid organization and decreased barrier function in atopic eczema patients**, *Journal of Lipid Research*, 2012; Vol. 53 12, 2755–2766.
- [119] I. Hatta, N. Ohta, K. Inoue, N. Yagi: **Coexistence of two domains in intercellular lipid matrix of stratum corneum**, *Biochimica et Biophysica Acta*, 2006; Vol. 1758 11, 1830–1836.
- [120] N. Ohta, S. Ban, H. Tanaka, S. Nakata, I. Hatta: **Swelling of intercellular lipid lamellar structure with short repeat distance in hairless mouse stratum corneum as studied by X-ray diffraction**, *Chemistry and Physics of Lipids*, 2003; Vol. 123 1, 1–8.
- [121] J. A. Bouwstra, G. S. Gooris, W. Bras, D. T. Downing: **Lipid organization in pig stratum corneum**, *Journal of Lipid Research*, 1995; Vol. 36 4, 685–695.

- [122] S. H. White, D. Mirejovsky, G. I. King: **Structure of lamellar lipid domains and corneocyte envelopes of murine stratum corneum. An X-ray diffraction study**, *Biochemistry*, 1988; Vol. 27 10, 3725–3732.
- [123] P. W. Wertz: **Integral lipids of hair and stratum corneum**, *EXS*, 1997; Vol. 78, 227–237.
- [124] T. N. Engelbrecht, T. Hauss, K. Süß, A. Vogel, M. Roark, S. E. Feller, R. H. H. Neubert, B. Dobner: **Characterisation of a new ceramide EOS species- synthesis and investigation of the thermotropic phase behaviour and influence on the bilayer architecture of stratum corneum lipid model membranes**, *Soft Matter*, 2011; Vol. 7 19, 8998.
- [125] S. Pfeiffer, G. Vielhaber, J. P. Vietzke, K. P. Wittern, U. Hintze, R. Wepf: **High-pressure freezing provides new information on human epidermis: simultaneous protein antigen and lamellar lipid structure preservation. Study on human epidermis by cryoimmobilization**, *The Journal of Investigative Dermatology*, 2000; Vol. 114 5, 1030–1038.
- [126] A. Al-Amoudi, J. Dubochet, L. Norlén: **Nanostructure of the epidermal extracellular space as observed by cryo-electron microscopy of vitreous sections of human skin**, *The Journal of Investigative Dermatology*, 2005; Vol. 124 4, 764–777.
- [127] T. J. McIntosh, M. E. Stewart, D. T. Downing: **X-ray diffraction analysis of isolated skin lipids: reconstitution of intercellular lipid domains**, *Biochemistry*, 1996; Vol. 35 12, 3649–3653.
- [128] J. A. Bouwstra, G. S. Gooris, F. E. R. Dubbelaar, M. Ponec: **Cholesterol sulfate and calcium affect stratum corneum lipid organization over a wide temperature range**, *Journal of Lipid Research*, 1999; Vol. 40 12, 2303–2312.
- [129] J. A. Bouwstra, K. Cheng, G. S. Gooris, A. M. Weerheim, M. Ponec: **The role of ceramides 1 and 2 in the stratum corneum lipid organisation**, *Biochimica et Biophysica Acta*, 1996; Vol. 1300 3, 177–186.
- [130] J. A. Bouwstra, F. E. R. Dubbelaar, G. S. Gooris, A. M. Weerheim, M. Ponec: **The role of ceramide composition in the lipid organisation of the skin barrier**, *Biochimica et Biophysica Acta - Biomembranes*, 1999; Vol. 1419 2, 127–136.
- [131] M. de Jager, G. S. Gooris, I. P. Dolbnya, W. Bras, M. Ponec, J. A. Bouwstra: **Novel lipid mixtures based on synthetic ceramides reproduce the unique stratum corneum lipid organization**, *Journal of Lipid Research*, 2004; Vol. 45 5, 923–932.
- [132] E. H. Mojumdar, G. S. Gooris, J. A. Bouwstra: **Phase behavior of skin lipid mixtures- the effect of cholesterol on lipid organization**, *Soft Matter*, 2015; Vol. 11 21, 4326–4336.
- [133] M. de Jager, G. S. Gooris, I. P. Dolbnya, M. Ponec, J. A. Bouwstra: **Modelling the stratum corneum lipid organisation with synthetic lipid mixtures- the importance of synthetic ceramide composition**, *Biochimica et Biophysica Acta*, 2004; Vol. 1664 2, 132–140.
- [134] J. A. Bouwstra, G. S. Gooris, M.-D. Vries, J. A. van der Spek, W. Bras: **Structure of human stratum corneum as a function of temperature and hydration: A wide-angle X-ray diffraction study**, *International Journal of Pharmaceutics*, 1992; Vol. 84 3, 205–216.
- [135] J. A. Bouwstra, G. S. Gooris, J. A. van der Spek, W. Bras: **Structural investigations of human stratum corneum by small-angle X-ray scattering**, *The Journal of Investigative Dermatology*, 1991; Vol. 97 6, 1005–1012.
- [136] J. A. Bouwstra, F. E. R. Dubbelaar, G. S. Gooris, M. Ponec: **The lipid organisation in the skin barrier**, *Acta dermatovenereologica. Supplementum*, 2000; Vol. 208, 23–30.
- [137] L. Norlén: **Molecular Skin Barrier Models and Some Central Problems for the Understanding of Skin Barrier Structure and Function**, *Skin Pharmacology and Physiology*, 2003; Vol. 16 4, 203–211.
- [138] E. H. Mojumdar, G. S. Gooris, D. J. Barlow, M. J. Lawrence, B. Demé, J. A. Bouwstra: **Skin lipids- localization of ceramide and fatty acid in the unit cell of the long periodicity phase**, *Biophysical Journal*, 2015; Vol. 108 11, 2670–2679.
- [139] E. H. Mojumdar, G. S. Gooris, D. Groen, D. J. Barlow, M. J. Lawrence, B. Demé, J. A. Bouwstra: **Stratum corneum lipid matrix: Location of acyl ceramide and cholesterol in the unit cell of the long periodicity phase**, *Biochimica et Biophysica Acta*, 2016.
- [140] M. Seul, M. J. Sammon: **Preparation of surfactant multilayer films on solid substrates by deposition from organic solution**, *Thin Solid Films*, 1990; Vol. 185 2, 287–305.
- [141] K. K. Sharma "Optics: Principles and Applications, Elsevier Science" 2006.
- [142] T. Hauß: **V1- Membrane Diffractometer at BER II**, *Journal of large-scale research facilities JLSRF*, 2016; Vol. 2.
- [143] T. D. Hong, S. Edgington, R. H. Ellis, M. A. de Muro, D. J. Moore: **Saturated salt solutions for humidity control and the survival of dry powder and oil formulations of Beauveria bassiana conidia**, *Journal of Invertebrate Pathology*, 2005; Vol. 89 2, 136–143.
- [144] T. D. Hong, R. H. Ellis, J. Gunn, D. J. Moore: **Relative humidity, temperature, and the equilibrium moisture content of conidia of Beauveria bassiana (Balsamo) Vuillemin- A quantitative approach**, *Journal of Stored Products Research*, 2002; Vol. 38 1, 33–41.
- [145] B. Demé, Cristiglio Viviana, Aguetz Olivier "D16: Instrument Specifications" 27.07.2017.
- [146] N. P. Franks, W. R. Lieb: **The structure of lipid bilayers and the effects of general anaesthetics. An x-ray and neutron diffraction study**, *Journal of Molecular Biology*, 1979; Vol. 133 4, 469–500.
- [147] D. L. Worcester, N. P. Franks: **Structural analysis of hydrated egg lecithin and cholesterol bilayers II. Neutron diffraction**, *Journal of Molecular Biology*, 1976; Vol. 100 3, 359–378.
- [148] J. F. Nagle, S. Tristram-Nagle, J. F. Nagle, S. Tristram-Nagle: **Structure of lipid bilayers**, *Biochimica et Biophysica Acta*, 2000; 1469 (3) 3, 159–195.
- [149] S. Dante, T. Hauss, N. A. Dencher: **Insertion of externally administered amyloid beta peptide 25-35 and perturbation of lipid bilayers**, *Biochemistry*, 2003; Vol. 42 46, 13667–13672.
- [150] H.-C. Chen, R. Mendelsohn, M. E. Rerek, D. J. Moore: **Effect of cholesterol on miscibility and phase behavior in binary mixtures with synthetic ceramide 2 and octadecanoic acid. Infrared studies**, *Biochimica et Biophysica Acta*, 2001; Vol. 1512 2, 345–356.
- [151] E. Brief, S. Kwak, J. T. Cheng, N. Kitson, J. L. Thewalt, M. Lafleur: **Phase behavior of an equimolar mixture of N-palmitoyl-D-erythro-sphingosine, cholesterol, and palmitic acid, a mixture with optimized hydrophobic matching**, *Langmuir*, 2009; Vol. 25 13, 7523–7532.
- [152] B. Skolova, K. Hudska, P. Pullmannova, A. Kováčik, K. Palát, J. Roh, J. Fleddermann, I. Estrela-Lopis, K. Vávrová: **Different phase behavior and packing of ceramides with long (C16) and very long (C24) acyls in model membranes- infrared spectroscopy using deuterated lipids**, *J Phys Chem B*, 2014; Vol. 118 35, 10460–10470.
- [153] L. Li, X. Tang, K. G. Taylor, D. B. DuPré, M. C. Yappert: **Conformational characterization of ceramides by nuclear magnetic resonance spectroscopy**, *Biophysical Journal*, 2002; Vol. 82 4, 2067–2080.

- [154] J. J. Bulgin, L. J. Vinson: **The use of differential thermal analysis to study the bound water in stratum corneum membranes**, *Biochimica et Biophysica Acta*, 1967; Vol. 136 3, 551–560.
- [155] A. Y. Gruzinov, A. V. Zabelin, M. A. Kiselev: **Short periodicity phase based on ceramide AP in the model lipid membranes of stratum corneum does not change during hydration**, *Chemistry and physics of lipids*, 2017; Vol. 202, 1–5.
- [156] M. A. Kiselev, N. Y. Ryabova, A. M. Balagurov, S. Dante, T. Hauss, J. Zbytovská, S. Wartewig, R. H. H. Neubert: **New insights into the structure and hydration of a stratum corneum lipid model membrane by neutron diffraction**, *European Biophysics Journal*, 2005; Vol. 34 8, 1030–1040.
- [157] S. Sonnenberger, A. Eichner, T. Schmitt, T. Hau, S. Lange, A. Langner, R. H. H. Neubert, B. Dobner: **Synthesis of specific deuterated derivatives of the long chained stratum corneum lipids [EOS] and [EOP] and characterization using neutron scattering**, *Journal of labelled compounds & radiopharmaceuticals*, 2017; Vol. 60 7, 316–330.
- [158] S. Sonnenberger, S. Lange, A. Langner, R. H. H. Neubert, B. Dobner: **Synthesis of ceramides NS and NP with perdeuterated and specifically ω deuterated N-acyl residues**, *Journal of labelled compounds & radiopharmaceuticals*, 2016; Vol. 59 12, 531–542.
- [159] T. Schmitt, S. Lange, B. Dobner, S. Sonnenberger, T. Hauss, R. H. H. Neubert: **Investigation of a CER[NP] and [AP] based stratum corneum modelling membrane system-** Using specifically deuterated CER together with a neutron diffraction approach, *Langmuir*, 2017.
- [160] J. A. Bouwstra, G. S. Gooris, F. E. R. Dubbelaar, M. Ponc: **Phase behavior of lipid mixtures based on human ceramides: coexistence of crystalline and liquid phases**, *Journal of Lipid Research*, 2001; Vol. 42 11, 1759–1770.
- [161] K. Ekelund, L. Eriksson, E. Sparr: **Rectangular solid domains in ceramide-cholesterol monolayers - 2D crystals**, *Biochimica et Biophysica Acta*, 2000; Vol. 1464 1, 1–6.
- [162] S. L. Souza, M. J. Capitan, J. Alvarez, S. S. Funari, M. H. Lameiro, E. Melo: **Phase behavior of aqueous dispersions of mixtures of N-palmitoyl ceramide and cholesterol: a lipid system with ceramide-cholesterol crystalline lamellar phases**, *The journal of physical chemistry. B*, 2009; Vol. 113 5, 1367–1375.
- [163] P. Garidel, B. Foltting, I. Schaller, A. Kerth: **The microstructure of the stratum corneum lipid barrier-** mid-infrared spectroscopic studies of hydrated ceramide:palmitic acid:cholesterol model systems, *Biophysical Chemistry*, 2010; Vol. 150 1-3, 144–156.
- [164] S. Raudenkolb, S. Wartewig, G. Brezesinski, S. S. Funari, R. H. H. Neubert: **Hydration properties of N-(alpha-hydroxyacyl)-sphingosine-** X-ray powder diffraction and FT-Raman spectroscopic studies, *Chemistry and Physics of Lipids*, 2005; Vol. 136 1, 13–22.
- [165] M. A. Lampe, A. L. Burlingame, J. Whitney, M. L. Williams, B. E. Brown, E. Roitman, P. M. Elias: **Human stratum corneum lipids: characterization and regional variations**, *Journal of Lipid Research*, 1983; Vol. 24 2, 120–130.
- [166] M. Ponc, A. M. Weerheim, P. Lankhorst, P. W. Wertz: **New acylceramide in native and reconstructed epidermis**, *The Journal of Investigative Dermatology*, 2003; Vol. 120 4, 581–588.
- [167] M. Mao-Qiang, P. M. Elias, K. R. Feingold: **Fatty acids are required for epidermal permeability barrier function**, *The Journal of Clinical Investigation*, 1993; Vol. 92 2, 791–798.
- [168] M. Oguri, G. S. Gooris, K. Bito, J. A. Bouwstra: **The effect of the chain length distribution of free fatty acids on the mixing properties of stratum corneum model membranes**, *Biochimica et Biophysica Acta*, 2014; Vol. 1838 7, 1851–1861.
- [169] T. Schmitt, S. Lange, S. Sonnenberger, B. Dobner, B. Demé, R. H. Neubert, G. Gooris, J. A. Bouwstra: **Determination of the influence of C24 D/(2R)- and L/(2S)-isomers of the CER[AP] on the lamellar structure of stratum corneum model systems using neutron diffraction**, *Chemistry and physics of lipids*, 2017; Vol. 209, 29–36.
- [170] Gunsteren WF van, Berendsen HJ: **Groningen molecular simulation (gromos) library manual**, *Biomos, Groningen* 1987;24(682704):13.
- [171] O. Berger, O. Edholm, F. Jähnig: **Molecular dynamics simulations of a fluid bilayer of dipalmitoylphosphatidylcholine at full hydration, constant pressure, and constant temperature**, *Biophysical journal*, 1997; Vol. 72 5, 2002–2013.
- [172] M. Höltje, T. Förster, B. Brandt, T. Engels, W. von Rybinski, H. D. Höltje: **Molecular dynamics simulations of stratum corneum lipid models: fatty acids and cholesterol**, *Biochimica et Biophysica Acta*, 2001; Vol. 1511 1, 156–167.
- [173] R. Gupta, D. B. Sridhar, B. Rai: **Molecular Dynamics Simulation Study of Permeation of Molecules through Skin Lipid Bilayer**, *The journal of physical chemistry. B*, 2016; Vol. 120 34, 8987–8996.
- [174] L. Martínez, R. Andrade, E. G. Birgin, J. M. Martínez: **PACKMOL-** A package for building initial configurations for molecular dynamics simulations, *Journal of computational chemistry*, 2009; Vol. 30 13, 2157–2164.
- [175] H. J. C. Berendsen, J. P. M. Postma, W. F. van Gunsteren, J. Hermans: **Interaction Models for Water in Relation to Protein Hydration**, in *Intermolecular Forces: Proceedings of the Fourteenth Jerusalem Symposium on Quantum Chemistry and Biochemistry Held in Jerusalem, Israel, April 13-16, 1981* (Ed.: B. Pullman); Vol. 14, Springer Netherlands; Imprint; Springer, p. 331" 1981.
- [176] M. J. Abraham, T. Murtola, R. Schulz, S. Páll, J. C. Smith, B. Hess, E. Lindahl: **GROMACS-** High performance molecular simulations through multi-level parallelism from laptops to supercomputers, *SoftwareX*, 2015; 1-2, 19–25.
- [177] W. Humphrey, A. Dalke, K. Schulten: **VMD-** Visual molecular dynamics, *Journal of molecular graphics*, 1996; Vol. 14 1, 33-8, 27-8.
- [178] P. W. Wertz, D. T. Downing: **Ceramides of pig epidermis: structure determination**, *Journal of Lipid Research*, 1983; Vol. 24 6, 759–765.
- [179] M. Janssens, G. S. Gooris, J. A. Bouwstra: **Infrared spectroscopy studies of mixtures prepared with synthetic ceramides varying in head group architecture-** coexistence of liquid and crystalline phases, *Biochimica et Biophysica Acta*, 2009; Vol. 1788 3, 732–742.
- [180] C. Das, M. G. Noro, P. D. Olmsted: **Fast cholesterol flip-flop and lack of swelling in skin lipid multilayers**, *Soft matter*, 2014; Vol. 10 37, 7346–7352.
- [181] A. Eichner, S. Sonnenberger, B. Dobner, T. Hau, A. Schroeter, R. H. H. Neubert: **Localization of methyl-branched ceramide [EOS] species within the long-periodicity phase in stratum corneum lipid model membranes-** A neutron diffraction study, *Biochimica et Biophysica Acta - Biomembranes*, 2016; Vol. 1858 11, 2911–2922.
- [182] Thomas Schmitt, DEME Bruno, R. H. H. Neubert "Investigation of the stratum corneum multilamellar lipid membrane structure in dependence of asymmetric CER[NP]-C24 and CER[AP]-C24, Institut Laue-Langevin (ILL)" 2016.

- [183] L. Opálka, A. Kováčik, J. Maixner, K. Vávrová: **Omega-O-Acylceramides in Skin Lipid Membranes- Effects of Concentration, Sphingoid Base, and Model Complexity on Microstructure and Permeability**, *Langmuir the ACS journal of surfaces and colloids*, 2016; Vol. 32 **48**, 12894–12904.
- [184] D. Groen, G. S. Gooris, J. A. Bouwstra: **New insights into the stratum corneum lipid organization by X-ray diffraction analysis**, *Biophysical Journal*, 2009; Vol. 97 **8**, 2242–2249.
- [185] M. de Jager, G. S. Gooris, I. P. Dolbnya, W. Bras, M. Ponec, J. A. Bouwstra: **The phase behaviour of skin lipid mixtures based on synthetic ceramides**, *Chemistry and Physics of Lipids*, 2003; Vol. 124 **2**, 123–134.
- [186] D. Groen, G. S. Gooris, J. A. Bouwstra: **Model membranes prepared with ceramide EOS, cholesterol and free fatty acids form a unique lamellar phase**, *Langmuir*, 2010; Vol. 26 **6**, 4168–4175.
- [187] D. de Sousa Neto, G. S. Gooris, J. A. Bouwstra: **Effect of the omega-acylceramides on the lipid organization of stratum corneum model membranes evaluated by X-ray diffraction and FTIR studies (Part I)**, *Chemistry and Physics of Lipids*, 2011; Vol. 164 **3**, 184–195.
- [188] D. Groen, D. S. Poole, G. S. Gooris, J. A. Bouwstra: **Investigating the barrier function of skin lipid models with varying compositions**, *European Journal of Pharmaceutics and Biopharmaceutics*, 2011; Vol. 79 **2**, 334–342.
- [189] G. Imokawa, A. Abe, K. Jin, Y. Higaki, M. Kawashima, A. Hidano: **Decreased level of ceramides in stratum corneum of atopic dermatitis: an etiologic factor in atopic dry skin?**, *The Journal of Investigative Dermatology*, 1991; Vol. 96 **4**, 523–526.
- [190] J. A. Bouwstra, G. S. Gooris, A. M. Weerheim, J. A. Kempenaar, M. Ponec: **Characterization of stratum corneum structure in reconstructed epidermis by X-ray diffraction**, *Journal of Lipid Research*, 1995; Vol. 36 **3**, 496–504.
- [191] I. Hatta, N. Ohta, S. Ban, H. Tanaka, S. Nakata: **X-ray diffraction study on ordered, disordered and reconstituted intercellular lipid lamellar structure in stratum corneum**, *Biophysical Chemistry*, 2001; Vol. 89 **2-3**, 239–242.
- [192] Y. Cho, B.-L. Lew, K. Seong, N.-I. Kim: **An inverse relationship between ceramide synthesis and clinical severity in patients with psoriasis**, *Journal of Korean medical science*, 2004; Vol. 19 **6**, 859–863.
- [193] E. Berardesca, M. Barbareschi, S. Veraldi, N. Pimpinelli: **Evaluation of efficacy of a skin lipid mixture in patients with irritant contact dermatitis, allergic contact dermatitis or atopic dermatitis- A multicenter study**, *Contact Dermatitis*, 2001; Vol. 45 **5**, 280–285.
- [194] M. Lodén: **The skin barrier and use of moisturizers in atopic dermatitis**, *Clinics in dermatology*, 2003; Vol. 21 **2**, 145–157.
- [195] E. Proksch, J.-M. Jensen, P. M. Elias: **Skin lipids and epidermal differentiation in atopic dermatitis**, *Clinics in dermatology*, 2003; Vol. 21 **2**, 134–144.
- [196] S. Stahlberg, B. Školová, P. K. Madhu, A. Vogel, K. Vávrová, D. Huster: **Probing the role of the ceramide acyl chain length and sphingosine unsaturation in model skin barrier lipid mixtures by (2)H solid-state NMR spectroscopy**, *Langmuir the ACS journal of surfaces and colloids*, 2015; Vol. 31 **17**, 4906–4915.
- [197] S. Stahlberg, S. Lange, B. Dobner, D. Huster: **Probing the Role of Ceramide Headgroup Polarity in Short-Chain Model Skin Barrier Lipid Mixtures by ²H Solid-State NMR Spectroscopy**, *Langmuir the ACS journal of surfaces and colloids*, 2016; Vol. 32 **8**, 2023–2031.
- [198] A. Herman, A. P. Herman: **Essential oils and their constituents as skin penetration enhancer for transdermal drug delivery- A review**, *The Journal of pharmacy and pharmacology*, 2015; Vol. 67 **4**, 473–485.
- [199] S. A. Ibrahim: **Spray-on transdermal drug delivery systems**, *Expert opinion on drug delivery*, 2015; Vol. 12 **2**, 195–205.
- [200] H. Trommer, R. H. H. Neubert: **Overcoming the stratum corneum- the modulation of skin penetration. A review**, *Skin Pharmacology and Physiology*, 2006; Vol. 19 **2**, 106–121.
- [201] R. H. H. Neubert, O. Bayrak, S. Steinbach, S. Sonnenberger, B. Dobner: **Development and Validation of Analytical Methods for the Detection and Quantification of a Novel Dimeric Ceramide in Stratum Corneum and Other Layers of the Skin**, *Chromatographia*, 2016; Vol. 79 **23-24**, 1615–1624.
- [202] L. Norlén, I. Nicander, A. Lundsjo, T. Cronholm, B. Forslind: **A new HPLC-based method for the quantitative analysis of inner stratum corneum lipids with special reference to the free fatty acid fraction.**, *Archives of Dermatological Research*, 1998; Vol. 290 **9**, 508–516.
- [203] A. Kováčik, M. Šilarová, P. Pullmannová, J. Maixner, K. Vávrová: **Effects of 6-Hydroxyceramides on the Thermotropic Phase Behavior and Permeability of Model Skin Lipid Membranes**, *Langmuir the ACS journal of surfaces and colloids*, 2017; Vol. 33 **11**, 2890–2899.
- [204] M. C. Wiener, S. H. White: **Fluid bilayer structure determination by the combined use of x-ray and neutron diffraction. II. "Composition-space" refinement method**, *Biophysical Journal*, 1991; Vol. 59 **1**, 174–185.
- [205] C. W. Bunn: **The crystal structure of long-chain normal paraffin hydrocarbons. The "shape" of the >CH₂ group**, *Trans. Faraday Soc.*, 1939; Vol. 35 **0**, 482–491.
- [206] R. H. H. Neubert, S. Sonnenberger, B. Dobner, C. W. Gray, K. N. Barger, K. Sevi-Maxwell, E. Sommer, J. Wohlrab: **Controlled Penetration of a Novel Dimeric Ceramide into and across the Stratum Corneum Using Microemulsions and Various Types of Semisolid Formulations**, *Skin pharmacology and physiology*, 2016; Vol. 29 **3**, 130–134.

7. Appendix

Lebenslauf

Thomas Schmitt, geboren: 16.06.1991

M. Sc. Biochemie (Biomedizin)



Persönliche Daten

Anschrift: Kunigundenstraße 5; 96129 Strullendorf
Telefonnummer: +49(0)9543 5201 **Mobil:** +49(0)170 958238
E-Mail: thomasschmitt2004@web.de **Researchgate:** [Thomas Schmitt11](#)
Geburtsort: Bamberg (BY) **Nationalität:** deutsch

Bildung



Lehranstalten: seit Feb.16 An-Institut für angewandte Dermatopharmazie e.V., an der Martin-Luther-Universität Halle-Wittenberg  
Promotion: Dr. rer. nat. Biochemie vsI. 1.HJ 2018



Okt.13 - Nov.15 Universität Leipzig -Alma Mater Lipsiensis-  
Studiengang: M. Sc. Biochemie (Biomedizin) Note: **1,4**

Okt.09 - Sep.13 Technische Hochschule Nürnberg Georg Simon Ohm  
B. Sc. angewandte Chemie (Biochemie) Note: **2,7**

Sep.07 - Jul.09 Staatliche berufliche Oberschule Bamberg  
Fachgebundene Hochschulreife Note: **2,7**
Fachrichtung: Wirtschaft und Verwaltung

Praktische Erfahrung

Promotion: seit Feb.16 An-Institut für angewandte Dermatopharmazie an der Martin-Luther-Universität Halle-Wittenberg e.V.  
“Investigation of the influence of asymmetric long chain ceramides [NP] and [AP] on stratum corneum lipid matrix architecture with neutron diffraction”

Masterarbeit (Uni.): Apr. - Sep.15 Universität Leipzig -Alma Mater Lipsiensis- Medizinische Fakultät, Arbeitsgruppe molekulare Onkologie  
„Regulation von Zellzyklusgenen durch E2F/CLE Tandemelemente“

- Bachelorarbeit (TH):** Mär.-Aug.13 Helmholtz-Zentrum München, deutsches Forschungszentrum für Gesundheit und Umwelt (Institut für Biochemische Pflanzenpathologie BIOP) 📍 🌐
 „Untersuchung der Protein-Protein-Interaktionen diverser immunaktiver Proteine aus *Arabidopsis thaliana* mittels Y2H-System“
- Praktische Semester:** Oct.14 - Jan.15 Universität Leipzig -Alma Mater Lipsiensis- Institut für Biochemie, Arbeitsgruppe für Bioorganische Chemie 📍 🌐
 „Synthesis and testing of carbaborane coupled peptides for use in neutron boron capture therapy“
- Mär. - Jul.11 Friedrich-Alexander-Universität Erlangen-Nürnberg, Lehrstuhl für Bioverfahrenstechnik, Arbeitsgruppe für Zellkultur und Immobilisierung 📍 🌐
 „Induktion der Expression von CD14 in THP-1 Monozyten“
- Nationale Kooperationen:**
- Helmholtz-Zentrum für Materialien und Energie (HZB), Berlin GER 📍 🌐
 - Meier-Leibnitz-Zentrum (MLZ), Garching b. München GER 📍 🌐
 - Universitätsklinikum (Dermatologie und Venerologie), Halle(Saale), GER 📍 🌐
- Internationale Kooperationen:**
- Institut Laue-Langevin, Grenoble (FR) 📍 🌐
 - Tata Research Development and Design Centre, Pune, (IND) 📍 🌐
 - Department of Pharmaceutical Technology, University of Chemistry and Technology, Prague (CZ) 📍 🌐
 - Leiden Academic Centre for Drug Research, Department of Drug Delivery Technology, Gorlaeus Laboratories, University of Leiden (NL) 📍 🌐

Liste wissenschaftlicher Beiträge

Originalpublikationen

T. Schmitt, S. Lange, S. Sonnenberger, B. Dobner, B. Demé, R. H. Neubert, G. Gooris, J. A. Bouwstra: **Determination of the influence of C24 D/(2R)- and L/(2S)-isomers of the CER[AP] on the lamellar structure of stratum corneum model systems using neutron diffraction**, *Chemistry and physics of lipids*, 2017; Vol. 209, 29–36.

T. Schmitt, S. Lange, B. Dobner, S. Sonnenberger, T. Hauss, R. H. H. Neubert: **Investigation of a CER[NP] and [AP] based stratum corneum modelling membrane system- Using specifically deuterated CER together with a neutron diffraction approach**, *Langmuir*, 2017.

T. Schmitt, R. Gupta, S. Lange, S. Sonnenberger, B. Dobner, T. Hauß, B. Rai, R. H. Neubert, R. H. H. Neubert: **Impact of the ceramide subspecies on the nanostructure of stratum corneum lipids using neutron scattering and molecular dynamics simulations. Part I- Impact of CER[NS]**, *Chemistry and physics of lipids*, 2018; Vol. 214, 58–68.

T. Schmitt, S. Lange, S. Sonnenberger, B. Dobner, B. Demé, A. Langner, R. H. Neubert: **The long periodicity phase (LPP) controversy Part I: The influence of a natural-like ratio of the CER[EOS] analogue [EOS]-br in a CER[NP]/[AP] based stratum corneum modelling system: A Neutron diffraction study**, *BBA-Biomembranes*, 2018 (just accepted)

Co-Autor Publiationen

S. Stahlberg, A. Eichner, S. Sonnenberger, A. Kováčik, S. Lange, T. Schmitt, B. Demé, T. Hauß, B. Dobner, R. H. H. Neubert, D. Huster: **Influence of a Novel Dimeric Ceramide Molecule on the Nanostructure and Thermotropic Phase Behavior of a Stratum Corneum Model Mixture**, *Langmuir the ACS journal of surfaces and colloids*, 2017; Vol. 33 36, 9211–9221.

S. Sonnenberger, A. Eichner, T. Schmitt, T. Hau, S. Lange, A. Langner, R. H. H. Neubert, B. Dobner: **Synthesis of specific deuterated derivatives of the long chained stratum corneum lipids [EOS] and [EOP] and characterization using neutron scattering**, *Journal of labelled compounds & radiopharmaceuticals*, 2017; Vol. 60 7, 316–330.

Ältere Publikationen

G. A. Müller, K. Stangner, T. Schmitt, A. Wintsche, K. Engeland: **Timing of transcription during the cell cycle- Protein complexes binding to E2F, E2F/CLE, CDE/CHR, or CHR promoter elements define early and late cell cycle gene expression**, *Oncotarget*, 2014

Konferenzbeiträge und andere Vorträge

(Poster) Thomas Schmitt: **“Investigation of a CER[NP] and [AP] based stratum corneum modelling membrane system: using specifically deuterated CER together with a neutron diffraction approach”**; *Gordon Research Conference: Barrier Function of Mammalian Skin*; 08.13.2017 – 08.18.2017.

(Poster) Thomas Schmitt, Reinhard H. H. Neubert: **“The Influence of a Novel Dimeric Ceramide Molecule on the Nanostructure and the Thermotropic Phase Behavior of a Stratum Corneum Model Mixture”**; *Gordon Research Conference: Barrier Function of Mammalian Skin*; 08.13.2017 – 08.18.2017.